1984

Effects of gravity load on composite floor diaphragm behavior

Michael Kerry Neilsen
Iowa State University

Effects of gravity load on composite floor diaphragm behavior

by

Michael Kerry Neilsen

A Thesis Submitted to the

Graduate Faculty in Partial Fullfillment of the

Requirements for the Degree of

MASTER OF SCIENCE

Department: Civil Engineering
Major: Structural Engineering

Approved:

Signatures redacted for privacy.

Iowa State University
Ames, Iowa
1984

TABLE OF CONTENTS

LIST OF SYMBOLS

a	length of the diaphragm or length of the push-off specimen, in.
a'	effective width of the "edge zone" perpendicular to the corrugations, in.
A_{cv}	net area of concrete section bounded by web thickness and length of section in the direction of shear force considered, in.
b	width of the diaphragm or width of the push-off specimen, in.
b'	effective width of the "edge zone" parallel to the corrugations, in.
d	effective width of a shear wall, in.
d_a	average diameter of an arc spot weld, in.
d_e	effective diameter of fused area, in.
D	actual out-to-out thickness of the concrete, in.
E_c	modulus of elasticity for concrete, ksi.
E_s	modulus of elasticity for steel, ksi.
f'_c	compressive strength of the concrete, psi.
f_y	yield strength of the steel, ksi.
F_{xx}	arc spot weld strength level designation in AWS electrode classification, ksi.
G_c	modulus of rigidity for concrete, ksi.
G_s	modulus of rigidity for steel, ksi.
h	shear wall depth, in.
I_c	moment of inertia of the composite web, in.
I_s	moment of inertia of the edge beams, in.
K_b	bending stiffness of the diaphragm, kips/in.
K_p	linear stiffness of the "edge zone" parallel to the corrugations, kips/in./in.

$K_{p'}$ linear stiffness perpendicular to the corrugations corresponding to $q_{p'}$, kips/in./in.

K_s shear stiffness of the diaphragm, kips/in.

K_t linear stiffness of the "edge zone" perpendicular to the corrugations, kips/in./in.

$K_{t'}$ linear stiffness parallel to the corrugations corresponding to $q_{t'}$, kips/in./in.

K_z diaphragm stiffness due to deformation in the "edge zone", kips/in.

K_T total calculated diaphragm stiffness, kips/in.

l_c length of the "edge zone" contributing to force on the fasteners, in.

l width of a shearwall or diaphragm, in.

l_p $(b^2 + 3bb' - 2b'^2)/6a$.

$l_{p'}$ $(b^2 + 4bb' - 4b'^2)/4a$.

l_t $a' - (2a'^2/3a)$.

$l_{t'}$ $2a' - (2a'^2/a)$.

n modular ratio of elasticity.

n_a number of edge fasteners along length a.

$n_{a'}$ number of edge fasteners along length a'.

n_b number of edge fasteners along length b.

n_c number of edge fasteners along length l_c.

n_s modular ratio of rigidity.

P_v load applied by vertical load mechanism, kips.

P_1 in-plane load applied to east end of the north edge beam, kips.

P_2 in-plane load applied to west end of the north edge beam, kips.

q_p interfacial shear force parallel to the corrugations, which occurs along edges that are parallel to the corrugations, kips/in.

q_p' interfacial shear force parallel to the corrugations, which occurs along edges that are perpendicular to the corrugations, kips/in.

q_t interfacial shear force perpendicular to the corrugations which occurs along edges that are perpendicular to the corrugations, kips/in.

q_t' interfacial shear force perpendicular to the corrugations, which occurs along edges that are parallel to the corrugations, kips/in.

Q_p ultimate strength value of q_p, kips/in.

Q_p' ultimate strength value of q_p', kips/in.

Q_t ultimate strength value of q_t, kips/in.

Q_t' ultimate strength value of q_t', kips/in.

Q_u ultimate fastener strength, kips.

Q_{up} ultimate strength of a fastener with the deck parallel to the edge member, kips.

Q_{ut} ultimate strength of a fastener with the deck perpendicular to the edge member, kips.

r width of one rib section, in.

s width of one up corrugation at the top, in.

t_a average thickness of the concrete, in.

t_e effective thickness of the diaphragm, in.

t_s thickness of the steel deck, in.

V applied shear force on the slab, kips.

v_{max} maximum shear stress, psi.

V_p applied shear force on the parallel push-off specimen, kips.

V_{up} ultimate shear force on the parallel push-off specimen, kips.

V_t applied shear force on the transverse push-off specimen, kips.

V_{ut} ultimate shear force on the transverse push-off specimen, kips.

w_c weight of the concrete slab, ksi.

w_l applied vertical load, ksi.

α coefficient that varies linearly from 3.0 for h/l equal to 1.5 to 2.0 for h/l equal to 2.0.

μ coefficient of friction between the steel deck and concrete.

μ_t cell force coefficient.

θ rotation of the concrete about its center.

ρ ratio of distributed shear reinforcement on a plane perpendicular to plane of A_{cv}.

σ_{ult} ultimate stress capacity of the steel, ksi.

σ_{ut} ultimate capacity per unit of projected area of the interface in the transverse direction, ksi.

σ_{up} ultimate capacity per unit of projected area of the interface in the parallel direction, ksi.

Δ_b bending deflection of the diaphragm, in.

Δ_p "edge zone" displacement in the longitudinal direction, in.

Δ_s shear deflection of the diaphragm, in.

Δ_t "edge zone" displacement in the transverse direction, in.

Δ_z deflection of the diaphragm due to deformation in the "edge zone", in.

Δ_T total deflection of the diaphragm, in.

Δ_1 displacement at east end of north edge beam, in.

Δ_2 displacement at west end of north edge beam, in.

1. INTRODUCTION

1.1. General

Cold-formed metal deck, composite floor slab systems have become more common in recent years. These floor systems reduce or eliminate the need for formwork and shoring, reduce field labor costs, and allow for the use of a minimum floor thickness. A minimum floor thickness results in a minimum weight floor slab system which results in material savings in many parts of the entire structure. The steel deck serves as formwork during construction. After the concrete cures on top of the steel deck, the two materials act together as a composite floor slab system. The steel deck provides the principal positive bending tension reinforcement. A typical system is shown in Figure 1.

Composite floor slabs are connected to support beams with arc spot welds or shear connectors welded through the steel deck to the support beams. Composite action between the steel deck and concrete is developed by chemical and mechanical bonding. Mechanical bonding is provided by cell geometry and/or mechanical devices such as embossments, indentations, holes in the steel deck or transverse wires attached to the deck. When shear connectors are used, additional composite action is directly developed between the support beams and the concrete.

Lateral forces on a building are generated by earthquakes or wind. These lateral forces are transferred through the plane of the floor slab into vertical shear resisting elements and finally into the foundation as horizontal shear. Floor slabs are designed to resist gravity loads but can also be designed to resist in-plane loads. Throughout this

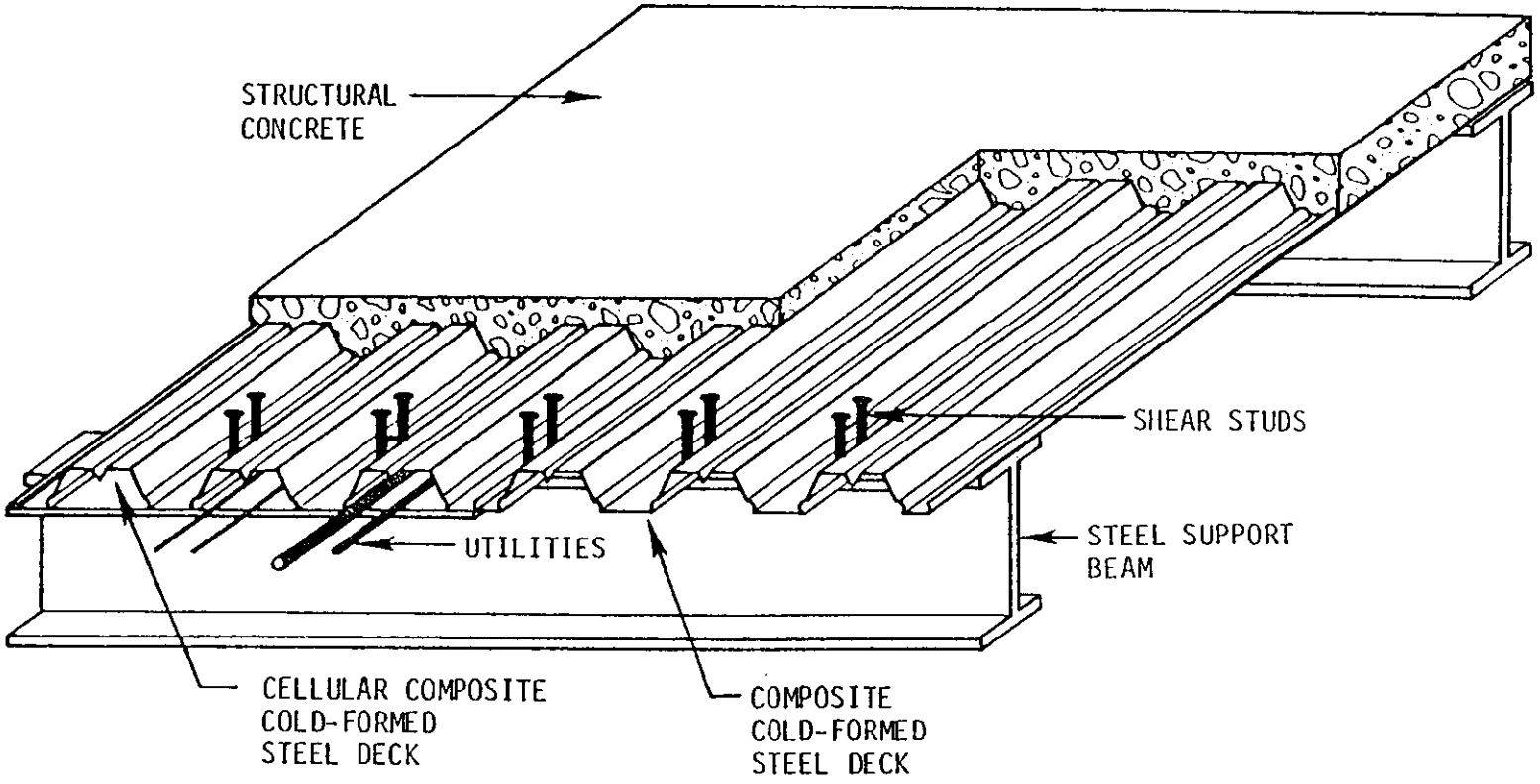

Figure 1. Typical construction utilizing cold-formed steel decking with composite support beams (30)

report, load applied in a direction normal to the concrete surface will be referred to as gravity or vertical load. Load applied in a direction parallel to the concrete surface will be referred to as in-plane load. A floor slab system, designed to resist in-plane load, is referred to as a diaphragm.

1.2. Objective of Overall Research Program

The objective of the overall research program is to investigate the behavioral and strength characteristics of composite steel-deck reinforced concrete floor diaphragms (30). Behavioral characteristics to be studied are failure mode, stiffness, maximum capacity and ductility. The entire research effort has been subdivided into the following phases:

1. Design and construction of a diaphragm test facility and performance of pilot tests on diaphragm specimens.
2. Full-scale testing of a series of diaphragm specimens subjected to in-plane loading only.
3. Testing of one-way slab element tests subjected to vertical loads to determine the effect of stud shear connectors on shear-bond strength.
4. Development of an analytical model using finite element analysis and definition of significant parameters for design equations.
5. Full-scale testing of composite slabs subjected to combined in-plane loads and distributed gravity loads.

6. Full-scale testing of composite slabs with different length to width ratios.
7. Investigation of the effects of continuity from adjoining floor slab panels.

Results from the experimental testing will be used to define and isolate various failure modes by the determination of the significant parameters which affect the diaphragm behavior. These parameters could include:

- deck parameters: strength, stiffness, thickness, cell geometry
- support framework
- shear connections
- concrete parameters: strength, stiffness, thickness, type
- specimen configuration: orientation, length, width
- loading program

Phases 1-3 of the research effort have been completed and are reported in References 8, 10, 16 and 30. Information presented in this report summarizes the work completed in Phase 5 of this research project.

1.3. Objective and Scope of this Study

The objective of Phase 5 was to experimentally and analytically investigate the effects of gravity load on composite floor diaphragm behavior. Efforts within Phase 5 included:

- A detailed review of previous diaphragm tests, gravity load tests and methods of analysis.

- Design and construction of a mechanism to apply a distributed vertical load.
- Testing of four full-scale specimens subjected to applied in-plane loading only.
- Testing of six full-scale specimens subjected to applied in-plane and distributed vertical load.
- Presentation of experimental results and evaluation of the test frame and vertical load mechanism.
- Determination of the effects of distributed vertical load on composite diaphragm behavior.
- Evaluation of existing methods of analysis and recommendation of modifications to existing methods and/or determination of new methods of analysis.
- Comparison of analytical and experimental results.

The primary purpose of these tests was to determine the effects of gravity load on composite floor diaphragm behavior. This report will include the procedures used and the results obtained from each of the efforts listed above.

2. REVIEW OF PREVIOUS RESEARCH

2.1. Gravity Load Research

Since 1967, an extensive experimental and theoretical investigation of gravity load effects on composite floor slabs has been conducted at Iowa State University's Engineering Research Institute. This investigation has included over 650 tests on various one-way slab elements, continuous slab elements, push-off specimens, and full-sized floor slabs. Results from this research are reported in References 15-16, 24-29, 31.

Shear-bond was found to be the primary mode of failure for steel deck reinforced concrete slabs subjected to gravity load (28). The shear-bond mode of failure is characterized by the formation of a diagonal crack near the point of applied vertical load or at the third point for uniform load (15) and a subsequent loss of bond between the steel-deck and concrete between the load point and the end. Several equations were developed to predict the gravity load capacity of slabs that experience shear-bond failure (31). The design equation that was finally accepted was based on a modified version of Equation 11-6 in the American Concrete Institute (ACI) Code 318-83 (1).

Results from the tests conducted on the full-scale floor slabs, simply supported on all four sides, indicate that the slabs behave principally as one-way slabs (29). This behavior is caused by the relatively large bending stiffness of the slabs in the direction parallel to the corrugations. Results from these tests also indicate

that when slabs are subjected to large concentrated loads, some two-way action may need to be considered. A procedure for predicting the amount of two-way action was developed by Porter and Ekberg (29).

2.2. Diaphragm Research

Prior to 1973, no general design equations for steel-deck reinforced concrete diaphragms existed. Experimental testing was conducted by various manufacturers to develop empirical design equations. This testing resulted in the development of several similar design equations that varied with manufacturer and deck type.

The first general design equations for steel deck reinforced concrete diaphragms were developed by C.W. Pinkham of S.B. Barnes and Associates of Los Angeles, California and published by the Department of Defense in a design manual, "Seismic Design of Buildings" (12). These empirical equations were based on a "guided cantilever" concept. Accurate ultimate load predictions were obtained from these equations for only a limited number of composite diaphragms. One possible reason for this limited accuracy is that several potential failure modes were not considered in the development of these equations.

An alternate method of analysis was proposed upon completion of the first three phases of this project. This proposed method of analysis was based on a consideration of the possible failure modes listed in Table 1. This list was based on a literature review by I.S.U. researchers (30) of prior work completed by various researchers (4, 5, 7, 8, 12, 15, 17, 18, 24-29, 31). The possible failure modes

Table 1. Failure modes for composite diaphragms

1. Composite Diaphragm
    a. Concrete Strength
        1. Diagonal tension
        2. Parallel to the deck corrugations
    b. Localized Failure
    c. Stability Failure
2. Deck / Concrete Interface
    a. Interfacial Shear Parallel to the Corrugations
    b. Interfacial Shear Perpendicular to the Corrugations
        1. Pop-up
        2. Deck foldover
        3. Concrete rib failure
3. Diaphragm / Edge Member Interface
    a. Arc Spot Welds
        1. Shearing of the weld
        2. Tearing and/or buckling of the deck around the weld
    b. Shear Connectors
        1. Connector shear
        2. Concrete shear failure around the connector

were divided into three categories based on the location of the failure.

Composite diaphragm failures occur when the floor slab system is behaving as a composite diaphragm at ultimate load. An example of this type of failure is diagonal tension failure. Diagonal tension failure is characterized by the concrete reaching its principal tensile stress limit and diagonal cracks forming at approximately 45° angles relative to the fixed edge (Fig. 2). A second type of composite diaphragm failure is characterized by a direct shearing of the concrete along a line parallel to the deck corrugations (Fig. 2). This failure mode will occur if the concrete cover above the top of the deck is thin or the shear strength of the concrete is not adequate. Localized failure is a third possible type of composite diaphragm failure. This failure mode will occur when there is a non-uniform shear distribution in the diaphragm and discrete regions of high stress. A fourth example of composite diaphragm failure is stability. This failure mode is characterized by out-of-plane buckling of the composite diaphragm.

If shear connectors are not used to transfer in-plane load to the concrete, then all of the in-plane load must be transferred to the concrete through the interface by interfacial shear forces. This interfacial load transfer was assumed to occur in a relatively narrow band near the framing members referred to as the "edge zone". If the applied interfacial shear forces exceed the interfacial capacity then interfacial shear failure will occur. Interfacial shear failure parallel to the corrugations is characterized by the concrete moving relative to the deck in a direction parallel to the deck corrugations.

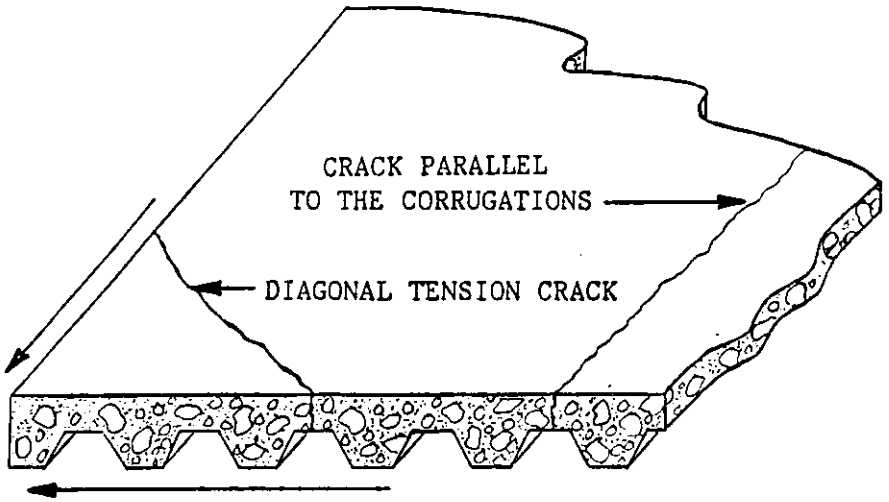

Figure 2. Shear failure of the concrete in diagonal tension and cracks parallel to the corrugations

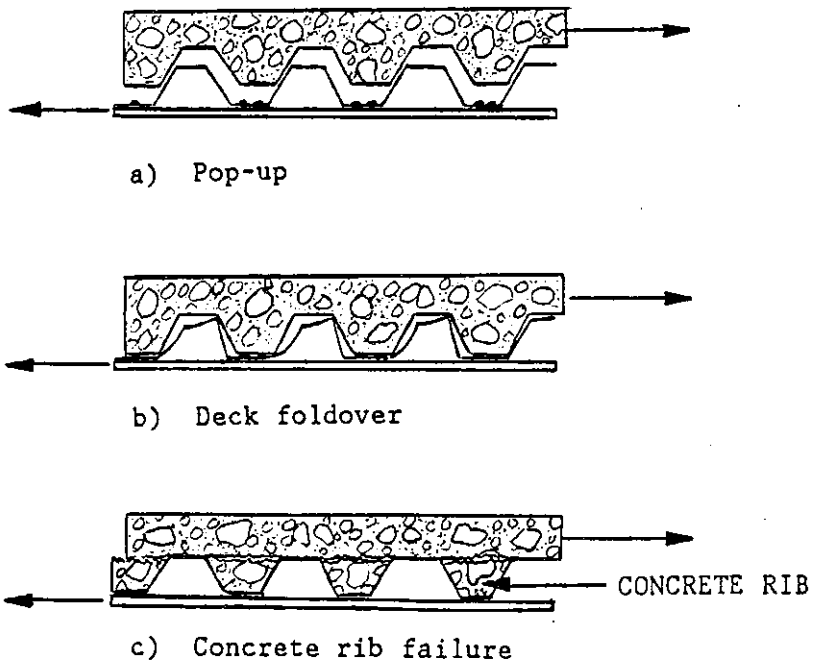

Figure 3. Interfacial failure perpendicular to the corrugations

When interfacial shear failure perpendicular to the corrugations controls, three types of behavior may occur (Fig. 3). If the steel deck corrugations are flexible, the concrete ribs will flatten the deck. This failure was termed deck foldover. If the steel deck corrugations are stiff, the concrete ribs will either slide up on the corrugations or the concrete ribs will be sheared from the rest of the concrete slab. These failure modes were termed pop-up and concrete rib failure, respectively.

Diaphragm to edge member interface failures occur when the load carrying capacity of edge connections is exceeded. Arc spot weld failure is characterized by a direct shearing of the weld or a buckling and/or tearing of the deck near the weld. When stud failure occurs, the stud is either sheared from the support beam or the concrete around the stud fails.

Separate equations were developed to predict ultimate capacities corresponding to each of the failure modes (30). The lowest predicted capacity corresponds to the failure mode that will control. Also, equations to predict the initial stiffness were developed. These were based in part on the "edge zone" concept. The total diaphragm deflection was given by the sum of the bending deflection of the equivalent plate girder, the shear deflection of the web and the deflection in the "edge zone". Stiffness of the "edge zone" was calculated from equations using results from the elemental push-off tests. A complete review of equation development is included in Section 5.1.3.

3. EXPERIMENTAL PROGRAM

To isolate the effects of gravity load on composite diaphragm behavior, similar slabs with and without gravity load were tested. Slabs 6, 9, 10 and 15 were subjected to in-plane load only. Slabs 12, 13, 14, 16, 17 and 18 were subjected to distributed gravity load and in-plane load.

3.1. Composite Floor Slab Specimens

Slabs 1-18 were all nominal 15 ft. X 15 ft. composite steel deck diaphragms. Centerline-to-centerline distance between framing beams was 15 ft. The length of the concrete slab and steel deck was 15 ft. 4 in. and the width was 15 ft. Composite diaphragms were connected to the test frame either by studs measuring a nominal 3/4 in.X 4 1/2 in. after burnoff or by arc spot welds measuring 3/4 in. in diameter using class E-60s-3 or E-70s-3 (Ms-21G) welding wire. Deck panels were connected to each other with 1/8 in. X 1 1/2 in. arc seam welds spaced 30 in. on center using 3/32 in. E7018 electrodes or E-60s-3 (Ms-21G) welding wire. All slabs were constructed using normal weight concrete. The concrete was compacted with an electric vibrator during casting and wet cured for 7-14 days under a plastic cover. A test parameter summary is given in Table 2.

Slabs 6 and 17 were constructed using a 16-gauge, 1 1/2 in. deep, embossed steel deck (Deck Type 2, Fig. 4). An 18-gauge, 1 1/2 in. deep, embossed steel deck was used on Slabs 15 and 16 (Deck Type 7, Fig. 5). Slabs 9 and 13 were constructed using a 16-gauge, 3 in.

Table 2. Summary of parameters for slab specimens

Slab Number	Concrete Parameters: Nom. Thick. (in)	Actual Thick. D (in)	f'c (psi)	Steel Deck Parameters: Deck Type	Deck Thick. (in)	Yield Strength (ksi)	Ultimate Strength (ksi)	Connections per side
1	5.50	5.38	5634	1	0.034	41.7	53.4	30 studs
2	5.50	5.50	5250	1	0.034	41.7	53.4	30 studs
3	5.50	5.65	4068	1	0.034	41.7	53.4	60 welds
4	5.50	5.28	3849	1	0.034	41.7	53.4	60 welds
5	3.50	3.53	2966	2	0.062	48.2	60.7	30 welds
6	7.50	7.44	4549	2	0.062	48.2	60.7	60 welds
7	5.50	5.40	5435	3	0.058	49.7	61.1	60 welds
8	5.50	5.47	3345	1	0.035	41.7	53.4	4-6 studs[a]
9	5.50	5.48	5142	4	0.058	51.8	63.2	60 welds
9 (pan)					0.057	52.4	64.9	
10	5.50	5.53	3311	5	0.062	40.4	53.4	60 welds
11	5.50	5.72	3533	6	0.047	89.7	93.6	60 welds
12	5.50	5.59	3412	5	0.062	40.4	53.4	60 welds
13	5.50	5.53	6187	4	0.058	51.8	63.2	60 welds
13 (pan)					0.057	52.4	64.9	
14	8.00	8.20	3699	5	0.062	40.4	53.4	60 welds
15	4.00	4.21	2844	7	0.047	89.7	93.6	60 welds
16	4.00	4.18	2952	7	0.047	89.7	93.6	60 welds
17	7.50	7.44	4261	2	0.062	46.0	54.4	60 welds
18	5.50	5.55	3052	5	0.062	40.4	53.4	60 welds

[a] 4 studs each E-W side, 6 studs each N-S side.

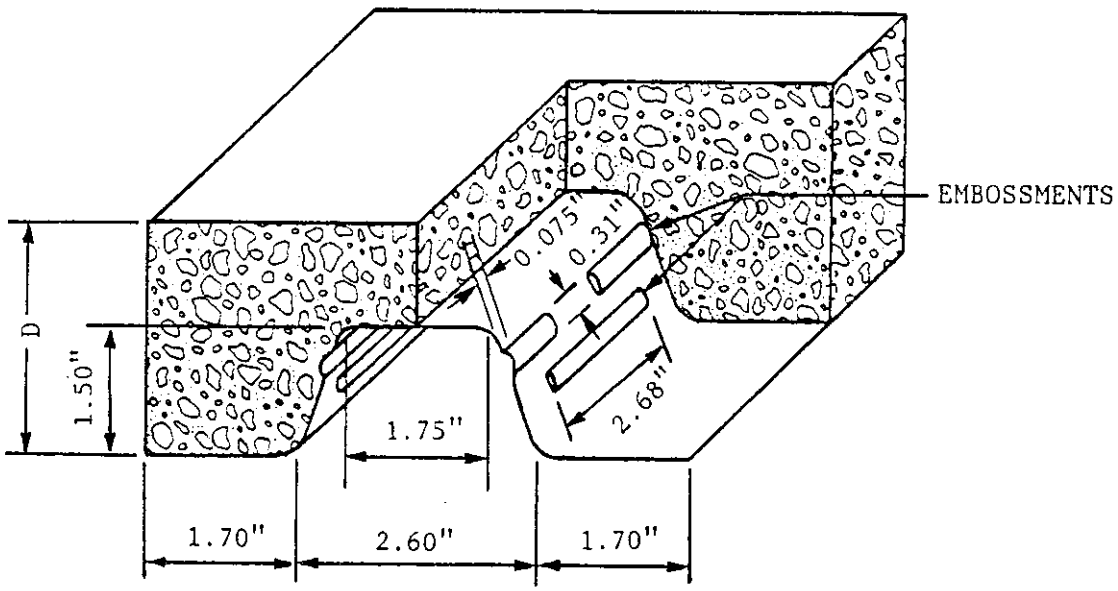

Figure 4. Typical view of Deck Type 2

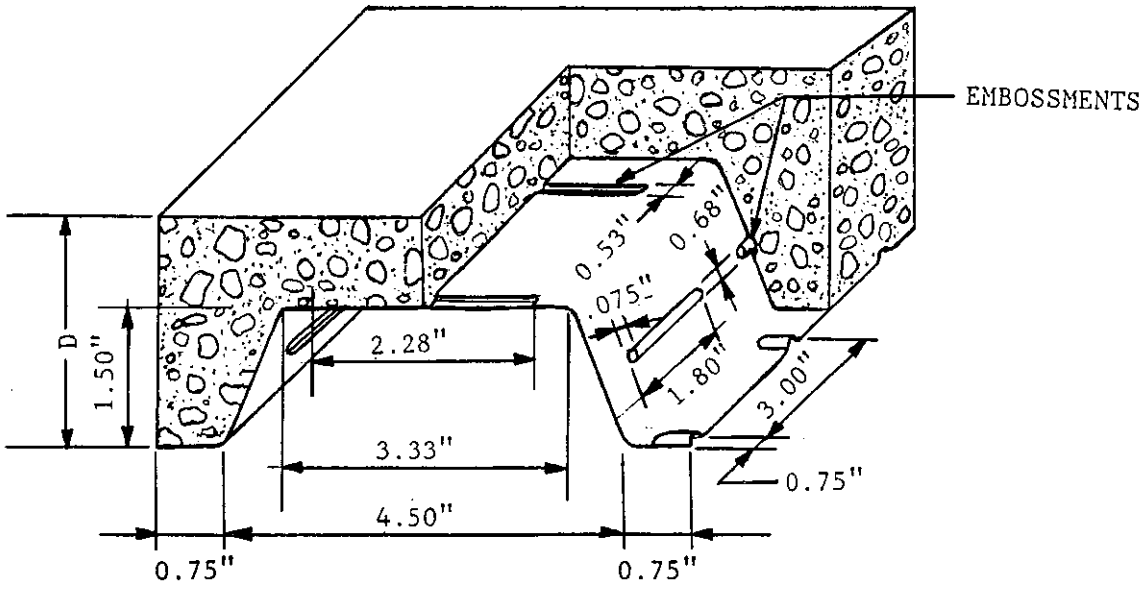

Figure 5. Typical view of Deck Type 7

deep, embossed, cellular deck type (Deck Type 4, Fig. 6). Cellular deck consists of a fluted section spot welded to a flat sheet. A 16-gauge, 3 in. deep, embossed steel deck was used on Slabs 10, 12, 14 and 18 (Deck Type 5, Fig. 7).

Slabs 6, 9 and 10 through 18 were connected to the test frame with 240 arc spot welds. These welds were evenly distributed around the perimeter of the slab (Figs. 8-10). The number of edge connectors used was purposely selected to be adequate to prevent diaphragm to edge member interface failure so that the other failure modes would occur. An extensive study of diaphragm to edge member interface failures and the effects of gravity load on diaphragm to edge member interface failures will need to be included in future research.

3.2. Test Frame

A cantilever diaphragm test frame with a fixed edge was used. The fixed edge models a continuously attached shear wall. Also, in most buildings using composite floor systems, an adjacent slab that provides restraint against rotation exists on at least one side. The free edge models an unbraced frame that provides little restraint against lateral loads. Thus, the lateral loads must be transferred by the diaphragm into the shear wall. Stiff edge beams were used because they provide a more uniform shear stress distribution than do flexible support beams.

The test frame consisted of three large reinforced concrete blocks, three perimeter framing beams and two hydraulic cylinders with support

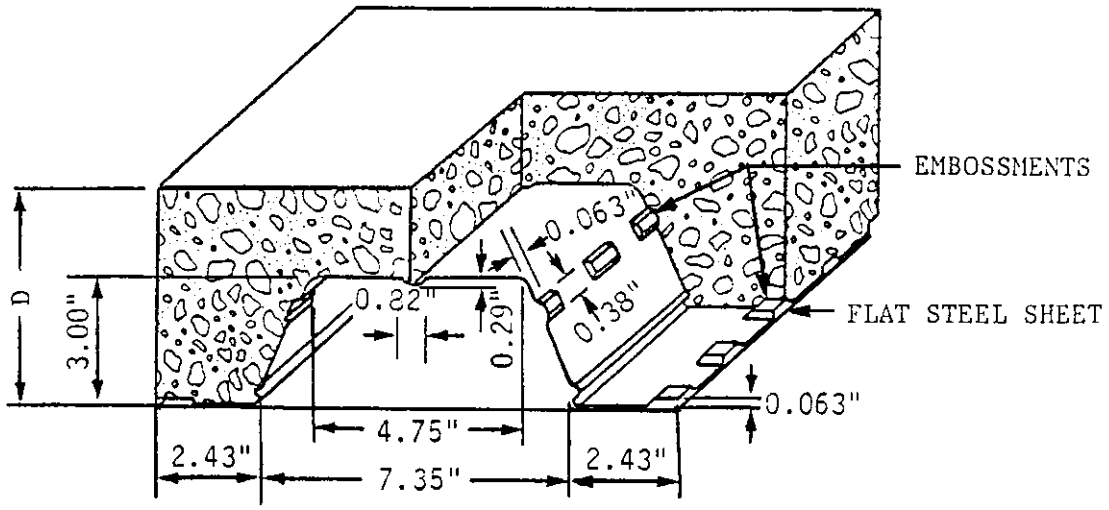

Figure 6. Typical view of Deck Type 4

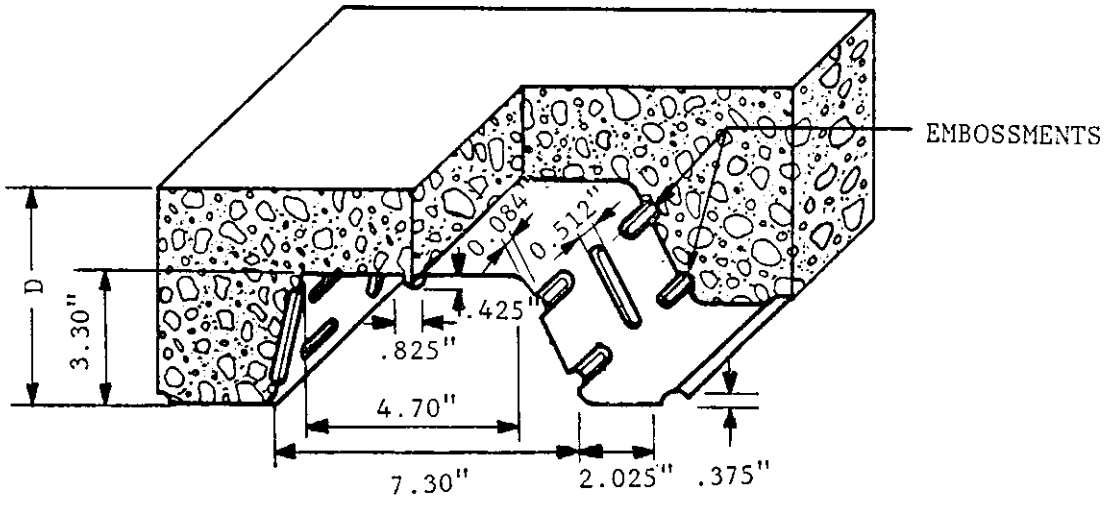

Figure 7. Typical view of Deck Type 5

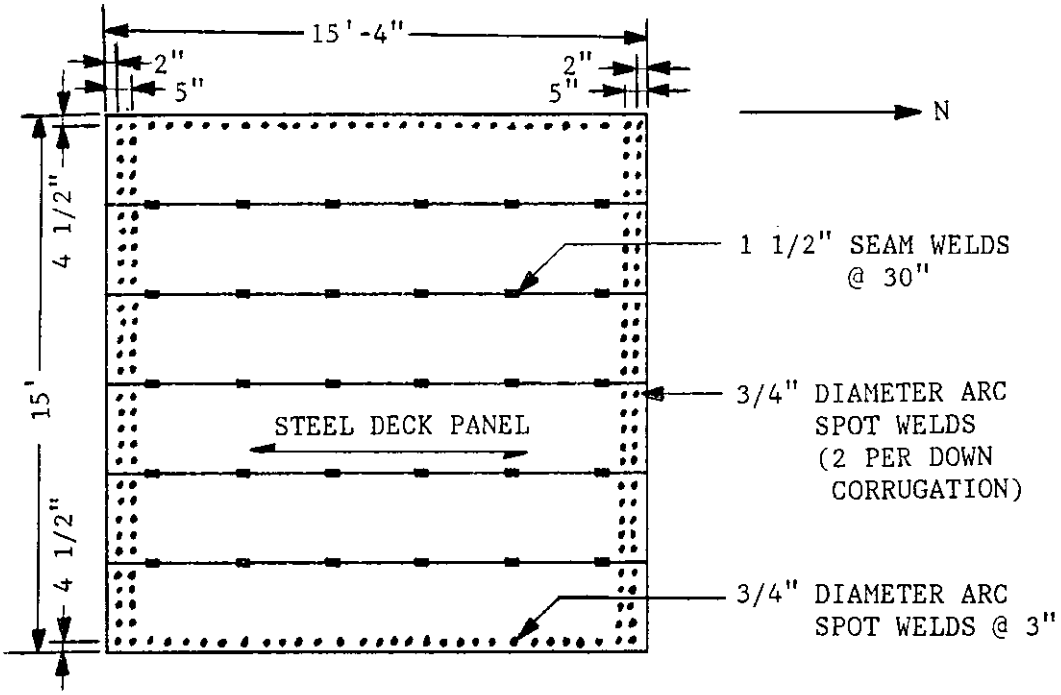

Figure 8. Plan view of edge connector layout for Slabs 6 and 17

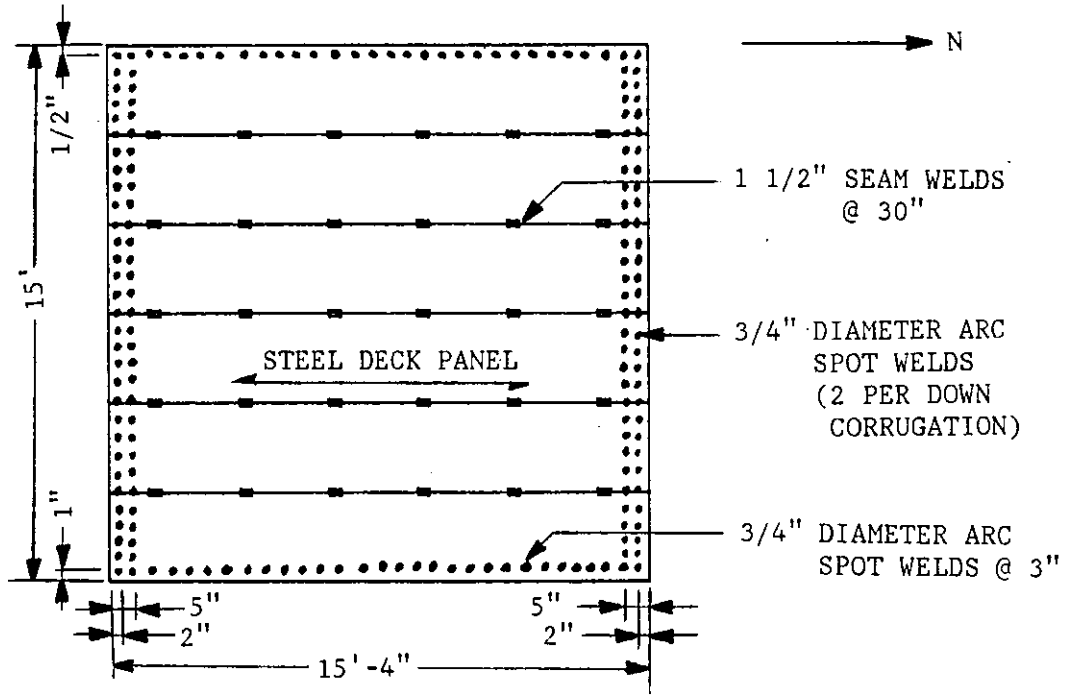

Figure 9. Plan view of edge connector layout for Slabs 15 and 16

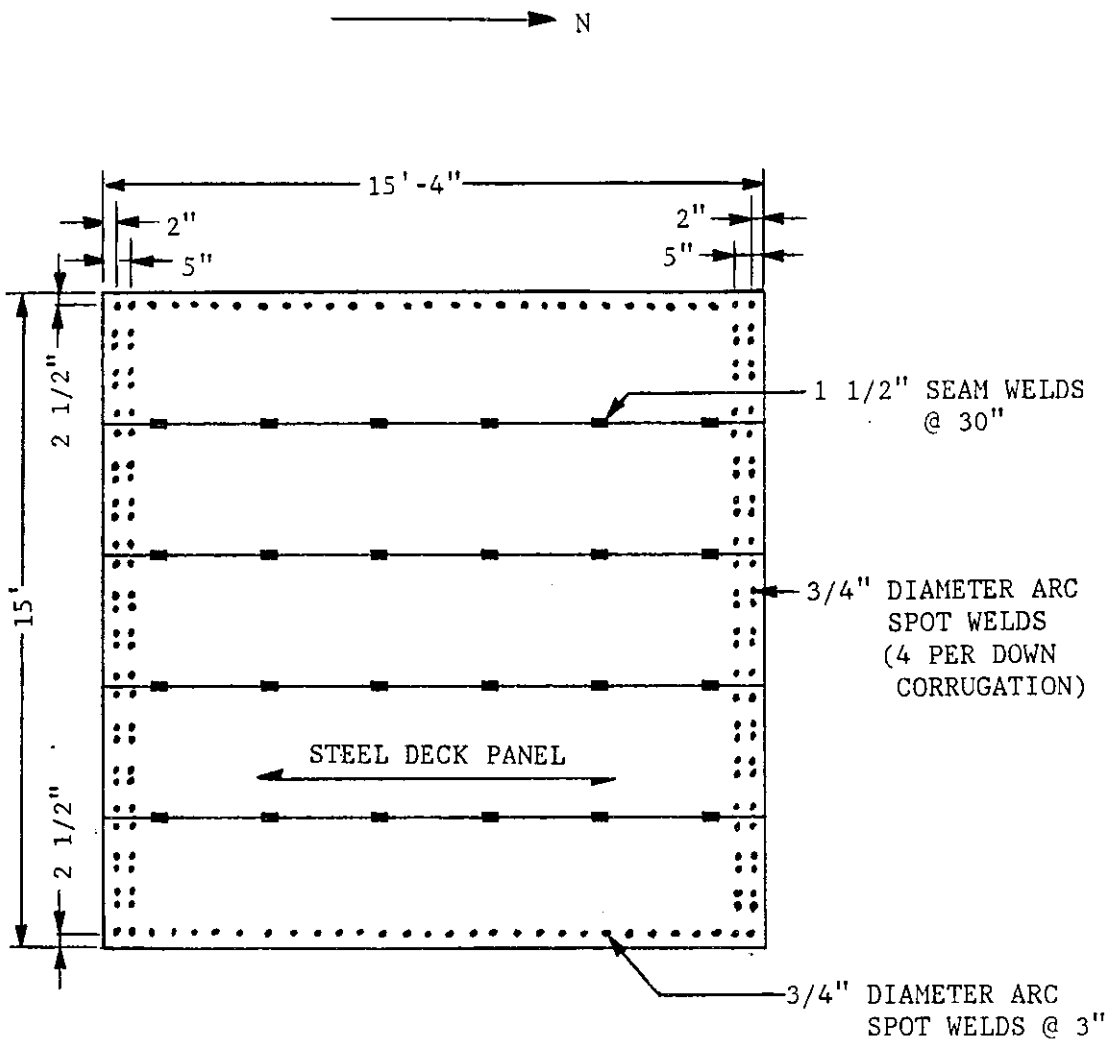

Figure 10. Plan view of edge connector layout for Slabs 9, 10, 12, 13, 14 and 18

frames. The test frame had a maximum displacement limit of ±6 inches and a maximum working load of ±400 KIPs. A layout of the test frame is shown in Figure 11.

An MTS closed-loop control system with a servo-valve was used to control the frame displacements during the test. The set point on the MTS servo-controller was manually operated to control the test frame displacements. The displacement signal was received from a direct current linear variable displacement transducer (DCDT) that was connected between the north edge of the test frame and the structural tie-down floor and oriented in a direction parallel to the north edge beam. This displacement signal was also continuously monitored by the data acquisition system. A schematic of the servo-hydraulic testing system is shown in Figure 12.

3.3. Vertical Load Mechanism

Vertical load was applied to 20 distributed neoprene pads on the surface of the specimens with the mechanisms shown in Figure 13. Each pad was subjected to the same load. The amount of vertical load applied was chosen to model an equivalent distributed load based on equivalent shear area in the one-way direction (parallel to the corrugations).

Each vertical load mechanism consisted of a hydraulic cylinder with a hollow piston, 1/2 in. diameter wire rope, 1/2 in. diameter threaded steel rod, 3 in. X 3 in. structural tubes used as spreader beams, steel plates and various connections. Wire rope was used so

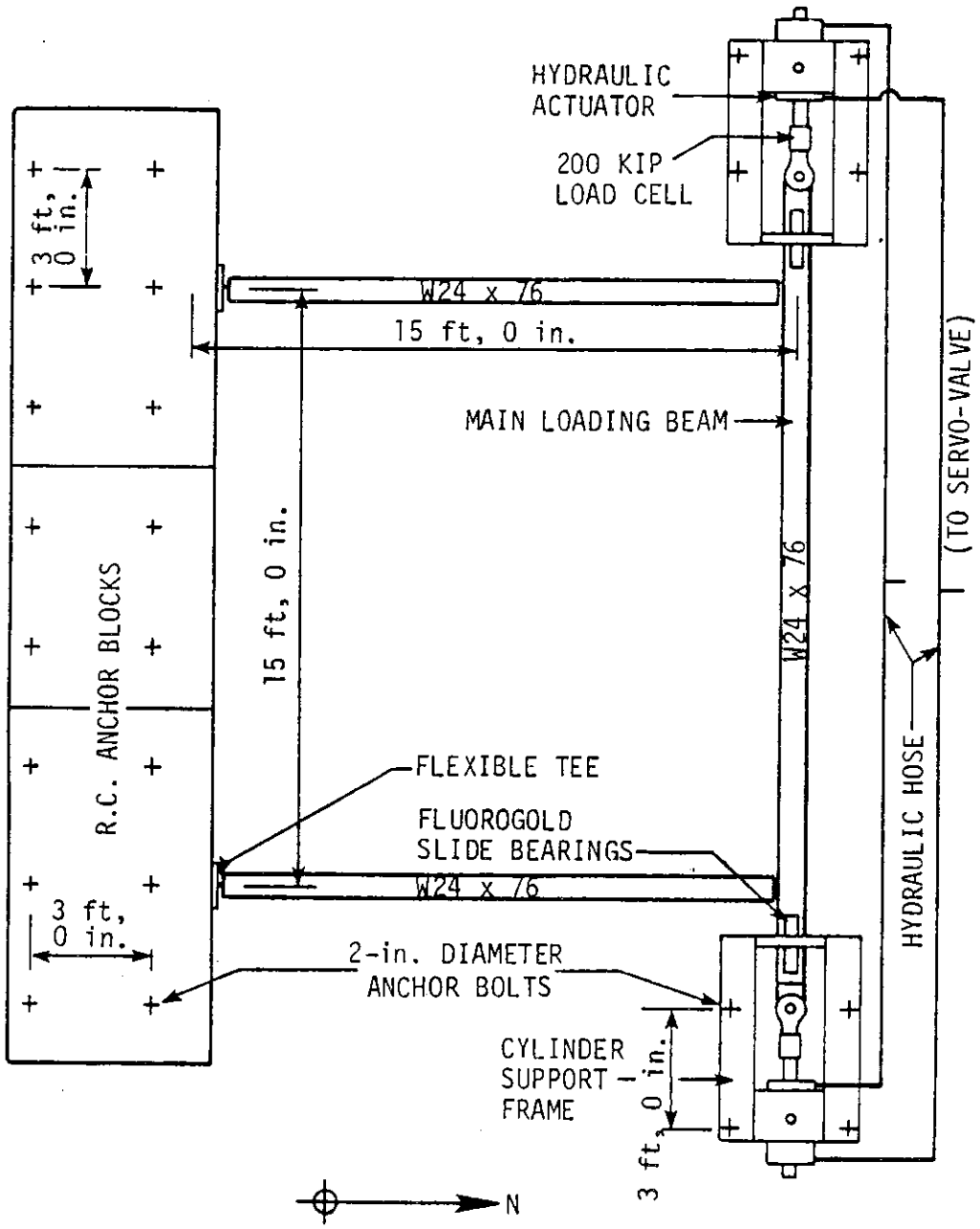

Figure 11. Diaphragm test frame schematic (8)

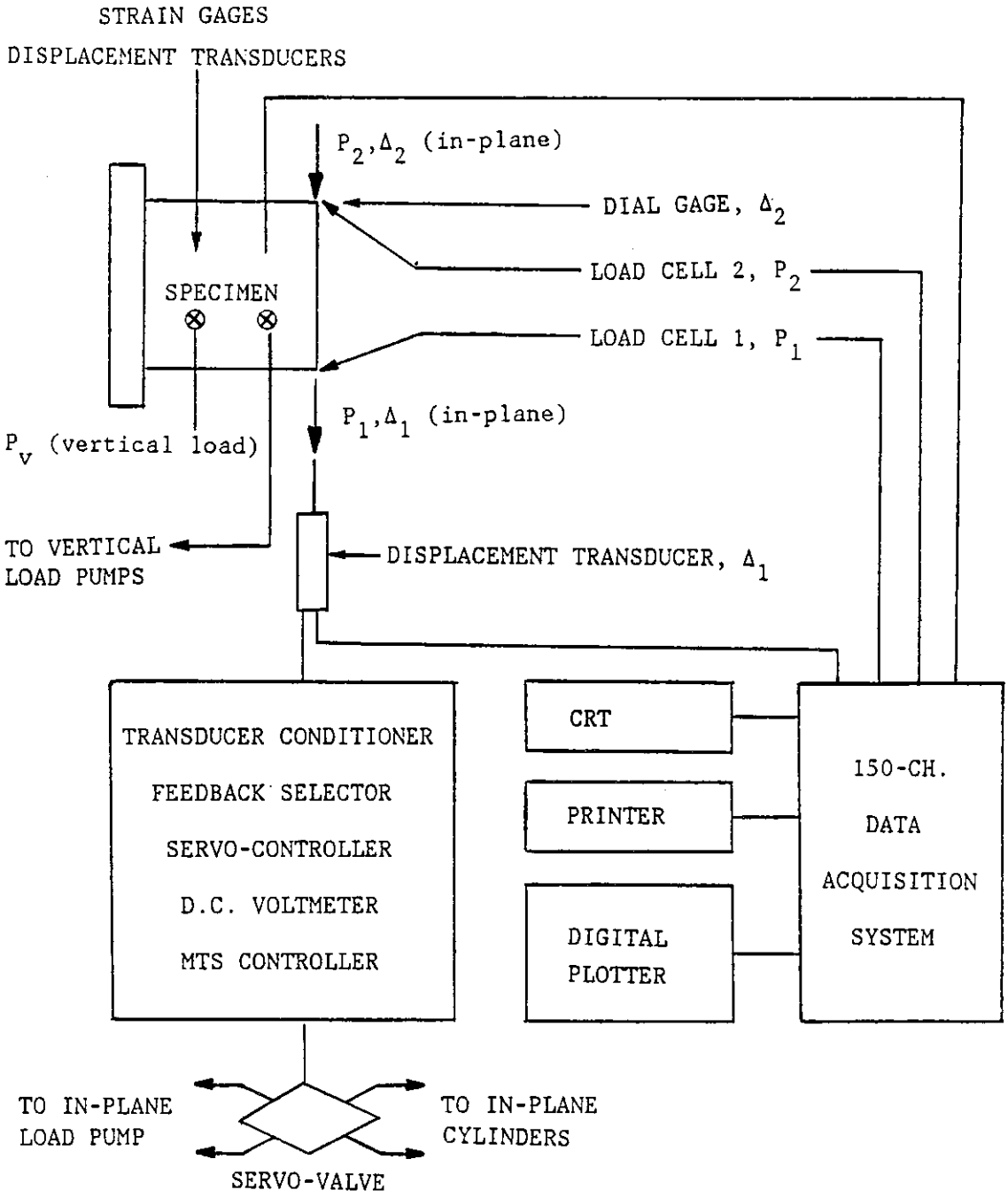

Figure 12. Schematic of servo-hydraulic testing system

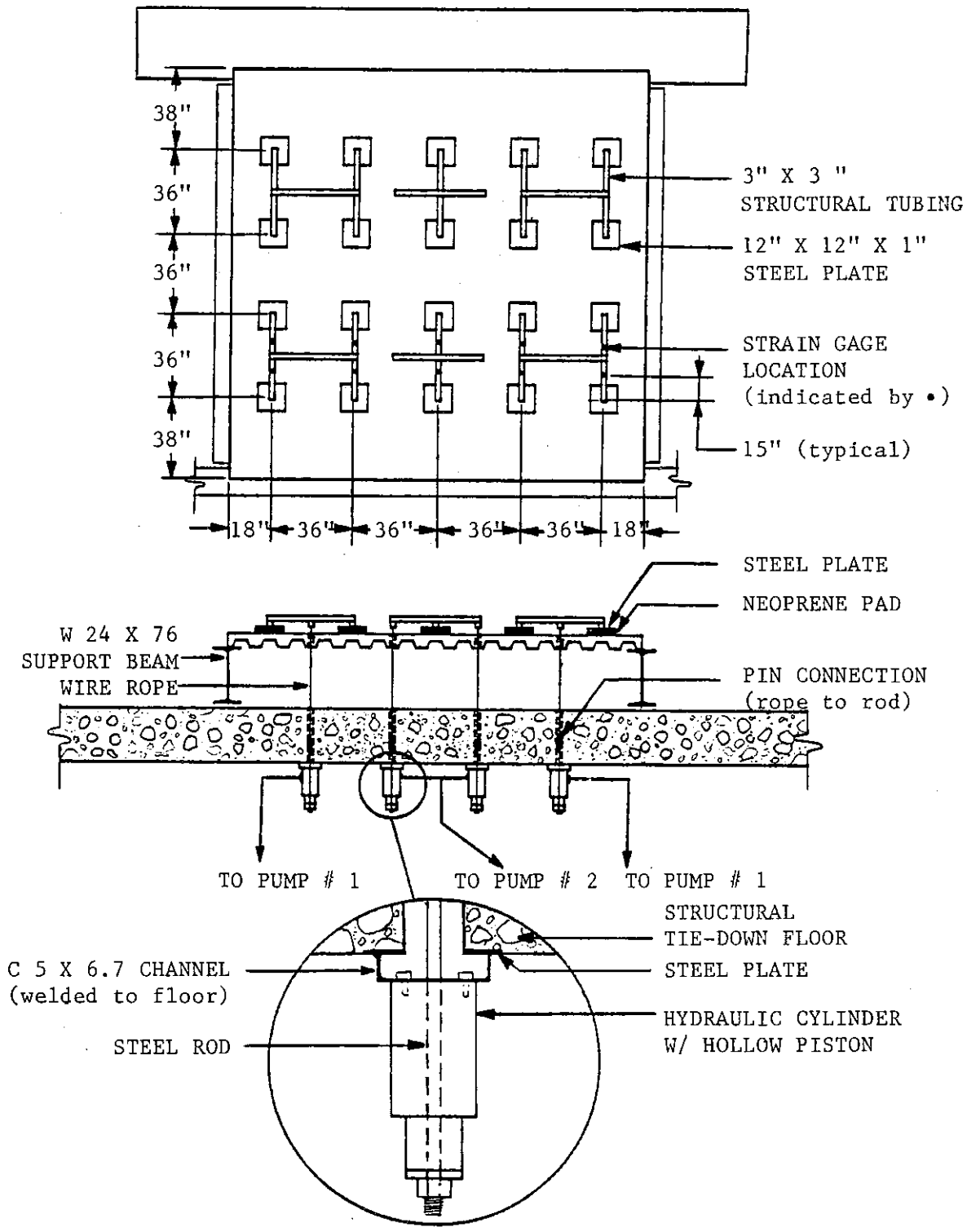

Figure 13. Vertical load mechanism schematic

that, as the diaphragm was cycled in-plane, the vertical load mechanism would apply little lateral restraint. Four mechanisms were used to apply load to four surface pads each and two mechanisms were used to apply load to two surface pads each (Fig. 13). The hydraulic cylinders that were used in mechanisms applying load to the same number of pads were connected with parallel hydraulic hoses to the same pump. Two separate pumps were used to apply the vertical load so that the amount of load being applied to each pad was the same. The vertical mechanisms had a design capacity of 200 psf and the hydraulic cylinders had a maximum capacity of 60 kips.

The amount of load being applied was manually controlled by adjusting the amount of hydraulic pressure being applied by the pumps. Strain gages were mounted on the bottom side of the spreader beams to measure the amount of load being applied (Fig. 13). These strain gages were monitored by the data acquisition system and readings obtained were displayed at every load point.

3.4. Data Acquisition System and Test Instrumentation

The data acquistion system (DAS) used on Slabs 10-18 consisted of a 150 channel Hewlett Packard (HP) model 3497A data acquisition control unit interfaced to an HP model 85 micro-computer which was interfaced to two disk drives, a digital plotter and a printer. This DAS recorded all strain gage, DCDT and load cell readings on magnetic disks at every load point. Also, between load points as the diaphragm was being dis-

placed in-plane, this DAS continuously monitored the in-plane load cells and the in-plane displacement DCDT and plotted load versus displacement with the digital plotter. An illustration of the load versus displacement results are indicated in a plot generated for Slab 12 as shown in Figure 14. Readings between load points were taken at the rate of one reading per second and approximately 30 readings were taken between any two load points depending on the rate of loading.

In-plane loads were measured by axial load cells that were connected in series with each of the hydraulic cylinder rods. Vertical loads were measured with strain gages that were placed on the bottom of the spreader beams that were distributing the load. The axial load cells and spreader beams were calibrated in a Satec test machine. Since hydraulic systems were used to apply both the in-plane and vertical loads, hydraulic pressure readings were taken and used to provide a check on the amount of load being applied.

In-plane and vertical displacements were measured with DCDTs and mechanical dial gages. A DCDT located near the northeast corner of the slab was used to provide the in-plane displacement feedback to the MTS servo-controller on all tests. Mechanical dial gages and DCDTs were also used to measure concrete movement relative to the steel deck, interfacial slip, along the edges of the diaphragm.

Uniaxial and three-gage rosette strain gages were used to measure strains at various locations (Fig. 15) on the diaphragm specimens. On Slab 10, embedment strain gages were used to measure strains in the concrete. These gages were oriented parallel to the deck corrugations.

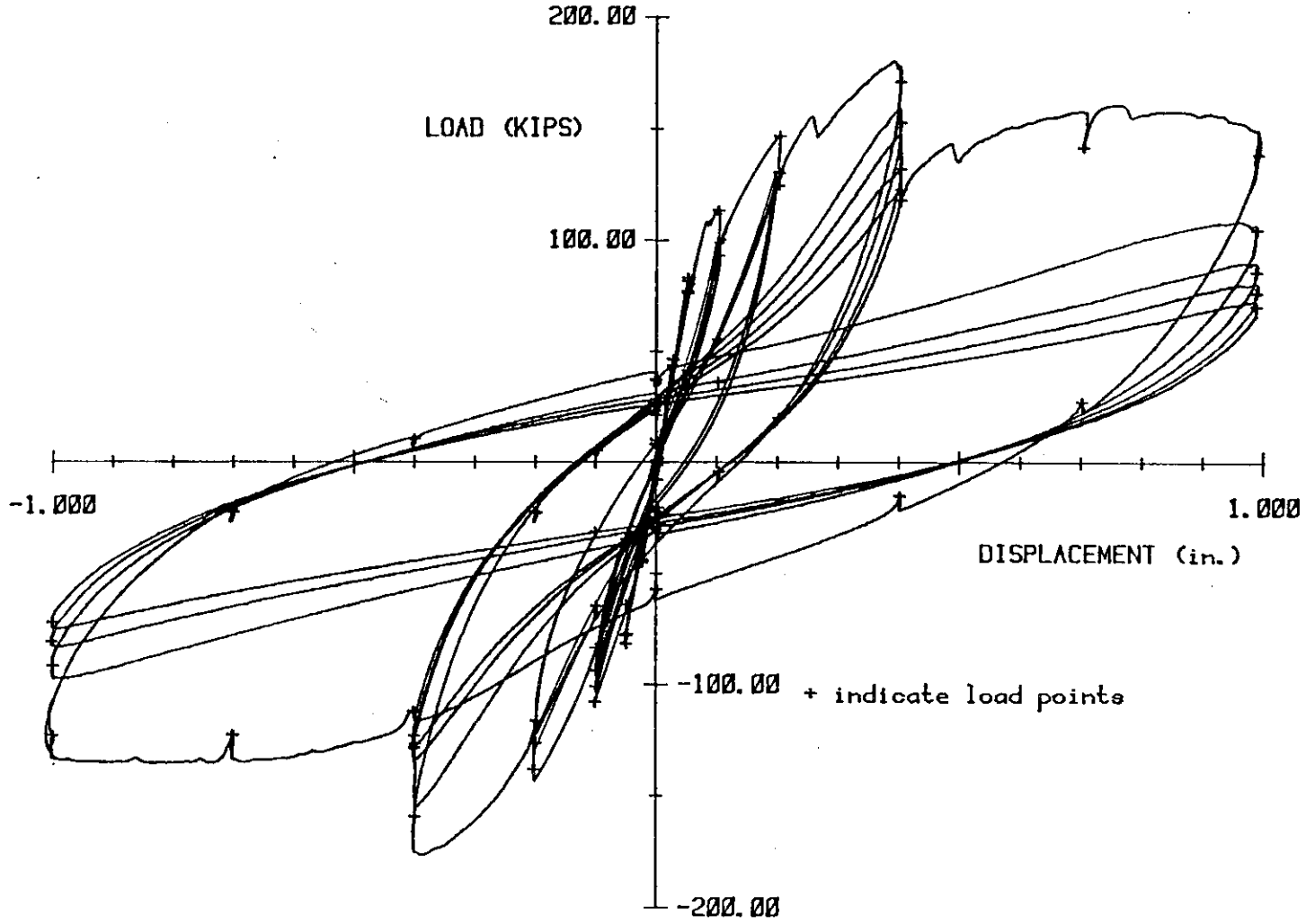

Figure 14. Load-displacement plot generated while testing Slab 12

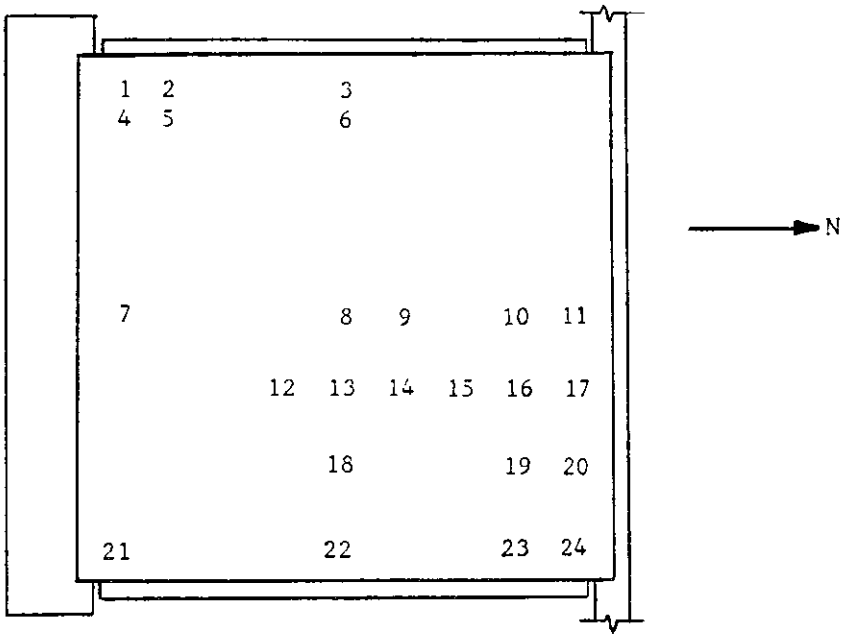

SLAB NUMBER	LOCATION 1	2	3	4	5	6	7	8	9	10	11	12	13	14	15	16	17	18	19	20	21	22	23	24
6	U'	-	-	-	-	-	U	R	-	-	U'	-	-	-	-	-	-	-	-	-	U	U	-	U
9	R	-	-	-	-	-	-	R	-	-	R	-	-	-	-	-	-	-	R'	-	-	R	-	R
10	R	U	R	U	U	U	-	R"	U	U	R"	-	U	-	-	-	U	U	U	U	-	R	U	R"
12	R	U	U	-	U	-	-	R	-	-	U	U	U	U	U	U	U	-	-	-	-	-	-	R
13	-	-	-	-	-	-	-	R	-	-	U	U	U	U	U	U	U	-	-	-	-	U'	-	R
14	-	-	-	-	-	-	-	R	-	-	-	-	U	-	U	-	U	-	-	-	-	-	-	R
15	-	-	-	-	-	-	-	R	-	-	-	-	U	-	U	-	U	-	-	-	-	-	-	R
16	-	-	-	-	-	-	-	R	-	-	-	-	U	-	U	-	U	-	-	-	-	-	-	R
17	R	-	-	-	-	-	U	R	-	-	U	-	-	-	-	-	-	-	-	-	R	U	U	R
18	-	-	-	-	-	-	-	R	-	-	-	-	U	-	U	-	U	-	-	-	-	-	-	R

R = ROSSETTE ON CONCRETE SURFACE AND BOTTOM OF STEEL DECK
U = UNIAXIAL GAGE ON CONCRETE SURFACE AND BOTTOM OF STEEL DECK
R'= ROSSETTE ON BOTTOM OF STEEL DECK ONLY
U'= UNIAXIAL GAGE ON BOTTOM OF STEEL DECK ONLY
R"= ROSSETTE ON CONCRETE SURFACE, BOTTOM OF STEEL DECK AND UNIAXIAL EMBEDMENT GAGE IN THE CONCRETE SLAB

Figure 15. Deck and slab strain gage layout and diagram

Uniaxial strain gages, attached to the webs of the W24 X 76 edge beams (Fig. 16), were used to measure strains along the edge beams.

During the test, cracks were marked and numbered with black markers. Pictures were taken with a camera mounted above the slab to record surface crack propagation. Pictures were also taken at various locations near the specimen. When available, a video camera was used to visually record slab behavior during the test. A tape recorder was used to verbally record observations made by researchers.

3.5. Load Program

A load program was established based on the expected design vertical load and in-plane displacement. A load point was assigned to each program increment where instrumentation readings were taken. This program was based on in-plane displacement control and at each load point the displacement was held constant.

The amount of vertical load applied was based on the design gravity load. The design gravity load was calculated by using the criteria given in Reference 28, and the m and k values listed in Table 3. These m and k values were derived from elemental one-way tests as described in Reference 28. Slabs 12, 13, 14, 16 and 17 were subjected to a distributed vertical load approximately equal in magnitude to their design gravity loads. Slab 18 was subjected to a distributed vertical load equal in magnitude to approximately twice its design gravity load.

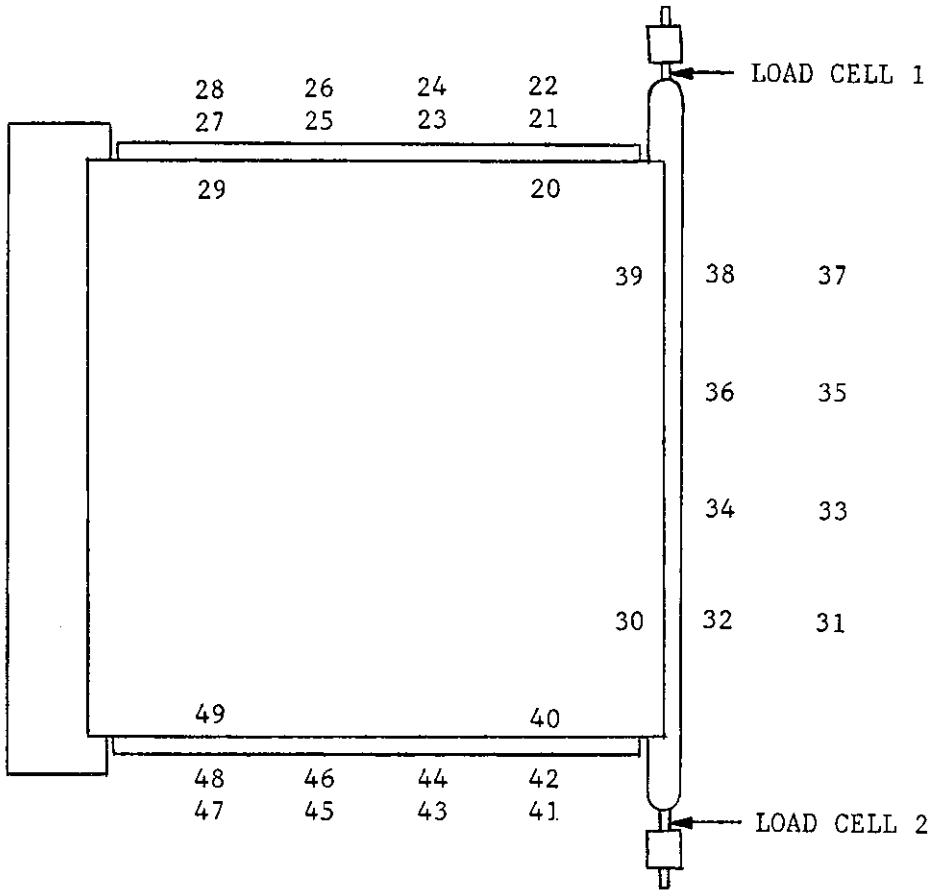

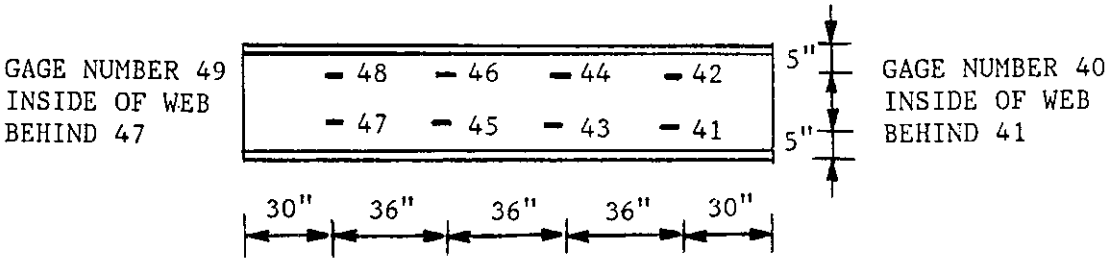

ELEVATION VIEW OF W24 X 76 EDGE BEAM (TYPICAL)

Figure 16. Edge beam strain gage locations

Prior to any in-plane loading, the specimen was incrementally subjected to the established vertical load for the given specimen (Table 3). With the applied vertical load being held constant, the slab was subjected to in-plane loads with progressively increasing displacement limits (Fig. 17). The initial cyclic limit was selected to be a displacement in the working load range of the slab. This limit was approximately doubled until a 1.000 in. displacement was reached. At every displacement limit, a minimum of three reversed displacement cycles were completed. If the load did not reach 95 percent of the previous cycles load after three cycles, additional cycles were completed at this displacement limit until this criterion was met. Four extra cycles were the most ever required.

Table 3. Design and applied vertical loads

Slab Number	Deck Type	m	k	A_s (in^2/ft)	Y_{sb} (in)	Design Load (psf)	Applied Load (psf)
12	5	7126	0.349	1.023	1.531	72	65
13	4	11857	0.375	1.675	0.843	204	200
14	5	7126	0.349	1.023	1.531	118	135
16	7	10838	0.089	0.755	0.943	40	35
17	2	11592	0.013	1.046	0.61	96	100
18	5	7126	0.349	1.023	1.531	72	135

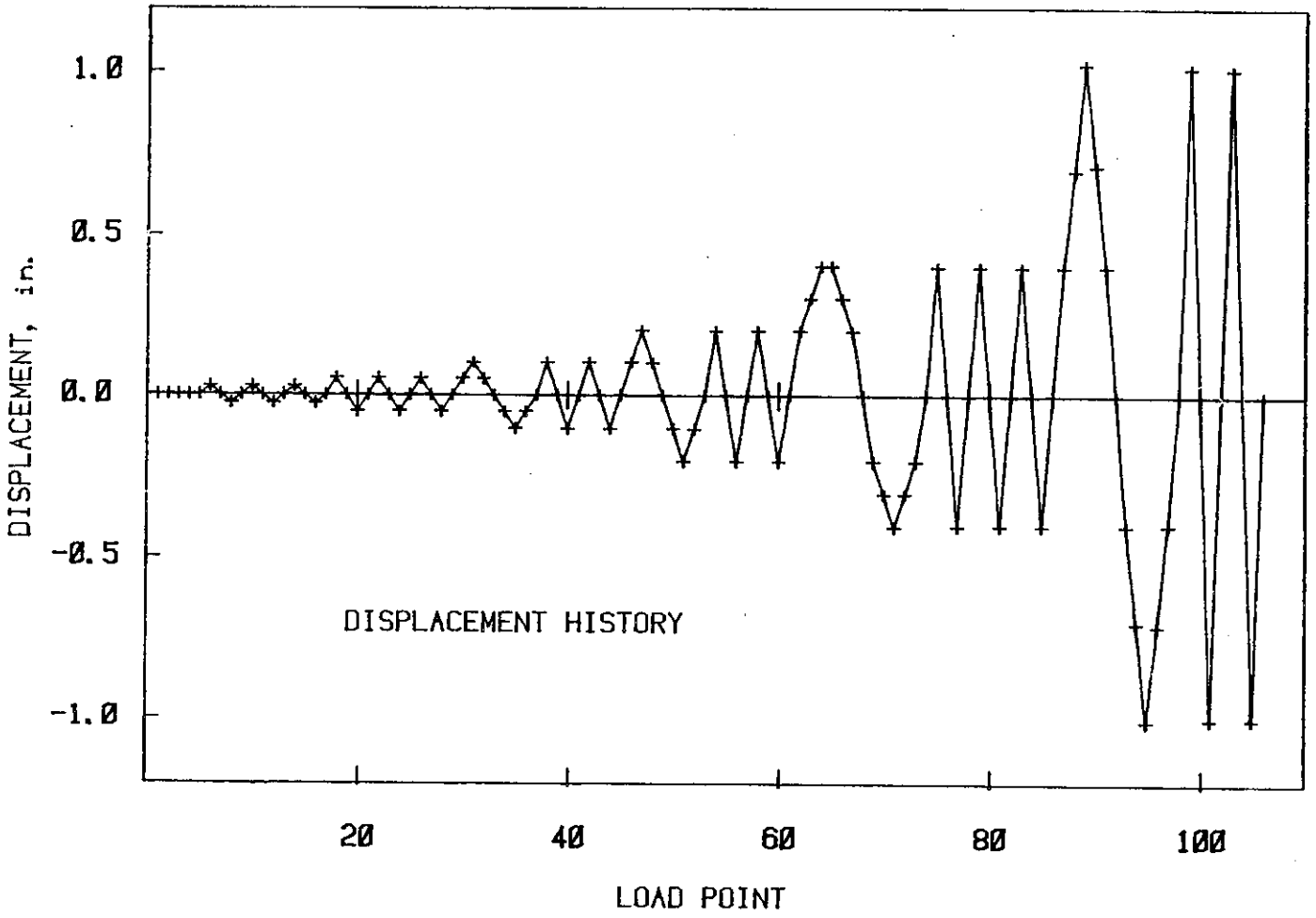

Figure 17. Typical in-plane displacement history

4. EXPERIMENTAL RESULTS

4.1. Slab Description and Behavior

This section includes a brief description of all slabs that were included in this study and a detailed description of slab behavior during the tests. Throughout this section, concrete movement relative to the steel deck will be referred to as slip. Slip in a direction parallel to the corrugations will be referred to as parallel slip. Slip in a direction perpendicular to the corrugations will be referred to as transverse slip.

4.1.1. Deck Type 2

Slabs 6 and 17 were constructed using a 16-gauge, 1 1/2 in. deep, embossed steel deck (Deck Type 2, Fig. 4). The steel deck was oriented so that the smaller width corrugations were up. This orientation made the steel deck stiff in the transverse direction and prevented deck foldover. Both slabs had a nominal concrete thickness of 7 1/2 in. This large thickness was used to prevent diagonal tension failure.

4.1.1.1. Slab 6 Slab 6 was tested as part of a previous research effort. Experimental results from this slab are reported by Porter and Greimann (30). The load program for Slab 6 consisted of reversed cyclic, in-plane loading with displacement limits of 0.025, 0.050, 0.100, 0.200, 0.400 and 1.000 in. A summary of experimental results for Slab 6 is included next to provide a basis for comparison with Slab 17.

Initial signs of distress were observed when the frame was displaced 0.025 in. to the east. Parallel slip of 0.002 in. and transverse

slip of 0.003 in. occurred near the corners of the diaphragm while cycling at this displacement limit. The magnitude of parallel and transverse slip increased as displacement limits were increased. The parallel slip magnitude increased at a faster rate than the tranverse slip magnitude.

A maximum load of 147 kips (Fig. 18) was reached while moving to a displacement of 0.100 in. The mode of failure at ultimate for this slab was interfacial shear parallel to the corrugations. The steel deck slipped relative to the concrete primarily in a direction parallel to the corrugations at ultimate. While cycling at a displacement limit of 0.100 in., the stiffness of the diaphragm slowly degraded.

When the frame was displaced 0.400 in. east, the steel deck moved relative to the concrete as shown in Figure 19. Slip both parallel and transverse to the corrugations occurred but the largest amount occurred parallel to the corrugations. Movement between the frame and steel deck was also measured. This movement was less than or equal to 0.002 in. at all measurement locations. While cycling at a displacement limit of 1.000 in., the concrete continued to slip relative to the deck. No cracks formed on the surface of the slab throughout the entire test.

4.1.1.2. Slab 17 Slab 17 was tested as part of this research effort. The purpose of Slab 17 was to study the behavioral changes caused by applying a distributed vertical load of 100 psf in addition and prior to in-plane load. The load program for this slab included the following steps. Vertical load was applied in increments of

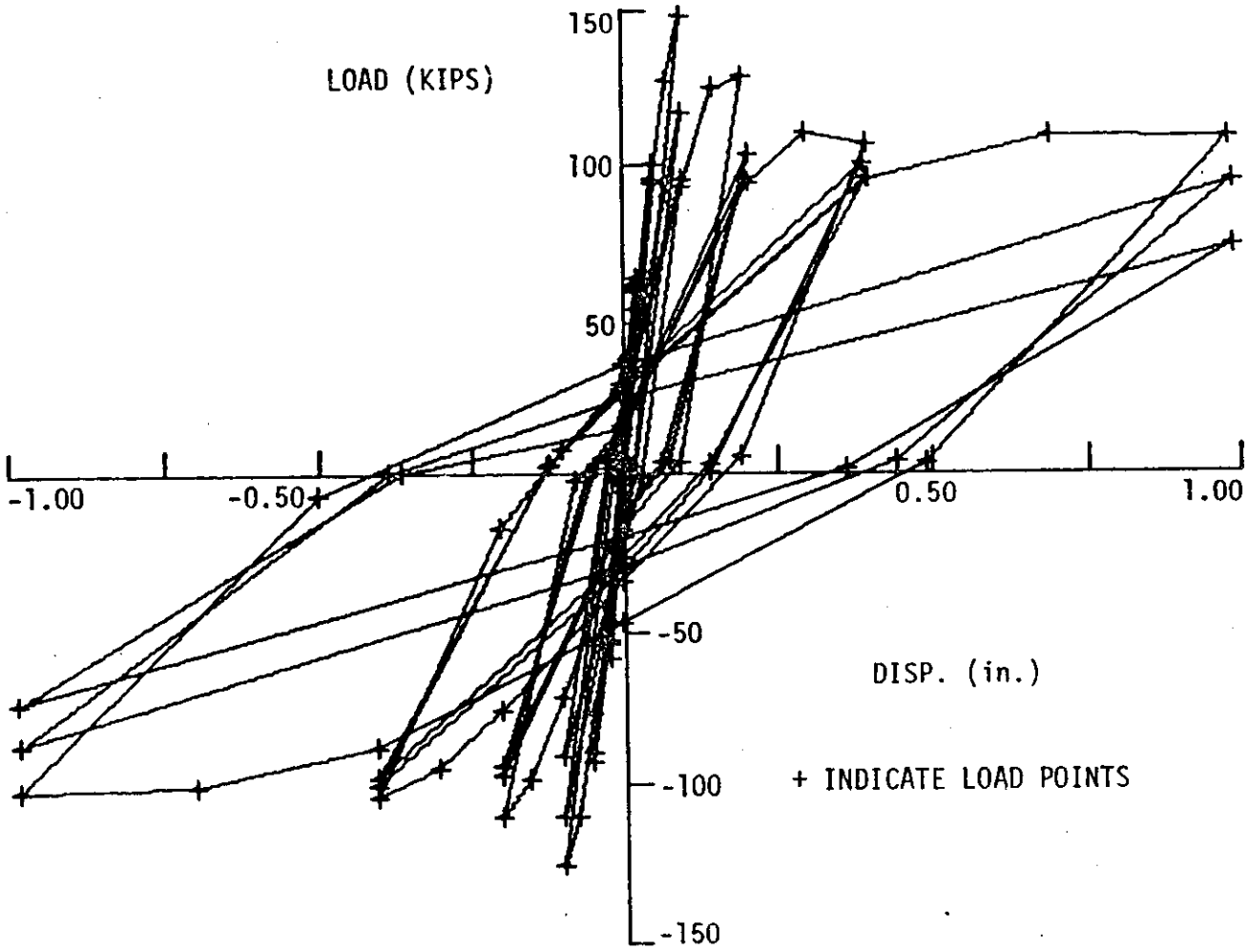

Figure 18. Load-displacement diagram for Slab 6 (30)

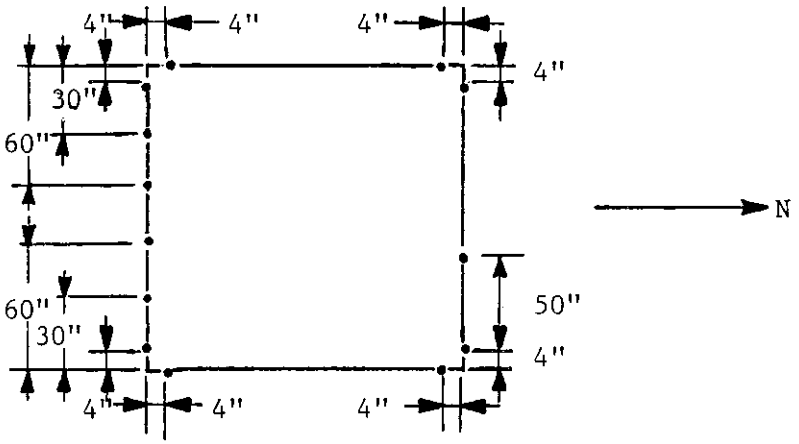

• indicates measurement location
for slip diagram shown below

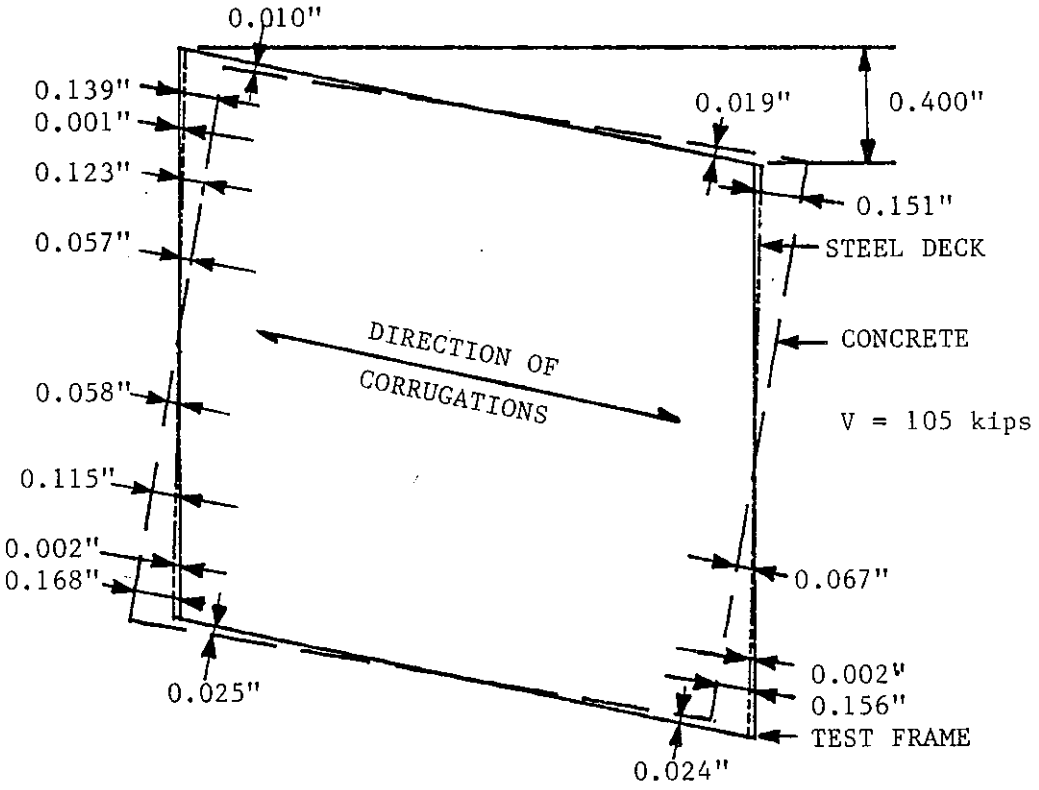

Figure 19. Interfacial slip diagram for Slab 6

20 psf until a total applied load of 100 psf was reached. With the vertical load held constant, this slab was subjected to the same reversed cyclic, in-plane load program as Slab 6.

When the slab was subjected to a distributed vertical load of 100 psf, the center of the diaphragm displaced 0.034 in. down. No slip greater than or equal to 0.001 in. had occurred. Parallel slip of 0.003 in. and transverse slip of 0.003 in. occurred while cycling at a displacement limit of 0.025 in. The amount of slip both parallel and transverse to the corrugations increased as in-plane displacement limits were increased. The parallel slip magnitude increased at a faster rate than the transverse slip magnitude.

A maximum load of 146 kips (Fig. 20) was reached while moving to a displacement limit of 0.400 in. At this point, the steel deck moved relative to the concrete as shown in Figure 21. Slip both parallel and transverse to the corrugations occurred. The magnitude of parallel slip was much larger than the magnitude of transverse slip. Movement between the steel deck and frame was also measured. This movement was less than 0.004 in. The mode of failure at ultimate was interfacial shear parallel to the corrugations. No surface cracks formed while cycling at a displacement limit of 0.400 in. As cycling continued, the stiffness of the diaphragm slowly degraded.

While moving to a displacement limit of 1.000 in., diagonal surface cracks appeared. The stiffness of the diaphragm was significantly reduced when these diagonal cracks formed (Fig. 20). A vertical displacement of 1.277 in. was measured at the center of the diaphragm

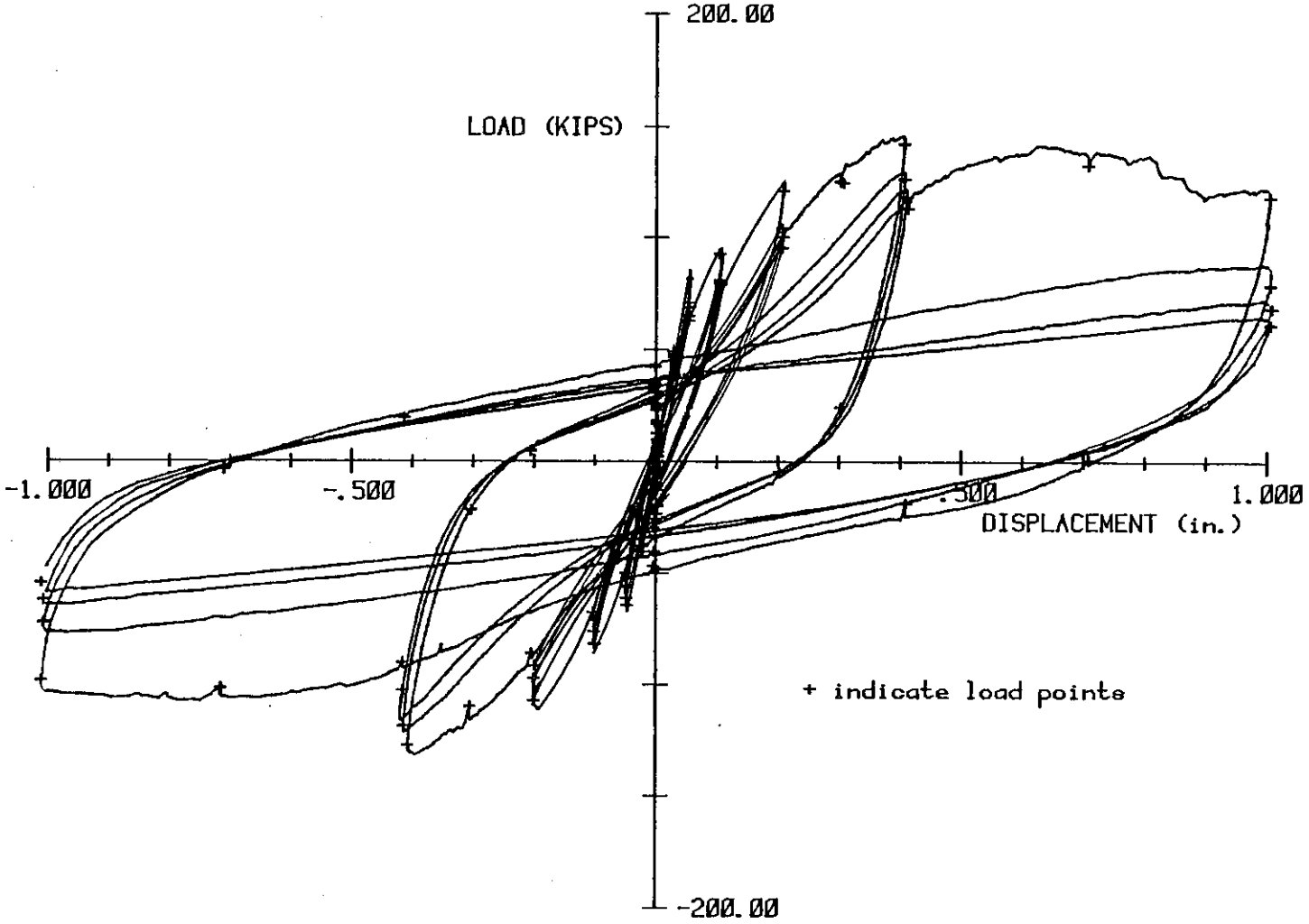

Figure 20. Load-displacement diagram for Slab 17

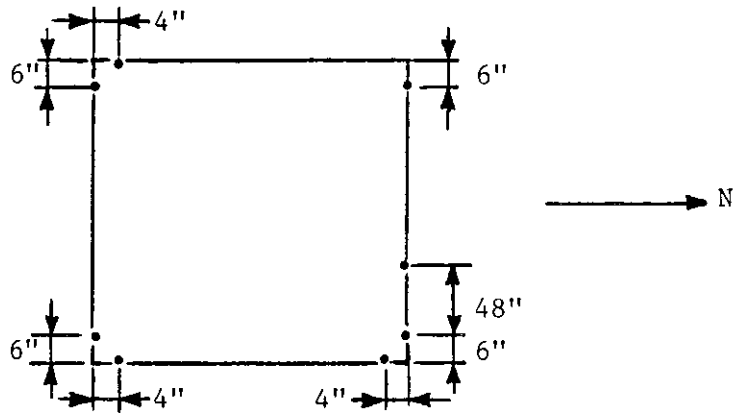

• indicates measurement location
for slip diagram shown below

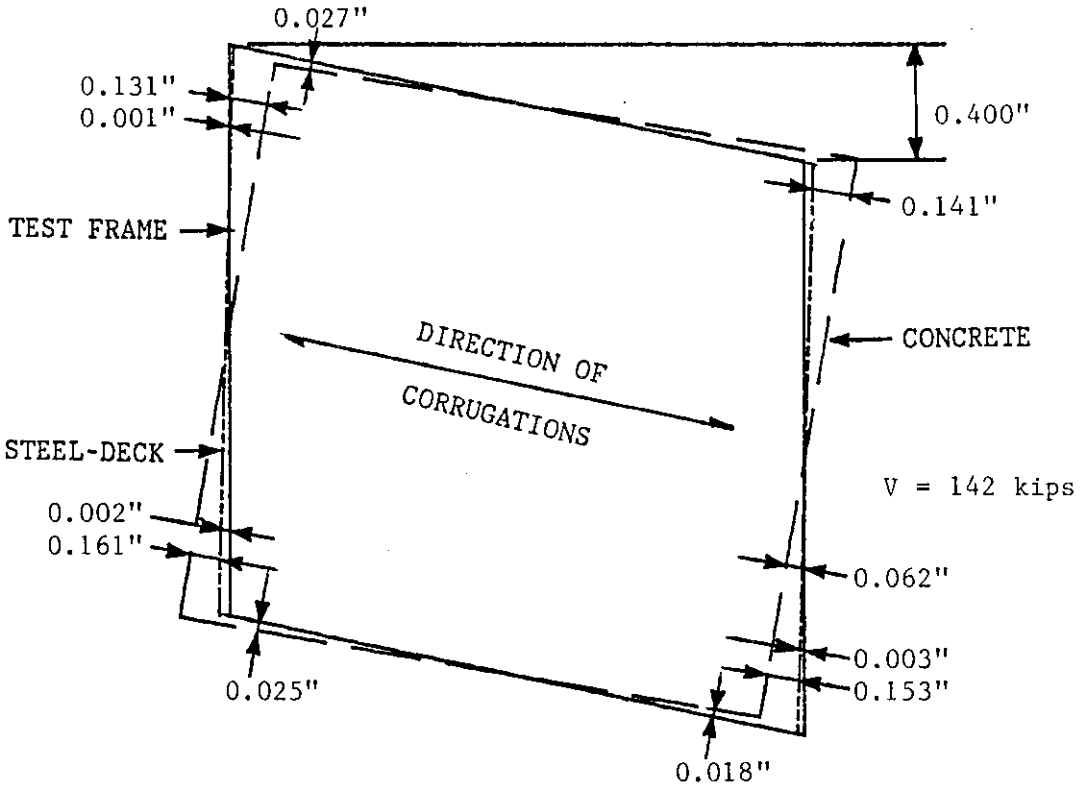

Figure 21. Interfacial slip diagram for Slab 17

after these diagonal cracks formed. After three complete reversed cycles at a displacement limit of 1.000 in were completed, the diaphragm was still able to carry the applied vertical load of 100 psf.

4.1.1.3. Comparison of Slab 17 with Slab 6 The behavior of Slabs 6 and 17 was very similar. Both slabs failed in interfacial shear parallel to the corrugations and had nearly the same ultimate in-plane capacity. Slab 6 reached an ultimate load of 147 kips while moving to a displacement limit of 0.100 in. Slab 17 reached an ultimate load of 146 kips while moving to a displacement limit of 0.400 in.

To compare the amount of interfacial slip, average parallel and transverse slip versus in-plane displacement was plotted (Fig. 22). Average slip was determined by averaging all slip measurements taken at locations within 12 in. of the diaphragm's corners. Parallel slip for both slabs was nearly the same. Transverse slip for Slab 17 was was less than the transverse slip for Slab 6. Vertical load had little effect on the amount of parallel slip but significantly reduced the amount of transverse slip.

An average vertical displacement was calculated by taking the average of measurements recorded from two DCDTs located near the center of the diaphragm. The vertical displacements for Slabs 6 and 17 are illustrated (Fig. 23) by a plot of average vertical displacement versus nominal cyclic displacement. Vertical displacements through ultimate for both slabs were less than 0.050 in. Large vertical displacements occurred on Slab 17 after cracks formed on the top surface of the diaphragm while cycling at a displacement limit of 1.000 in.

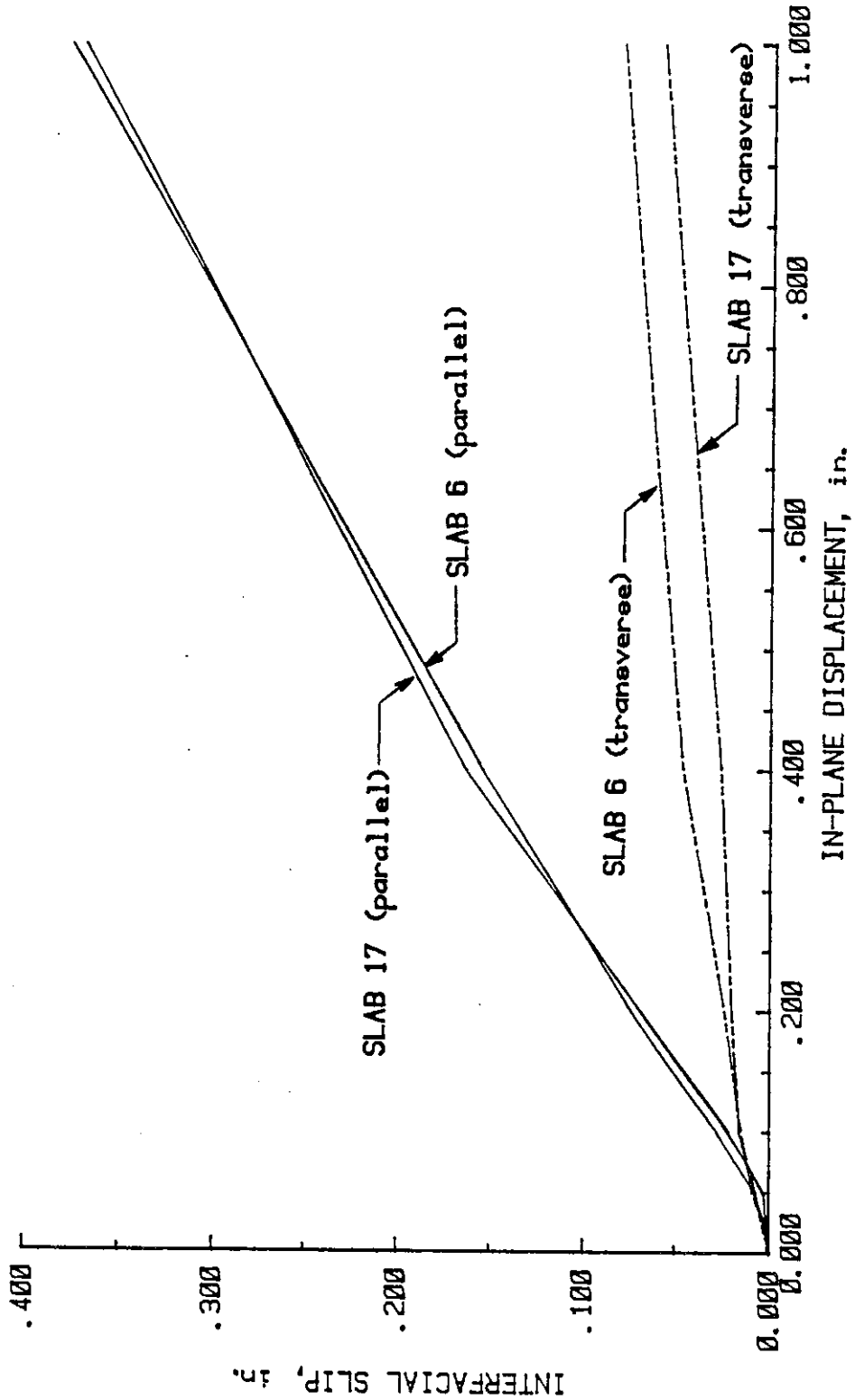

Figure 22. Interfacial slip for Slabs 6 and 17

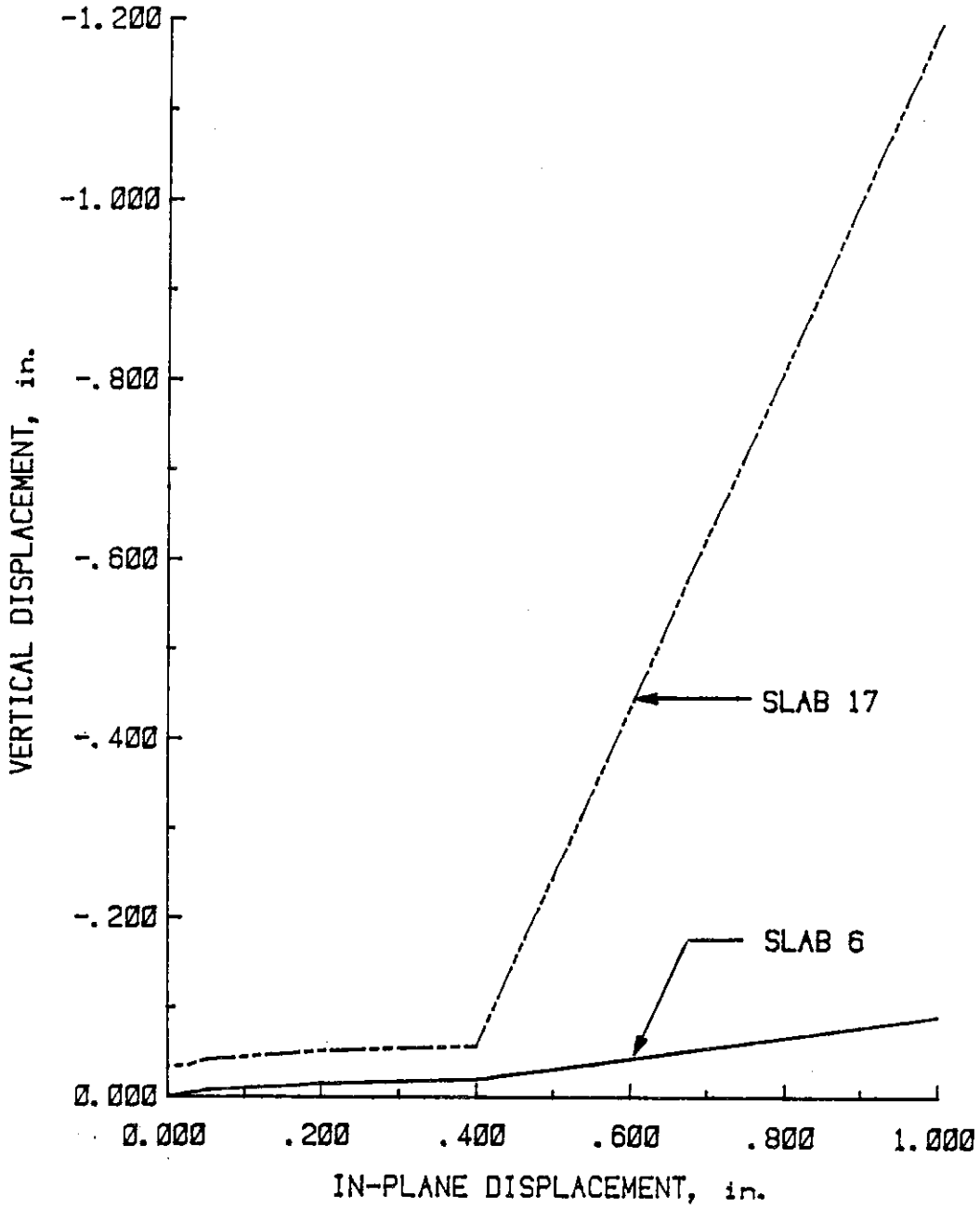

Figure 23. Vertical displacement for Slabs 6 and 17

4.1.2. Deck Type 4

Slabs 9 and 13 were constructed using a 16-gauge, 3 in. deep, embossed, cellular deck type (Deck Type 4, Fig. 6). This type of deck consists of a fluted section spot welded to a flat sheet. This flat sheet makes cellular steel deck stiffer than non-cellular steel deck in both directions transverse and parallel to the corrugations. Both slabs had a nominal concrete thickness of 5 1/2 in.

4.1.2.1. Slab 9 Slab 9 was tested as part of a previous research effort. Experimental results from Slab 9 are reported by Porter and Greimann (30). The load program for Slab 9 consisted of in-plane loading with displacement limits of 0.025, 0.050, 0.100, 0.200, 0.400 and 1.000 in. A summary of experimental results from Slab 9 are included next to provide a basis for comparison with Slab 13.

When the front edge of the test frame was displaced 0.050 in. east, a diagonal crack propagated across the southwest corner of the concrete slab (Fig. 24). Another diagonal crack formed across the northwest corner when the frame was displaced 0.100 in. west (Fig. 24). As cycling continued at this displacement limit, no new cracks formed and the stiffness of the diaphragm stabilized.

While moving to a displacement limit of 0.200 in. east, a diagonal crack appeared across the northeast corner of the diaphragm (Fig. 24). A maximum load of 220 kips (Fig. 25) was reached while moving to this displacement limit of 0.200 in. As cycling continued, diagonal cracks continued to form in both directions. The stiffness of the diaphragm degraded (Fig. 25). Corner sections of concrete began to slip out

SURFACE CRACK NUMBER	IN-PLANE DISPLACEMENT (in)	IN-PLANE LOAD (KIPs)
1	0.050 east	82
2	0.100 west	166
3	0.200 east	214

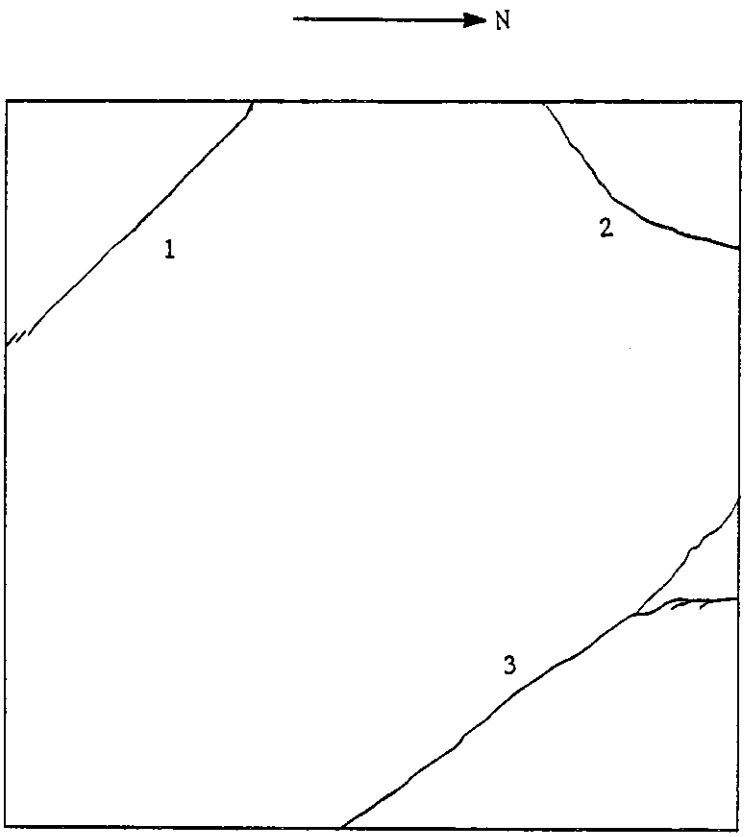

Figure 24. Top surface crack pattern for Slab 9

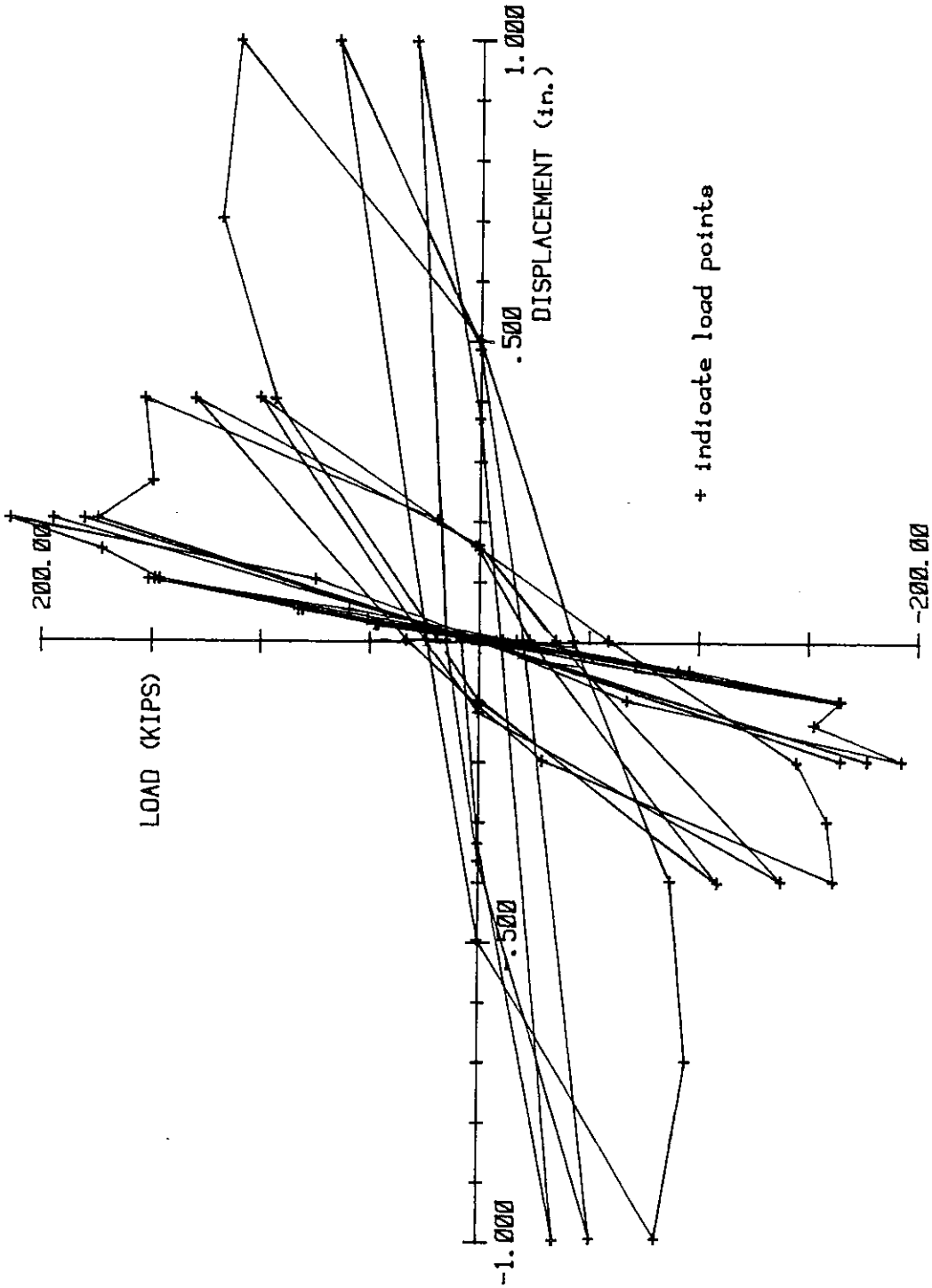

Figure 25. Load-displacement diagram for Slab 9 (30)

parallel to the corrugations. While cycling at a displacement limit of 1.000 in., welds along the seams between the deck panels and welds along the north and south edges failed. Deck panels began to slip relative to one another along the seams. This relative displacement, along the seams, will be referred to as seam slip.

4.1.2.2. Slab 13 Slab 13 was tested as part of this research effort. The purpose of Slab 13 was to study the behavioral changes caused by applying a distributed vertical load of 200 psf in addition and prior to in-plane load. The load program for this slab included the following steps. Vertical load was applied in increments of 40 psf until a total applied vertical load of 200 psf was reached. With vertical load held constant at 200 psf, the slab was subjected to the same reversed cyclic, in-plane load program as Slab 9.

While cycling at displacement limits of 0.025, 0.050 and 0.100 in., no cracks appeared on the surface of the diaphragm. A transverse slip of 0.013 in. and a parallel slip of 0.004 in. occurred while cycling at a displacement limit of 0.100 in. A maximum load of 250 kips (Fig. 26) was reached while moving to a displacement limit of 0.200 in. No surface cracks were observed at this point. While cycling at this displacement limit, short surface cracks appeared parallel to the corrugations in the southeast and northeast corners (Fig. 27). After these cracks appeared, a diagonal crack formed across the southwest corner. Parallel slip of 0.017 in. and transverse slip of 0.021 in. occurred while cycling at this displacement limit.

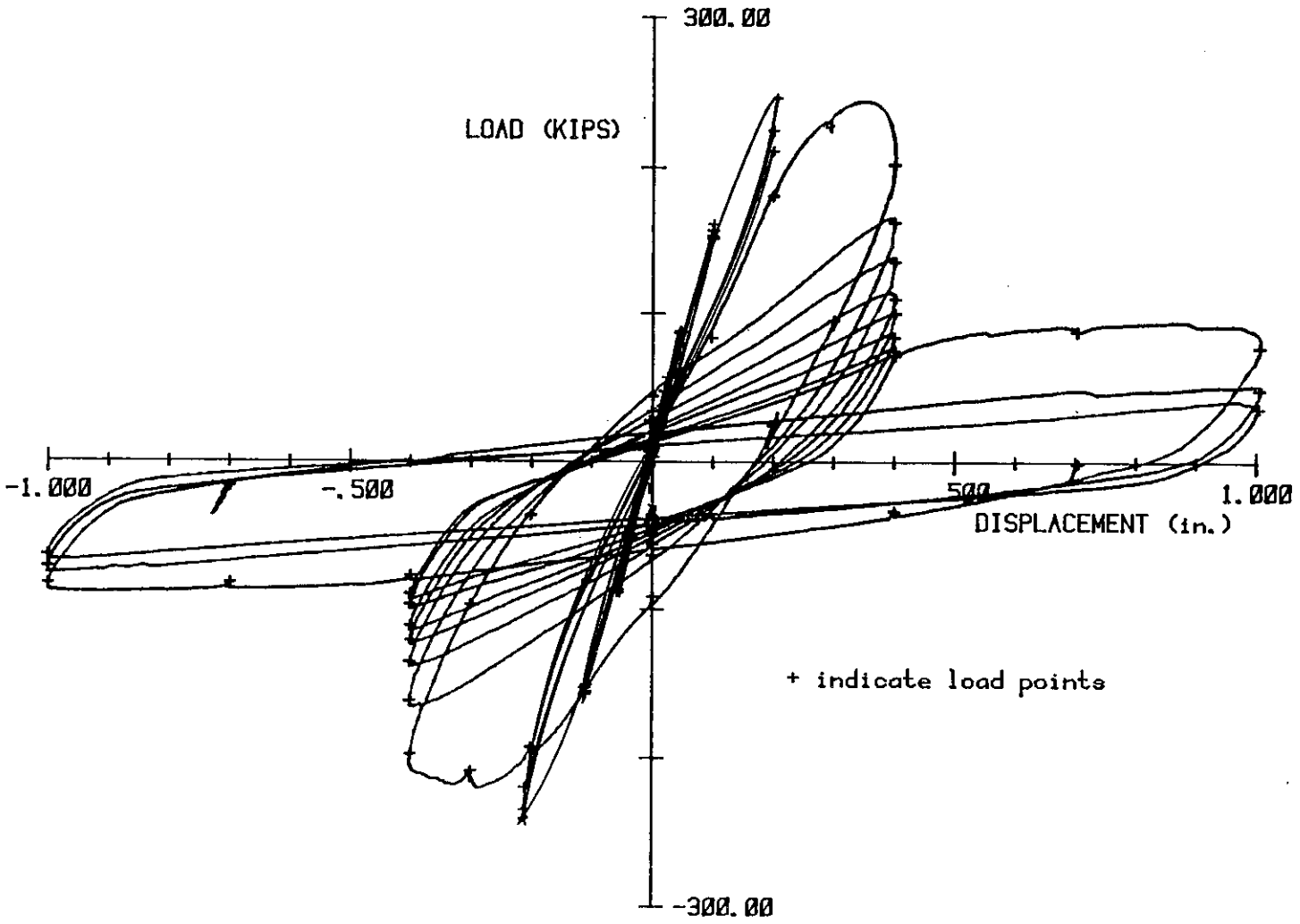

Figure 26. Load-displacement diagram for Slab 13

SURFACE CRACK NUMBER	IN-PLANE DISPLACEMENT (in)	IN-PLANE LOAD (KIPs)
1	0.200 west	237
2	0.200 east	199
3	0.200 east	193
4	0.400 east	240

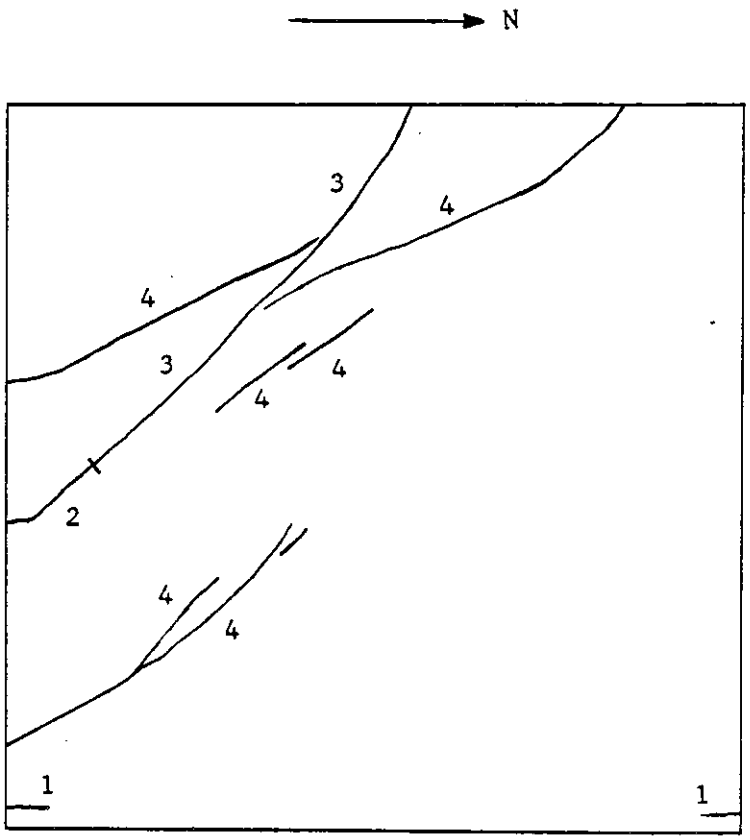

Figure 27. Top surface crack pattern for Slab 13

While moving to a displacement limit of 0.400 in., a load of 248 kips was reached and additional diagonal surface cracks appeared across the southwest corner of the concrete slab (Fig. 27). Additional diagonal cracks in both directions formed on the surface of the slab as cycling continued at this displacement limit. When these cracks formed, the stiffness of the diaphragm was reduced (Fig. 26). More diagonal cracks appeared while cycling at a displacement limit of 1.000 in. Welds failed along the north and south edges and along the seams and seam slip started to occur. After the in-plane load program was completed, the center of the diaphragm displaced down 1.174 in. At this point, the diaphragm was still able to carry the applied distributed vertical load of 200 psf.

4.1.2.3. Comparison of Slab 13 with Slab 9 The behavior of Slabs 9 and 13 was very similar. Both slabs failed in diagonal tension and reached ultimate loads while cycling at a displacement limit of 0.200 in. Slab 13 had a concrete compressive strength of 6187 psi and an ultimate capacity of 250 kips. Slab 9 had a concrete compressive strength of 5142 psi and an ultimate capacity of 220 kips.

An average slip was determined by taking the average of all slip measurements taken at locations less than 12 in. from the corners of the diaphragm. To compare the amount of interfacial slip, the average parallel and transverse slip versus nominal in-plane displacement was plotted (Fig. 28). Parallel slips for both slabs were approximately the same. Transverse slips for both slabs were similar prior

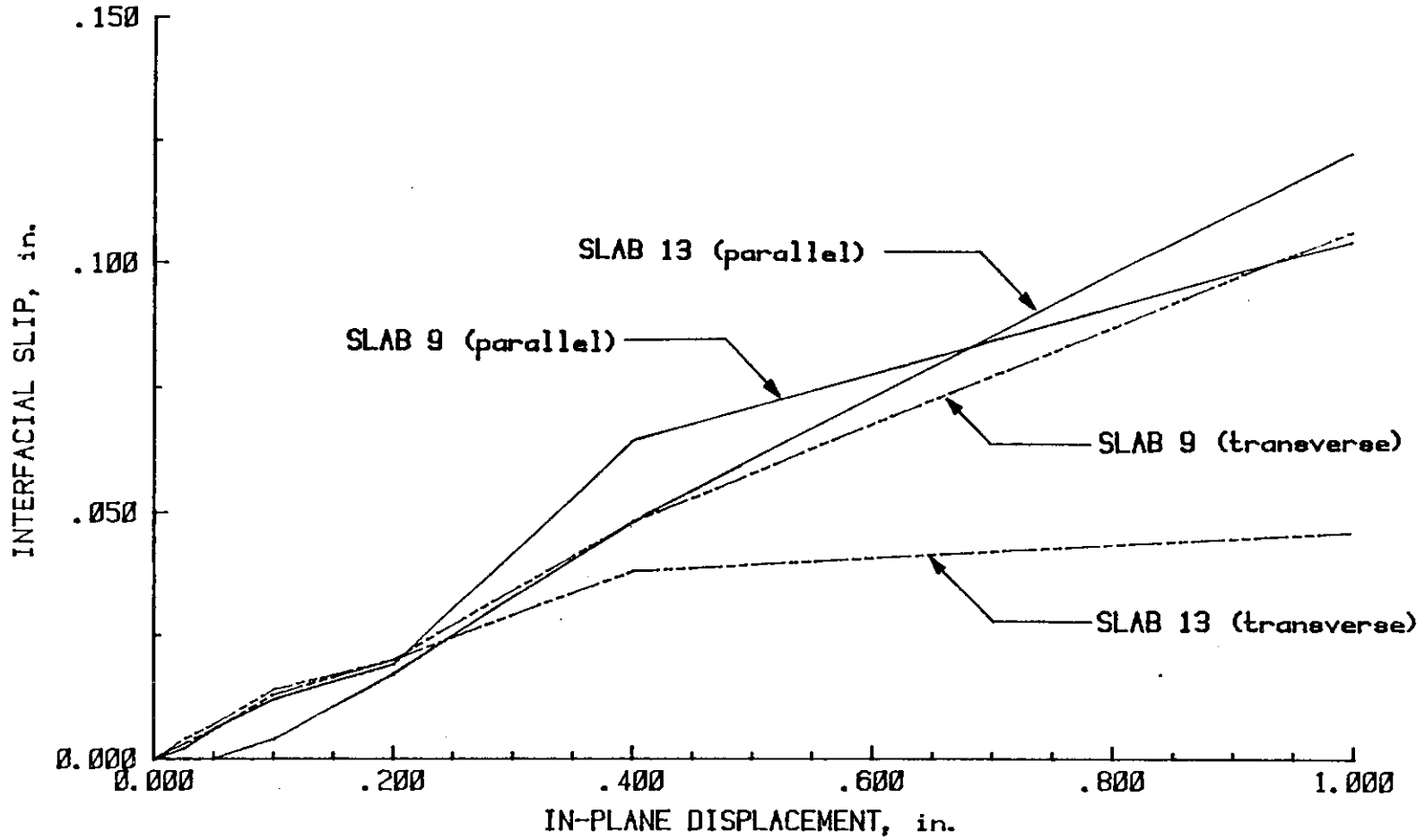

Figure 28. Interfacial slip for Slabs 9 and 13

to ultimate. After ultimate, Slab 13 experienced less transverse slip than Slab 9. Vertical load had little effect on parallel slip and transverse slip before ultimate but significantly reduced the amount of transverse slip after ultimate.

An average vertical displacement was calculated by taking the average of measurements recorded from two DCDTs located near the center of the diaphragm. Vertical displacements for Slabs 9 and 13 are illustrated by a plot (Fig. 29) of average vertical displacement versus nominal cyclic displacement. Prior to ultimate, the vertical displacement of Slab 13 was larger than the vertical displacement of Slab 9. After cracks formed on the top surface of Slab 13, large vertical displacements occurred.

4.1.3. Deck Type 5

A 16-gauge, 3 in. deep, embossed steel deck (Deck Type 5, Fig. 7) was used on Slabs 10, 12, 14 and 18. Slabs 10, 12 and 18 had a nominal concrete thickness of 5 1/2 in. Slab 14 had a nominal concrete thickness of 8 inches. This large thickness was used on Slab 14 to prevent diagonal tension failure. Slabs 10, 12, 14 and 18 were all tested as part of this research project.

4.1.3.1. Slab 10 The purpose of Slab 10 was to provide a control slab without vertical load that could be used for comparison with other slabs with vertical load. The load program for Slab 10 included reversed cyclic, in-plane loading with displacements limits of 0.025, 0.050, 0.100, 0.200, 0.400 and 1.000 in.

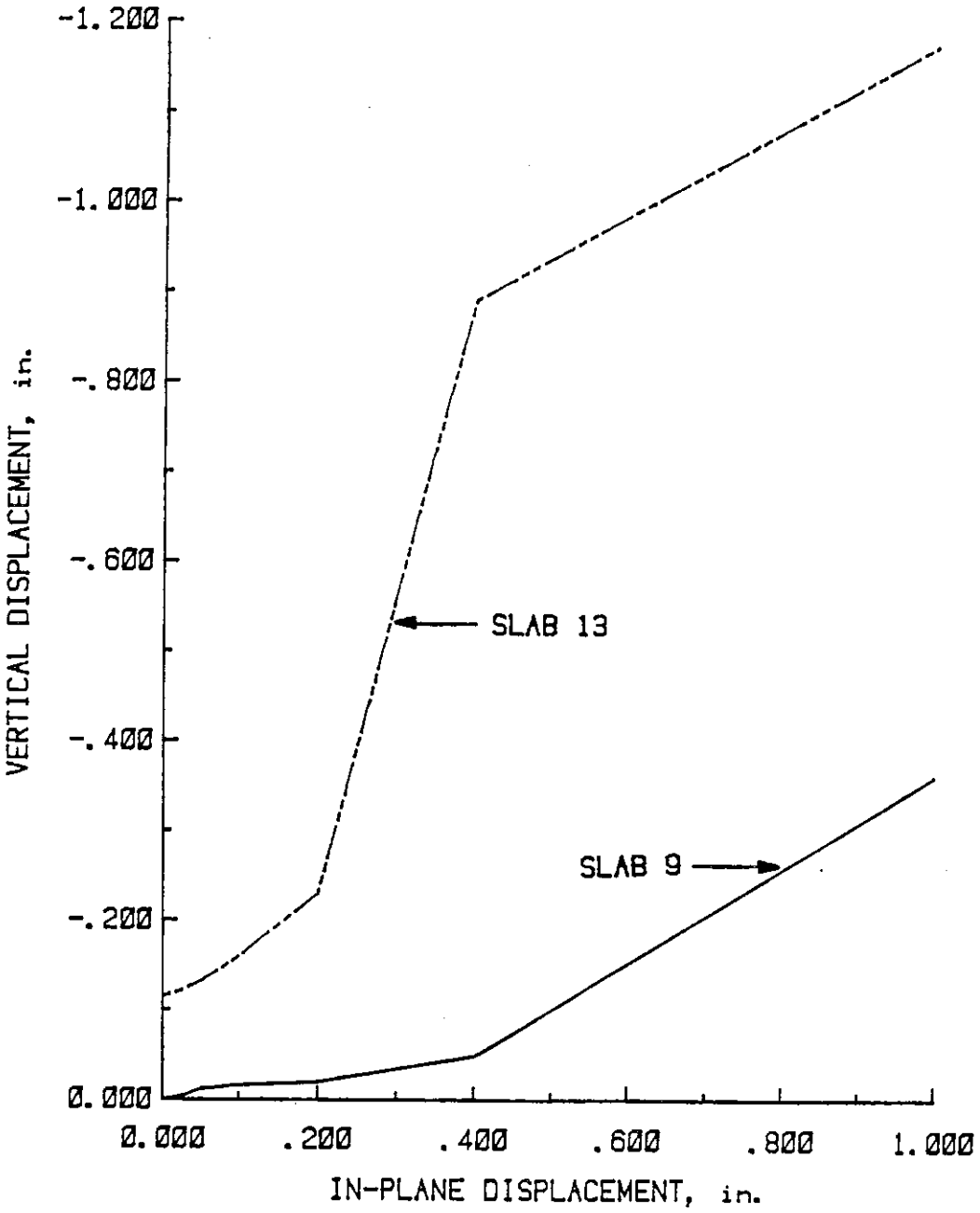

Figure 29. Vertical displacement for Slabs 9 and 13

Initial signs of distress were observed while cycling at a displacement limit of 0.100 in. At this displacement limit, diagonal cracks at the seams formed on the north and south faces of the slab. Parallel slip of 0.018 in. and transverse slip of 0.025 in. occurred. When the frame was displaced 0.200 in. west, a diagonal, surface crack appeared across the southeast corner (Fig. 30). A short surface crack near the northwest corner and parallel to the west edge also appeared.

Slab 10 reached a maximum load of 161 kips (Fig. 31) while cycling at a displacement limit of 0.400 in. The mode of failure at ultimate for this slab was diagonal tension. Diagonal cracks appeared across the northeast and southwest corners of the slab prior to ultimate load when the frame was displaced 0.400 in to the east. When the frame was moved 0.400 in. to the west, ultimate load was reached and a diagonal crack formed across the northwest corner of the slab (Fig. 30). The stiffness of the diaphragm was significantly reduced after these diagonal cracks formed. Additional diagonal cracks appeared in both directions while cycling at a displacement limit of 1.000 in.

4.1.3.2. Slab 12 The purpose of Slab 12 was to study behavioral changes caused by applying a distributed vertical load of 65 psf in addition and prior to in-plane load. This diaphragm's load program included the following steps. Vertical load was applied in increments of 13 psf until a total applied vertical load of 65 psf was reached. With this vertical load held constant, the diaphragm was subjected to the same reversed cyclic in-plane load program as Slab 10.

SURFACE CRACK NUMBER	IN-PLANE DISPLACEMENT (in)	IN-PLANE LOAD (KIPs)
1	0.200 west	132
2	0.400 east	138
3	0.400 west	153

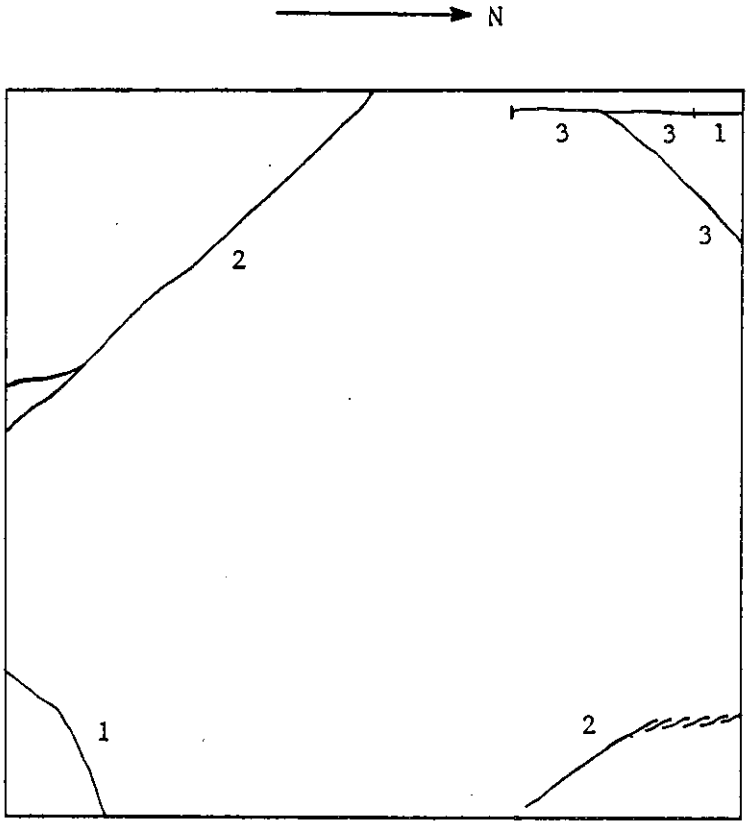

Figure 30. Top surface crack pattern for Slab 10

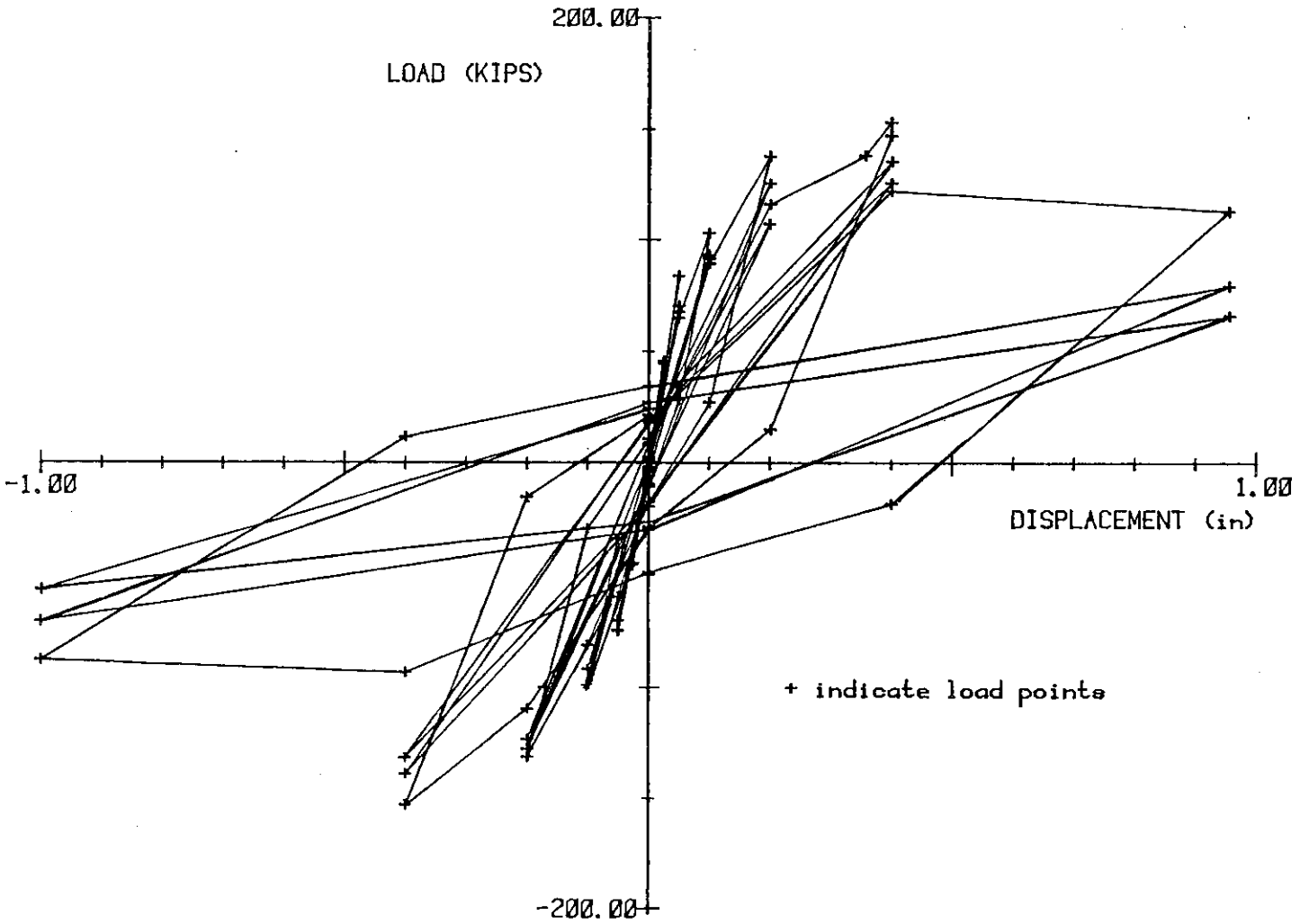

Figure 31. Load-displacement diagram for Slab 10

The center of the diaphragm displaced down 0.022 in. when the total vertical load of 65 psf was applied. While cycling at a displacement limit of 0.100 in., 0.011 in. of parallel slip and 0.014 in. of transverse slip occurred. Short surface cracks appeared parallel to the corrugations near the southwest, northeast and southeast corners of the slab (Fig. 32) while cycling at a displacement limit of 0.200 in.

A maximum load of 180 kips (Fig. 33) was reached while moving to a displacement limit of 0.400 in. A diagonal crack appeared across the southwest corner of the concrete slab at this point. With the displacement held constant at 0.400 in., the in-plane load dropped 9 kips before stabilizing. Several more diagonal cracks formed while cycling at this displacement limit. The in-plane and vertical stiffness of the diaphragm degraded significantly while cycling at this displacement limit and the center of the diaphragm displaced down 0.268 in. While cycling at a displacement limit of 1.000 in., more diagonal surface cracks appeared and the center of the diaphragm displaced down 1.524 in. The diaphragm was still able to carry the applied vertical load of 65 psf after the in-plane load program had been completed.

4.1.3.3. Slab 14 Slab 14 was tested to determine the effects of gravity load on diaphragms that do not fail in diagonal tension. The load program for Slab 14 included the following steps. Vertical load was applied in increments of 27 psf until a total applied vertical load of 135 psf was reached. With this distributed

SURFACE CRACK NUMBER	IN-PLANE DISPLACEMENT (in)	IN-PLANE LOAD (KIPs)
1	0.200 east	147
2	0.200 west	139
3	0.200 west	127
4	0.400 east	171

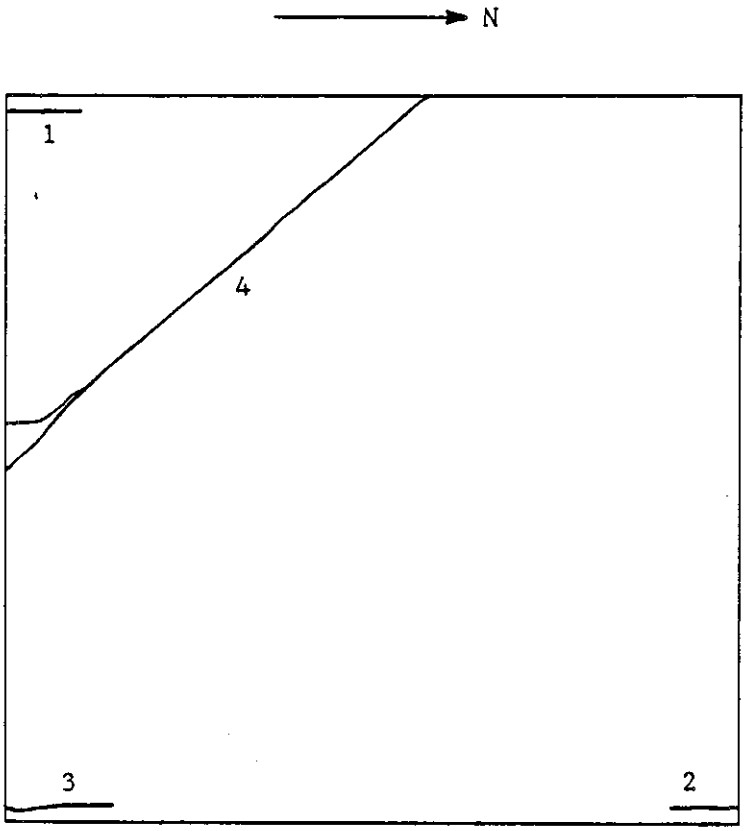

Figure 32. Top surface crack pattern for Slab 12

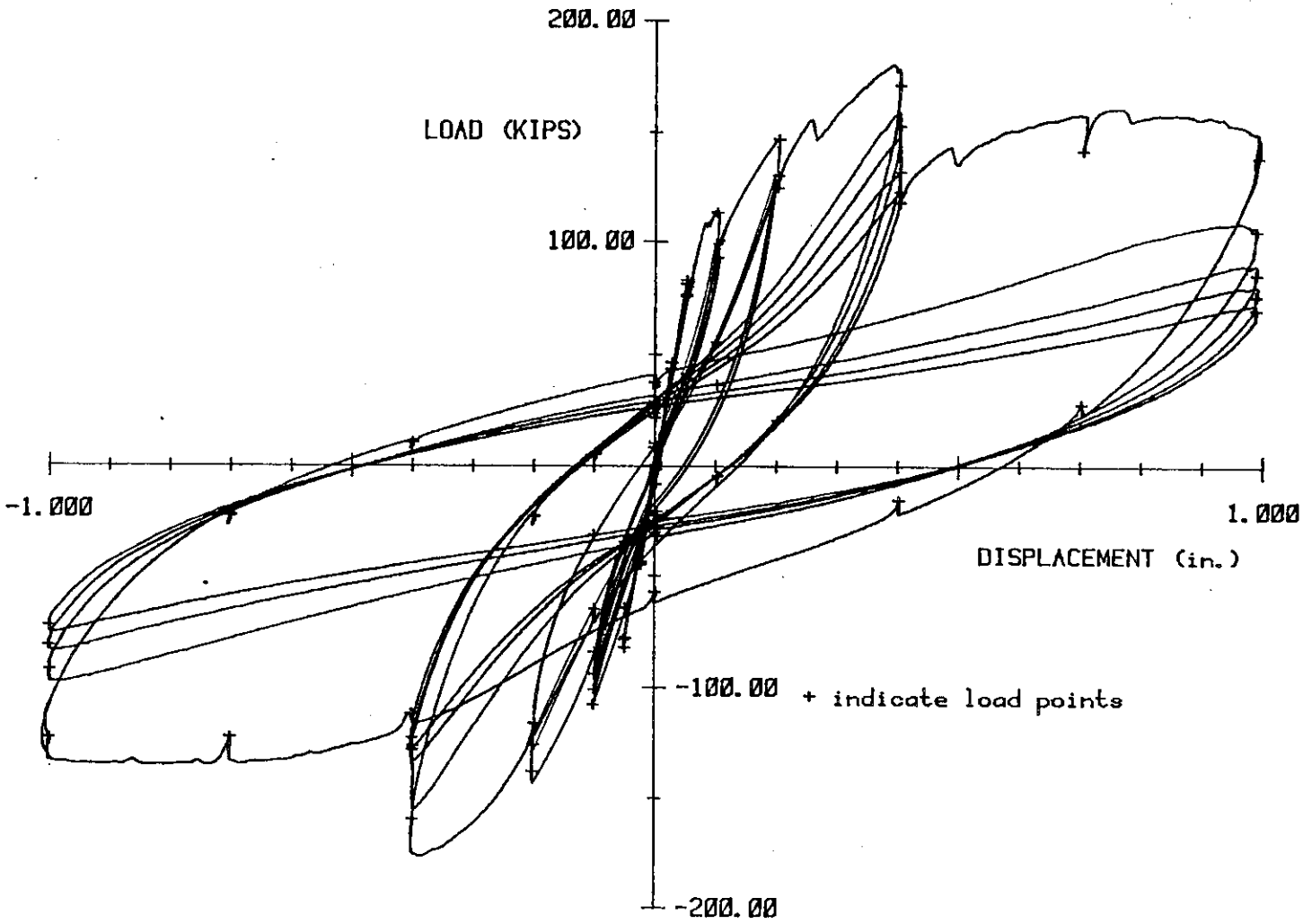

Figure 33. Load-displacement diagram for Slab 12

vertical load held constant, the diaphragm was subjected to the same reversed cyclic, in-plane load program as Slab 10.

Initial signs of distress were observed while cycling at a displacement limit of 0.100 in. Parallel slip of 0.018 in. and transverse slip of 0.017 in. was measured. As displacement limits were increased, the amount of parallel and transverse slip also increased. The parallel slip magnitude increased at nearly the same rate as the transverse slip magnitude.

While moving to a displacement limit of 0.400 in., a maximum load of 208 kips (Fig. 34) was reached. The mode of failure at ultimate for this slab was interfacial slip both parallel and transverse to the corrugations. Both parallel and transverse slip occurred. Elements of the composite diaphragm and the test frame moved relative to each other as shown in Figure 35 when the frame was moved to a displacement limit of 0.400 in. Parallel slip of 0.076 in. and transverse slip of 0.072 in. occurred. Three complete reversed displacement cycles were completed at a limit of 0.400 in. and no surface cracks appeared.

At a displacement of 0.700 in., a diagonal surface crack appeared. The in-plane load dropped 35 kips when this crack appeared (Fig. 34). Additional diagonal surface cracks appeared while cycling at a displacement limit of 1.000 in. The stiffness of the diaphragm was reduced by the formation of these diagonal cracks. A displacement of 1.588 in. down was measured at the center of the diaphragm. After the in-plane load program was completed, the diaphragm was still able to carry the applied vertical load of 135 psf.

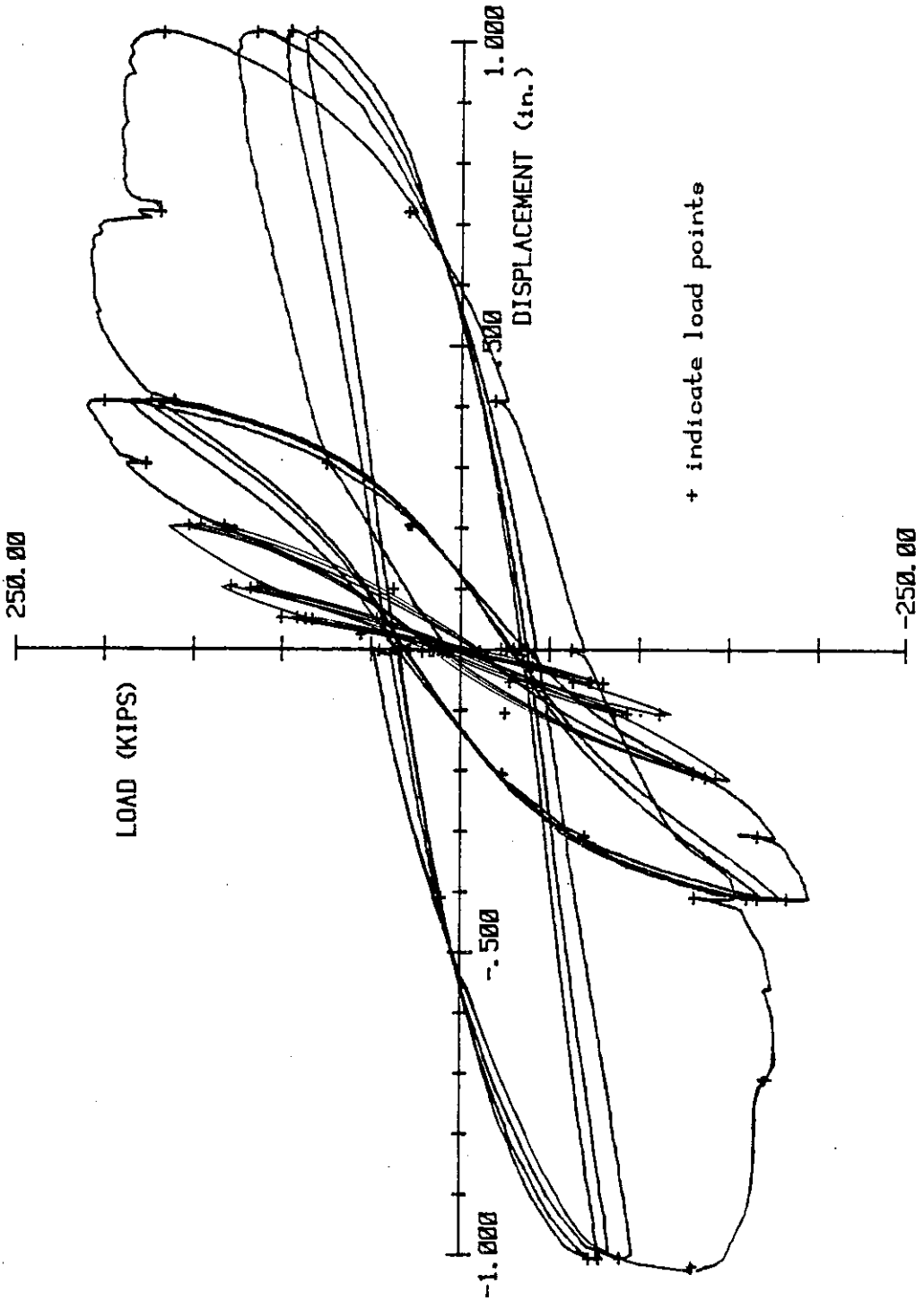

Figure 34. Load-displacement diagram for Slab 14

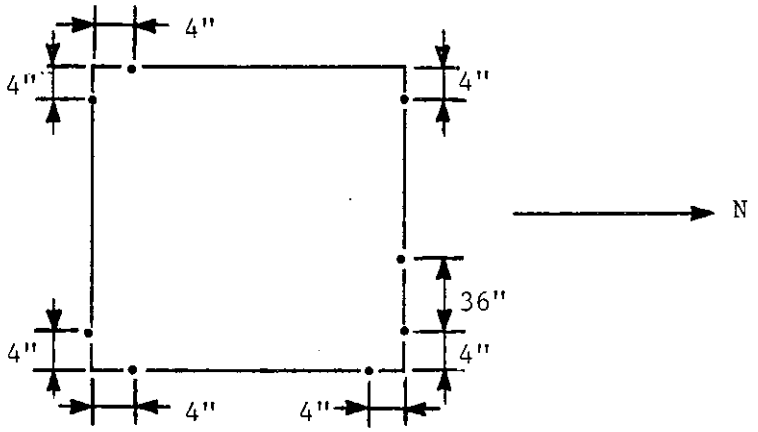

• indicates measurement location
for slip diagram shown below

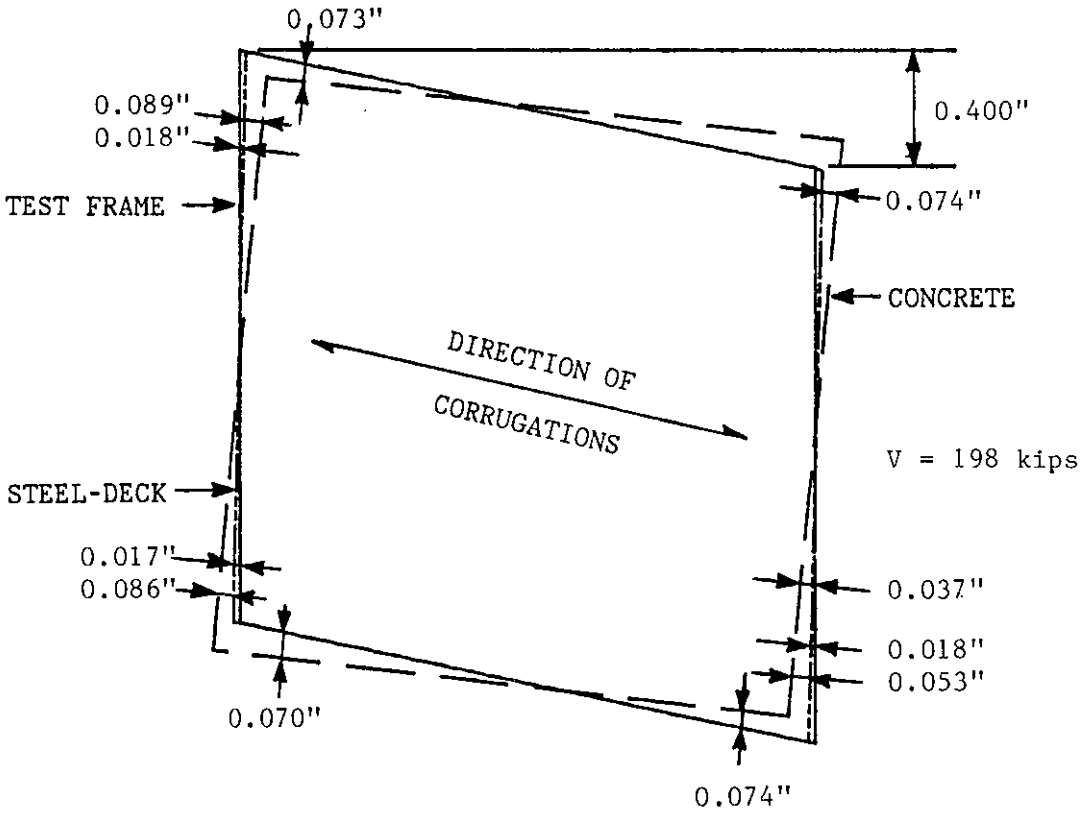

Figure 35. Interfacial slip diagram for Slab 14

4.1.3.4. Slab 18 The purpose of Slab 18 was to study the behavioral changes caused by applying a distributed vertical load of 135 psf in addition and prior to in-plane load. This slab's load program was similar to the load program used on Slab 14. Vertical load was applied in increments of 27 psf until a total applied load of 135 psf was reached. With the vertical load held constant, the slab was then subjected to the same in-plane load program as Slab 10.

The center of the diaphragm displaced down 0.122 in. when the vertical load of 135 psf was applied. Parallel slip of 0.018 in. and transverse slip of 0.017 in. occurred while cycling at a displacement limit of 0.100 in. The amount of parallel and transverse slip increased as displacement limits were increased.

Slab 18 reached a maximum load of 161 kips (Fig. 36) when the frame displaced 0.400 in. east. While moving to this displacement, diagonal cracks appeared across the southwest and northeast corners of the diaphragm (Fig. 37). Both the in-plane and vertical stiffnesses were reduced when these cracks formed. The center of the diaphragm displaced 0.411 in. down. Surface cracks, parallel to the east and west edges and in approximately 3 ft. from the east and west edges (Fig. 37) appeared after the diagonal cracks had formed. Additional diagonal surface cracks formed as cycling continued. After the in-plane load program was completed, a vertical displacement of 2.520 in. was measured at the center of the diaphragm. At this point, the diaphragm was still able to carry the distributed vertical load of 135 psf.

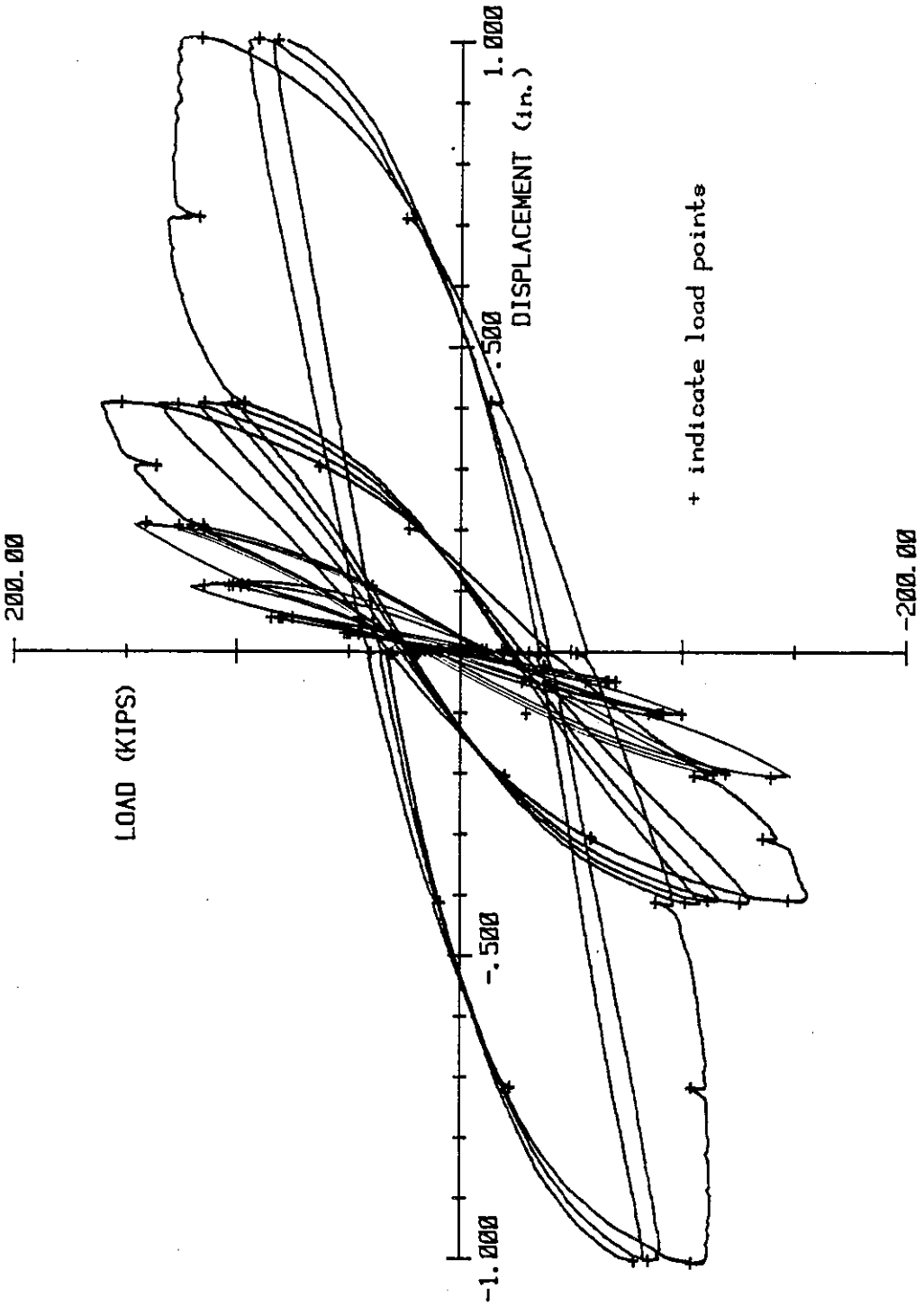

Figure 36. Load-displacement diagram for Slab 18

SURFACE CRACK NUMBER	IN-PLANE DISPLACEMENT (in)	IN-PLANE LOAD (KIPs)
1	0.300 east	137
2	0.400 east	152

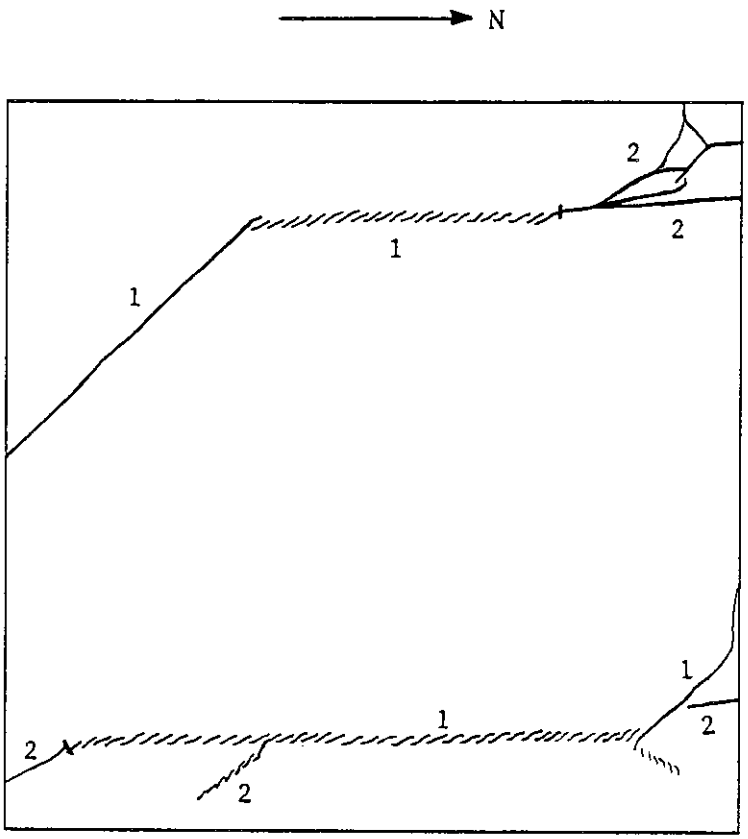

Figure 37. Top surface crack pattern for Slab 18

4.1.3.5. Comparison of Slabs 12, 14 and 18 with Slab 10

The behavior of Slabs 10, 12 and 18 was very similar. These slabs all failed in diagonal tension. Slabs 10, 12 and 18 had concrete compressive strengths of 3311, 3412 and 3052 psi and ultimate capacities of 161, 180 and 161 kips, respectively. Slab 14 had a nominal concrete thickness of 8 in. and failed in interfacial slip. The amount of interfacial slip was compared by plotting average parallel and transverse slip versus nominal in-plane displacement (Fig. 38). Average slip was determined by taking the average of all slip measurements taken at locations within 12 in. from the corners of the slab. Slab 14 experienced larger parallel and transverse slips than Slabs 10, 12 or 18. Slab 18 slipped less than Slab 10 in the transverse direction but more than Slab 10 in the parallel direction. Slab 12 slipped less than Slab 10 in both directions.

Vertical displacements for Slabs 10, 12, 14 and 18 are illustrated by a plot of average vertical displacement versus nominal cyclic displacement (Fig. 39). Average vertical displacement was calculated by averaging measurements recorded by two DCDTs located near the center of the diaphragm. Prior to ultimate load, the vertical displacements of Slabs 10, 12 and 14 were less than 0.100 in. The vertical displacement of Slab 10 remained small throughout the entire test. Slabs 12 and 14 experienced large vertical displacements after cracks formed on the top surfaces of these diaphragms. Slab 18 experienced large vertical displacements even before ultimate load was reached.

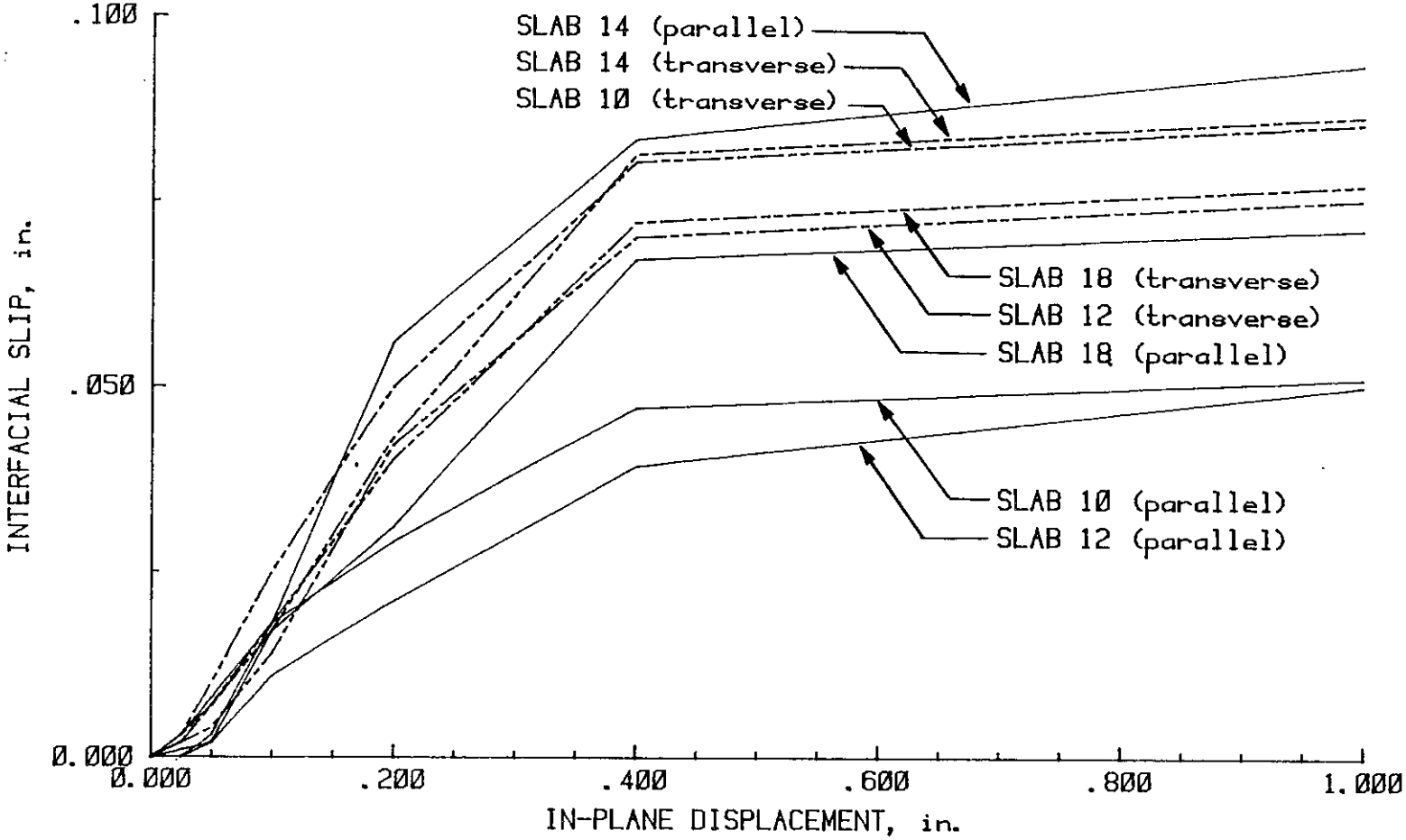

Figure 38. Interfacial slip for Slabs 10, 12, 14 and 18

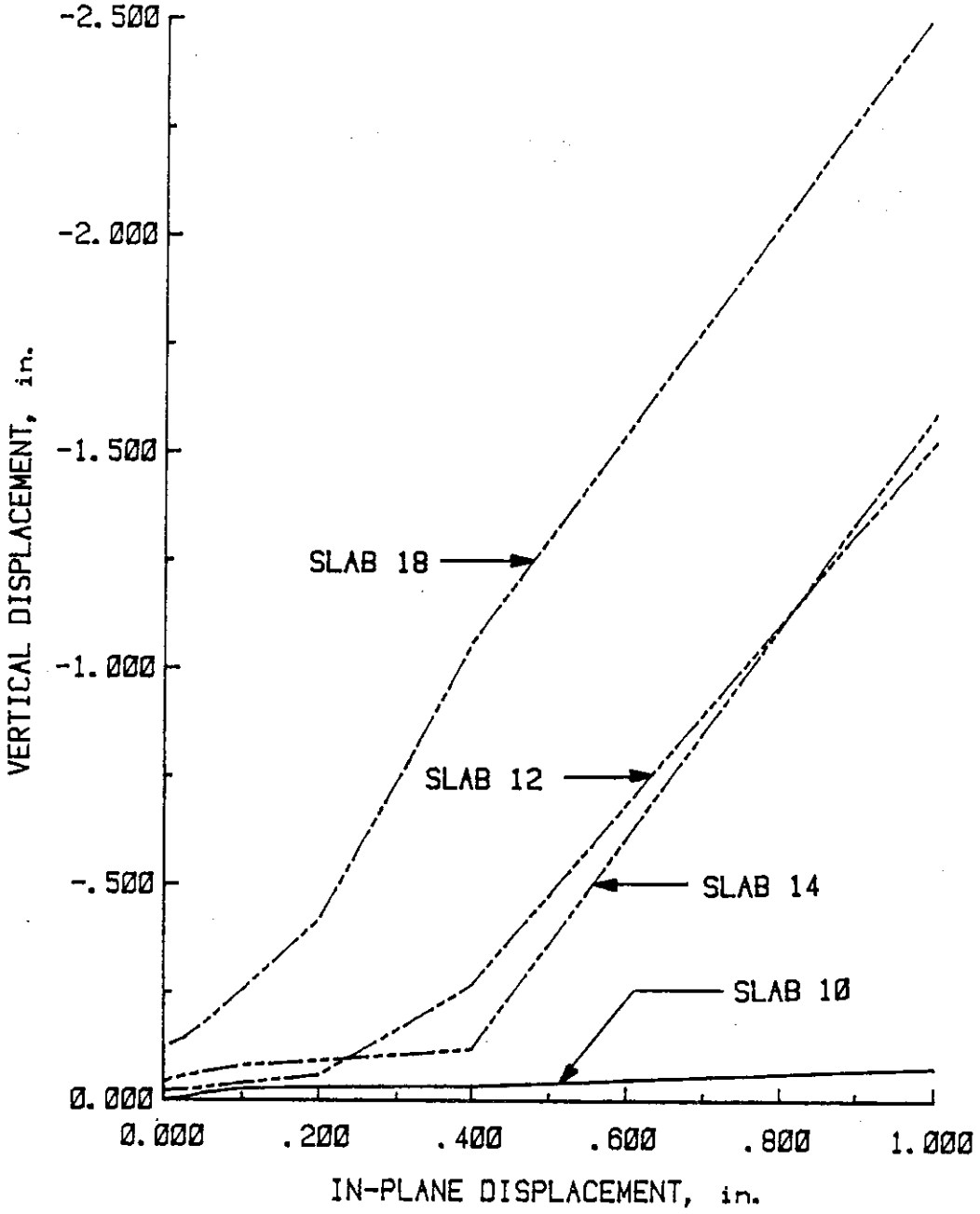

Figure 39. Vertical displacement for Slabs 10, 12, 14 and 18

4.1.4. Deck Type 7

Slabs 15 and 16 were constructed using an 18-gauge, 1 1/2 in. deep, embossed steel deck (Deck Type 7, Fig. 5). This deck was oriented so that the smaller width corrugations were down. This orientation saves concrete and is commonly used in practice. Both slabs had a nominal concrete thickness of 4 in. Slabs 15 and 16 were tested as part of this research effort.

4.1.4.1. Slab 15 Slab 15 was tested to provide a control slab for comparison with Slab 16. The load program for Slab 15 included reversed cyclic, in-plane loading with displacement limits of 0.025, 0.050, 0.100, 0.200, 0.400 and 1.000 in.

While the slab was cycled at a displacement limit of 0.050 in., parallel slip of 0.007 in. and transverse slip of 0.013 in. occurred. Concrete in the down corrugations near the north and south edges of the diaphragm, sheared from the concrete slab when the test frame was cycled at a displacement limit of 0.100 in. This behavior was described as concrete rib failure in Section 2.2 and is shown in Figure 3. The concrete ribs that had been sheared from the concrete slab did not slip. The rest of the concrete slab experienced transverse slip of 0.032 in. and parallel slip of 0.019 in. As cycling continued at a displacement limit of 0.200 in., more concrete ribs sheared from the concrete slab.

An ultimate load of 103 kips (Fig. 40) was reached while moving to a displacement limit of 0.400 in. The steel deck moved relative to the concrete as shown in Figure 41 at this point. Slip both parallel

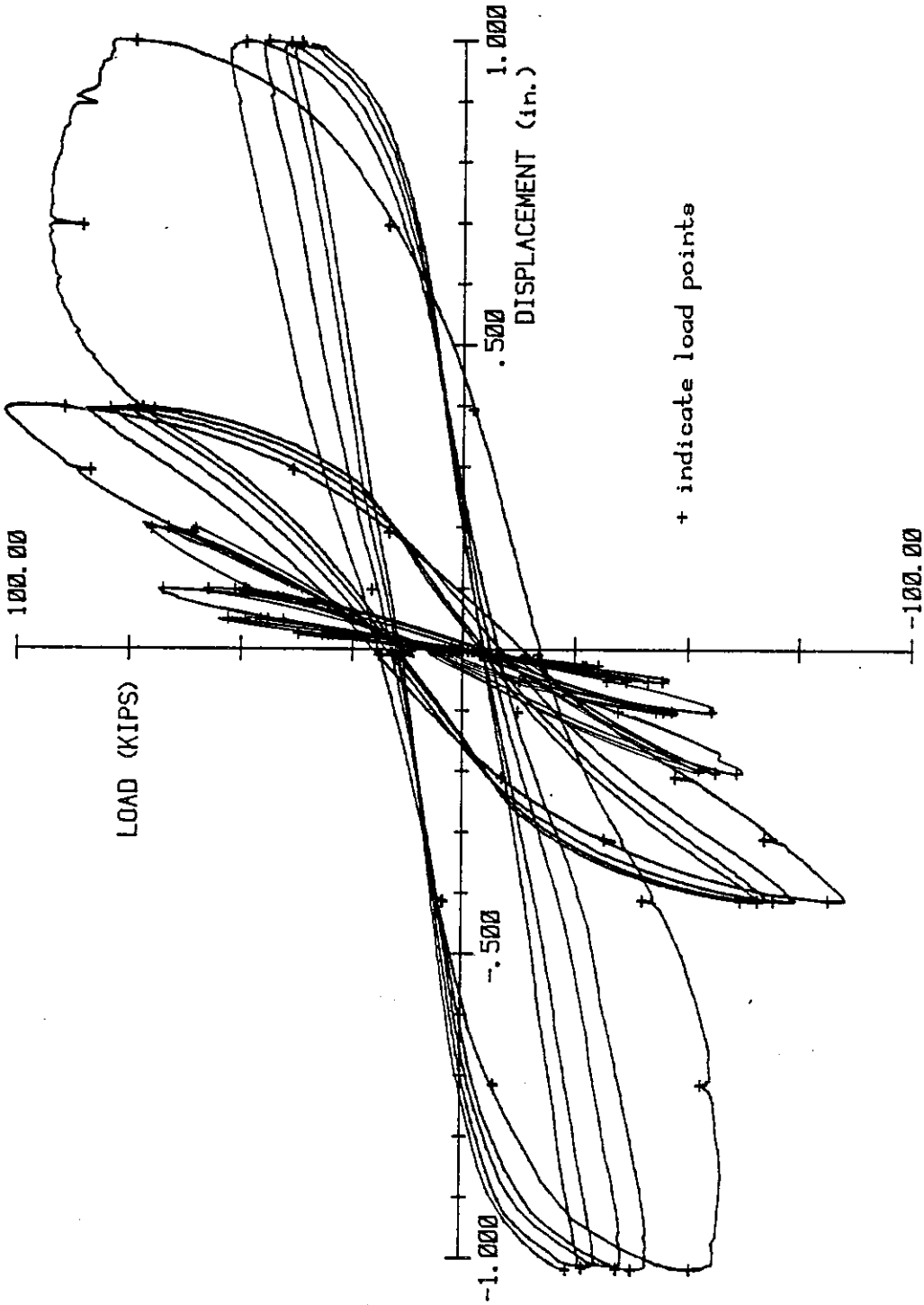

Figure 40. Load-displacement diagram for Slab 15

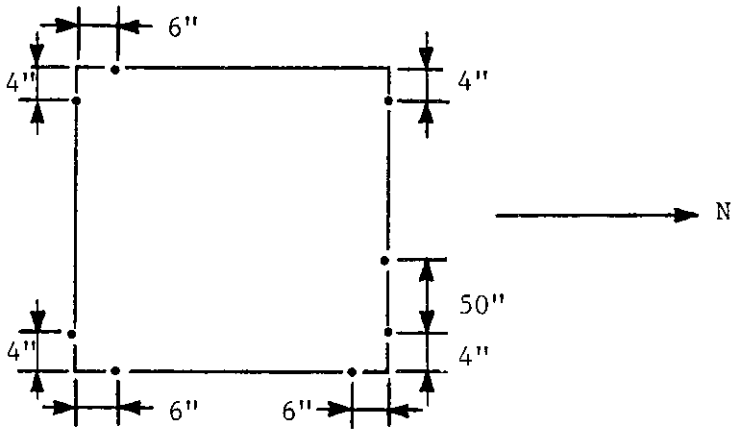

• indicates measurement location for slip diagram shown below

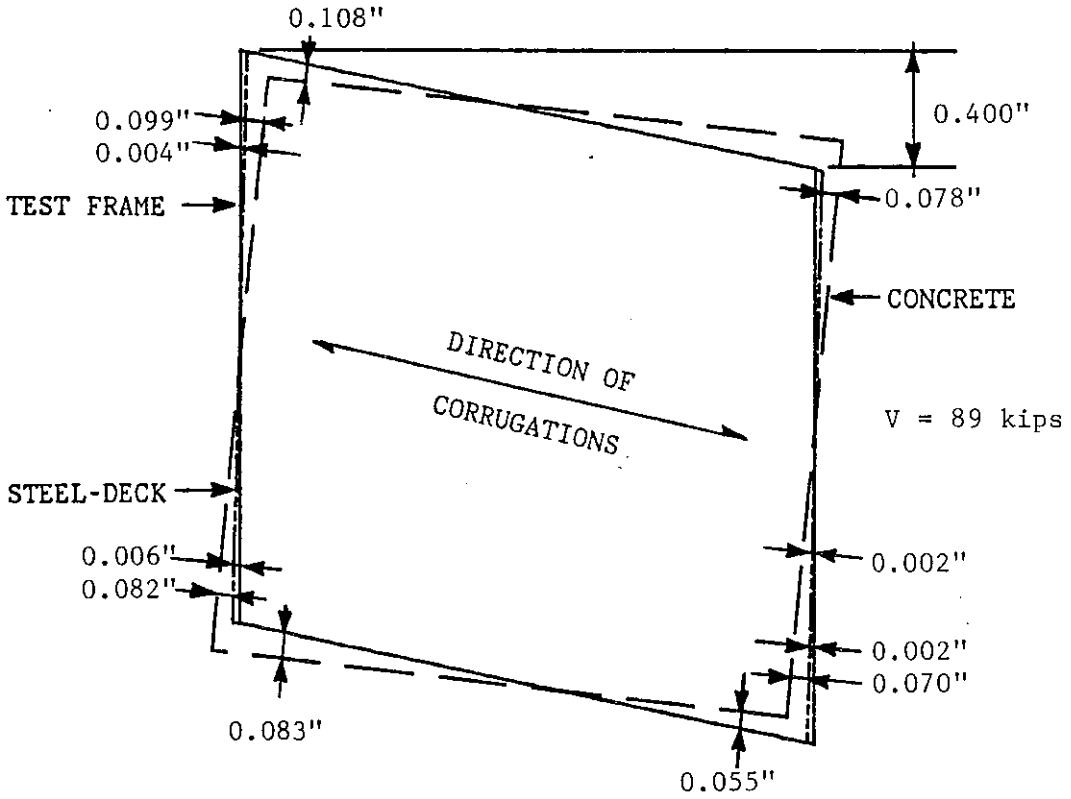

Figure 41. Interfacial slip diagram for Slab 15

and transverse to the corrugations occurred. As cycling continued at a displacement limit of 0.400 in., the diaphragm's stiffness slowly degraded. No surface cracks formed while cycling at this displacement limit.

While cycling at a displacement limit of 1.000 in., diagonal cracks appeared across the surface of the diaphragm. The diaphragm's load carrying capacity was reduced when these diagonal cracks formed (Fig. 40). After the test had been completed, the top concrete surface was removed to reveal the extent of concrete rib failure. The concrete ribs that had been sheared from the rest of the slab extended inwards 18 in. from the north and south edges.

4.1.4.2. Slab 16 The purpose of Slab 16 was to study the behavioral changes caused by applying a distributed vertical load of 35 psf in addition and prior to in-plane load. Vertical load was applied in increments of 7 psf until a total applied vertical load of 35 psf was reached. With the vertical load held constant, the diaphragm was subjected to the same in-plane load program as Slab 15.

When the vertical load was applied, the center of the diaphragm displaced down 0.081 in. No parallel or transverse slip occurred when the vertical load was applied. Parallel slip of 0.007 in. and transverse slip of 0.008 in. occurred while cycling at a displacement limit of 0.050 in. Most of the concrete in the down corrugations sheared from the rest of the concrete slab while cycling at a displacement limit of 0.100 in. This concrete rib failure is described in Section 2.2 and is shown in Figure 3.

A maximum load of 124 kips (Fig. 42) was reached while moving to a displacement limit of 0.400 in. Diagonal cracks appeared across the surface of the concrete slab at this point (Fig. 43). With the in-plane displacement held constant at 0.400 in., the in-plane load dropped 40 kips before stabilizing. The mode of failure at ultimate for this slab was diagonal tension failure of the concrete slab. More diagonal cracks appeared as cycling continued at displacement limits of 0.400 and 1.000 in. After the in-plane load program was completed, the center of the diaphragm displaced down 2.517 in. The diaphragm was still able to carry the applied vertical load of 35 psf. After the test was completed, the concrete slab was removed to reveal the extent of concrete rib failure. The ribs that had sheared from the concrete slab and remained in the down corrugations extended inwards from the north and south ends 18 in.

4.1.4.3. Comparison of Slab 16 with Slab 15 Slab 15 experienced concrete rib failure and had an ultimate capacity of 103 kips. Slab 16 was constructed exactly like Slab 15 and was subjected to an applied vertical load of 35 psf in addition and prior to being loaded in-plane. Slab 16 failed in diagonal tension and had an ultimate capacity of 124 kips.

The amount of interfacial slip was compared by plotting average slip versus displacement (Fig. 44). Average slip was determined by taking the average of all slip measurements taken at locations within 12 in. of the corners of the diaphragm. Slab 16 slipped less than Slab 15 in both the parallel and transverse directions.

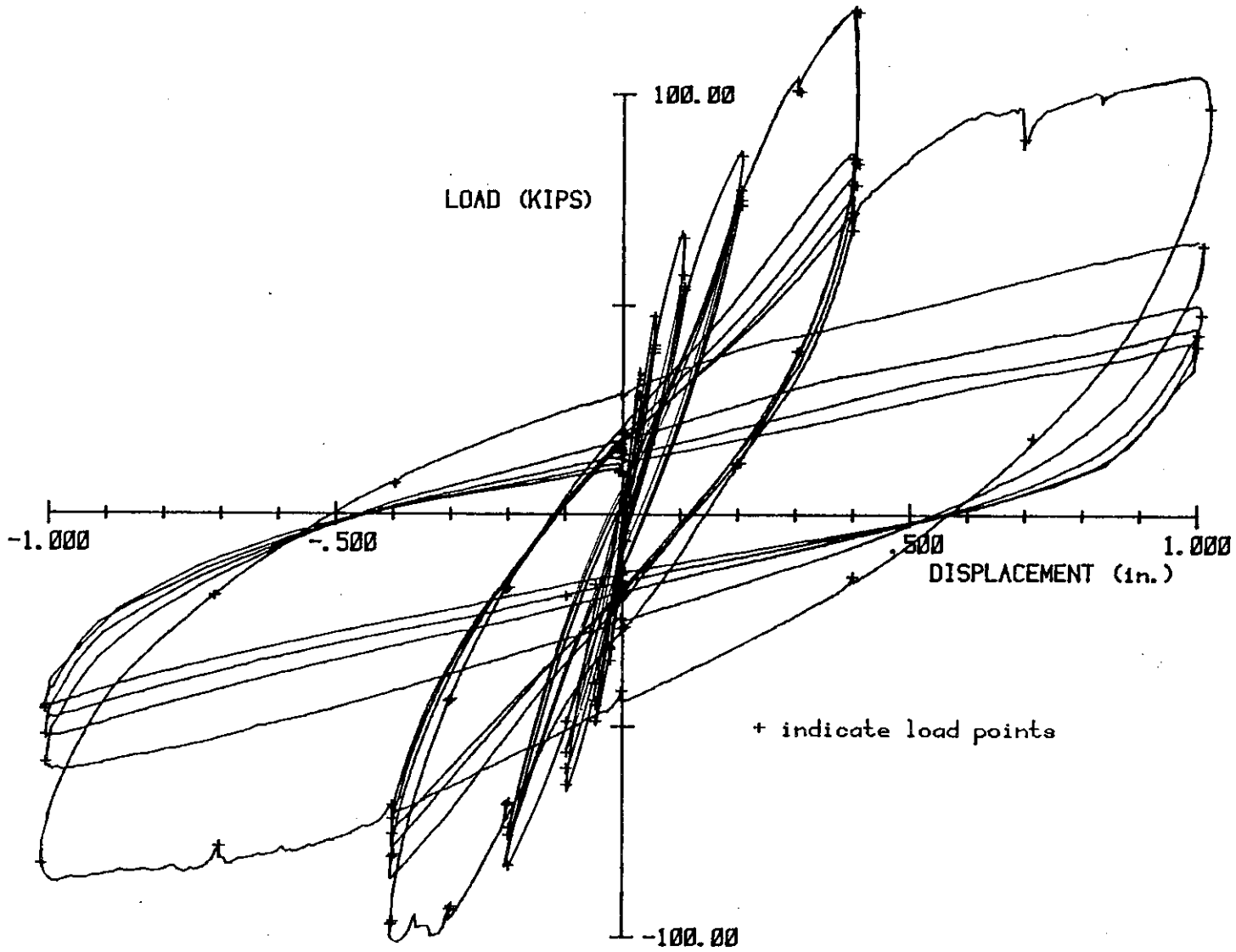

Figure 42. Load-displacement diagram for Slab 16

SURFACE CRACK NUMBER	IN-PLANE DISPLACEMENT (in)	IN-PLANE LOAD (KIPs)
1	0.400 east	84

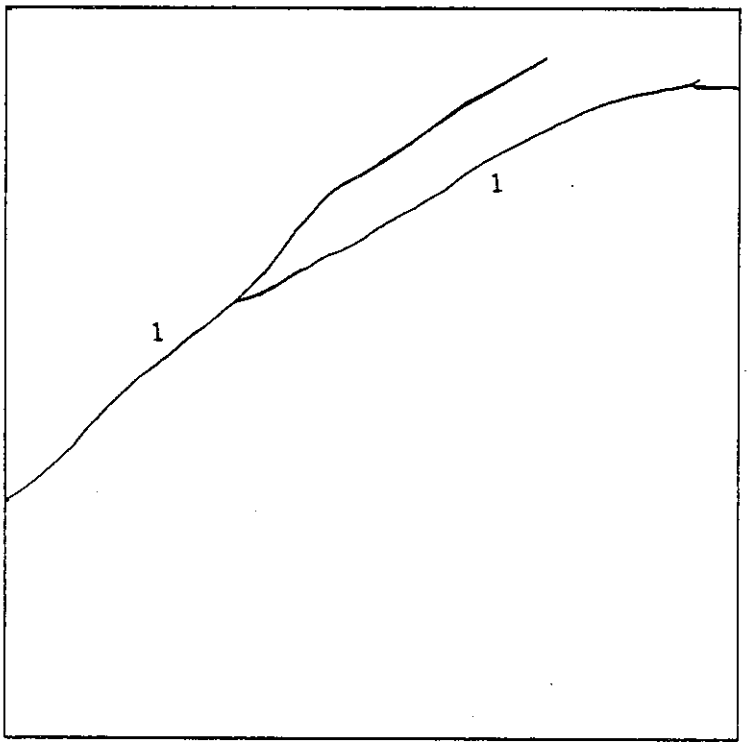

Figure 43. Top surface crack pattern for Slab 16

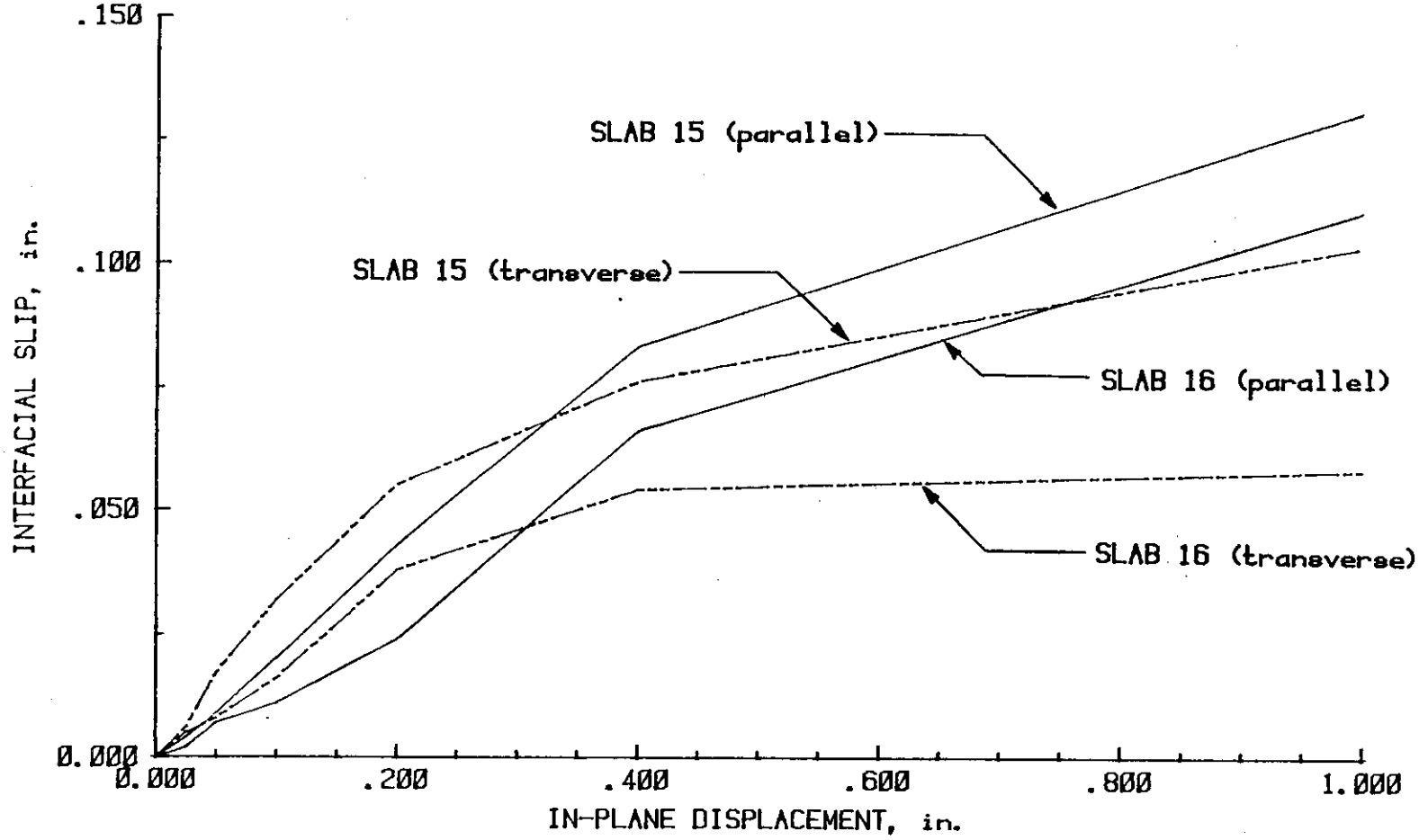

Figure 44. Interfacial slip for Slabs 15 and 16

An average vertical displacement was calculated by taking the average of measurements recorded from two DCDTs located near the center of the diaphragm. Average vertical displacement is illustrated by a plot of average vertical displacement versus nominal in-plane displacement (Fig. 45). Prior to ultimate, the vertical displacement of both slabs was less than 0.200 in. Vertical displacements for both slabs remained small until cracks appeared on the surface of the slabs. Large vertical displacements occurred after surface cracks appeared. After the in-plane load program was completed, the center of Slab 16 displaced down 2.517 in.

4.2. Measured Results

Measured results helped to identify general behavioral trends both before and after ultimate load. This section includes results from strain measurements.

A variety of uniaxial and rosette concrete surface gages and concrete embedment gages were used to measure in-plane strain distributions across the diaphragms during each test. Rosettes were used to identify principal strains and principal strain directions. When the diaphragms were subjected to vertical load, resulting principal surface strains at the center of the diaphragm were oriented in a direction parallel to the edges of the diaphragm (Fig. 46a). The largest principal compressive strains were oriented parallel to the steel deck corrugations. When the diaphragms were subjected to in-plane loading

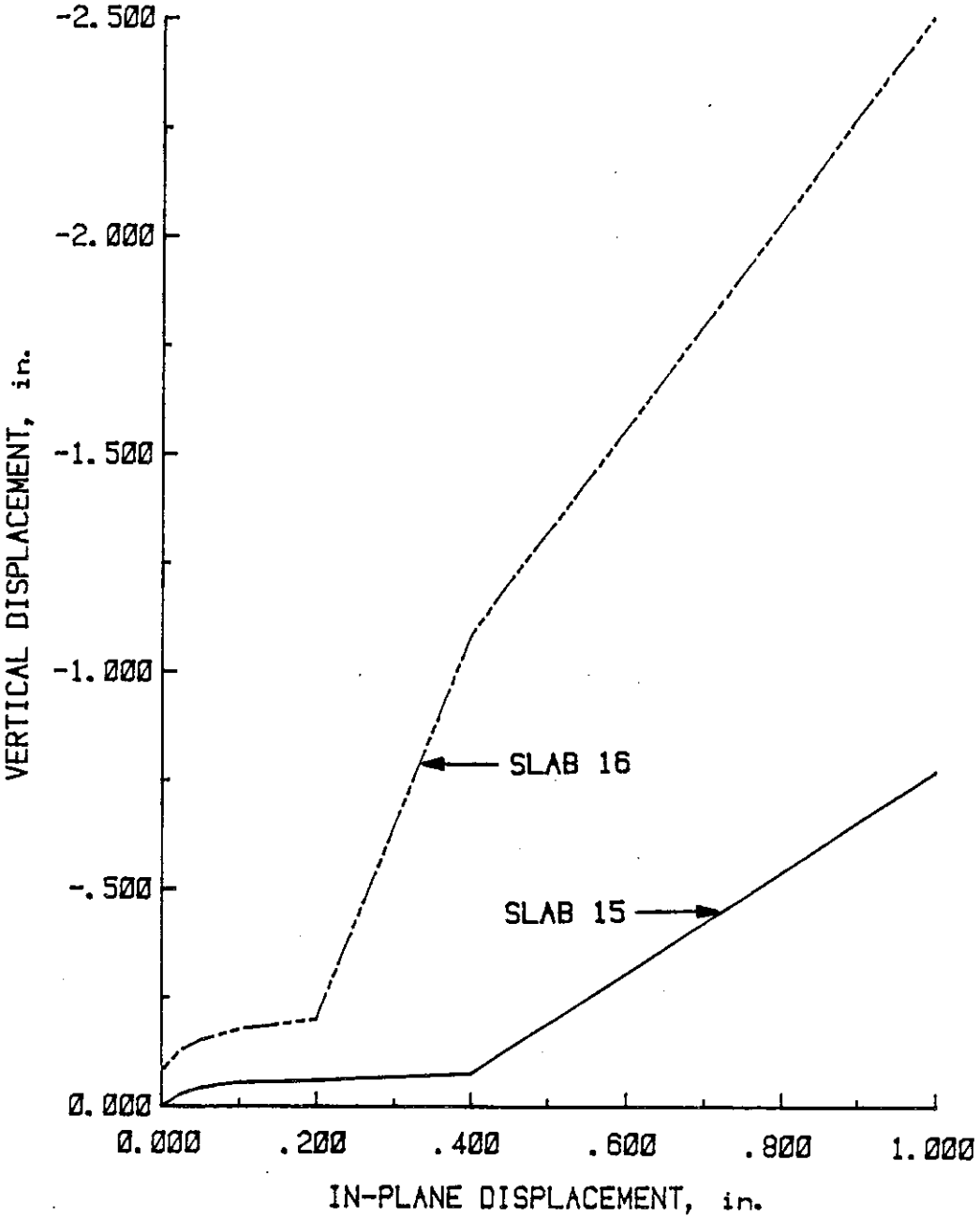

Figure 45. Vertical displacement for Slabs 15 and 16

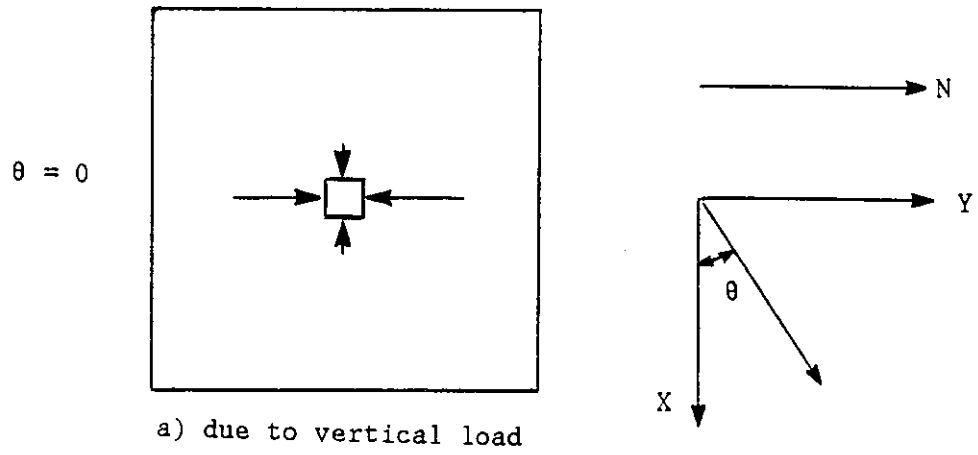

a) due to vertical load

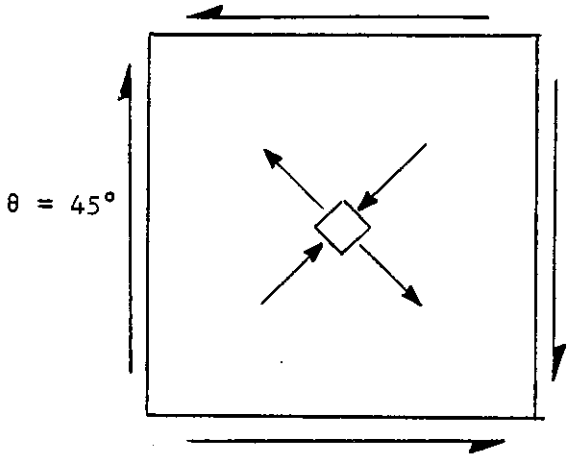

b) due to in-plane load

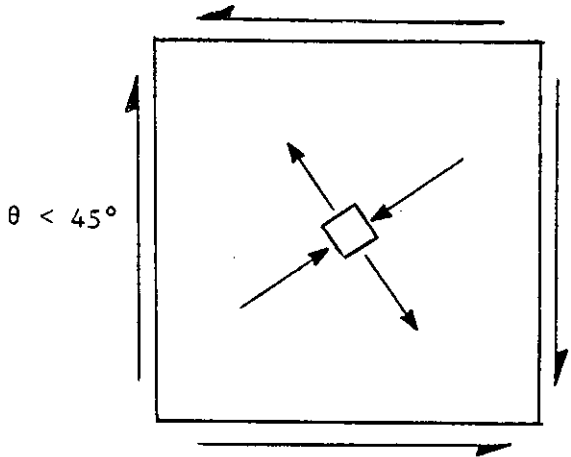

c) due to a combination of vertical and in-plane load

Figure 46. Orientation of principal strains on the concrete surface

only, principal surface strains were oriented in a direction measuring approximately 45° from a line (X-axis) parallel to the north or south edges (Fig. 46b). Principal tensile strain magnitudes were equal to principal compressive strain magnitudes. When the diaphragms were subjected to both in-plane and vertical load, principal tensile strains were oriented in a direction measuring less than 45° from the X-axis (Fig. 46c). Principal concrete surface strains due to in-plane load were calculated by subtracting the strain measurements obtained after the vertical load was applied from the subsequent strain measurements and then using these adjusted strain measurements to calculate principal strains.

Principal tensile surface strains, due to in-plane load, are illustrated in Figure 47 by a plot of principal surface strains versus in-plane load. Results from Slab 13 are not shown because the rosette used on this slab malfunctioned. These measured results indicated that a linear relationship exists between the principal tensile strains on the concrete surface and the in-plane load. These measured results also indicate that the principal tensile strains per unit load on the concrete surface are related to the average thickness of the concrete slab and the concrete compressive strength. Slabs with larger concrete thicknesses experience smaller principal tensile strains per unit load. Slabs with higher concrete strengths experience smaller principal tensile strains per unit load. This relationship between principal tensile strains per unit load and concrete compressive strength is probably due to the relationship between modulus of elasticity for

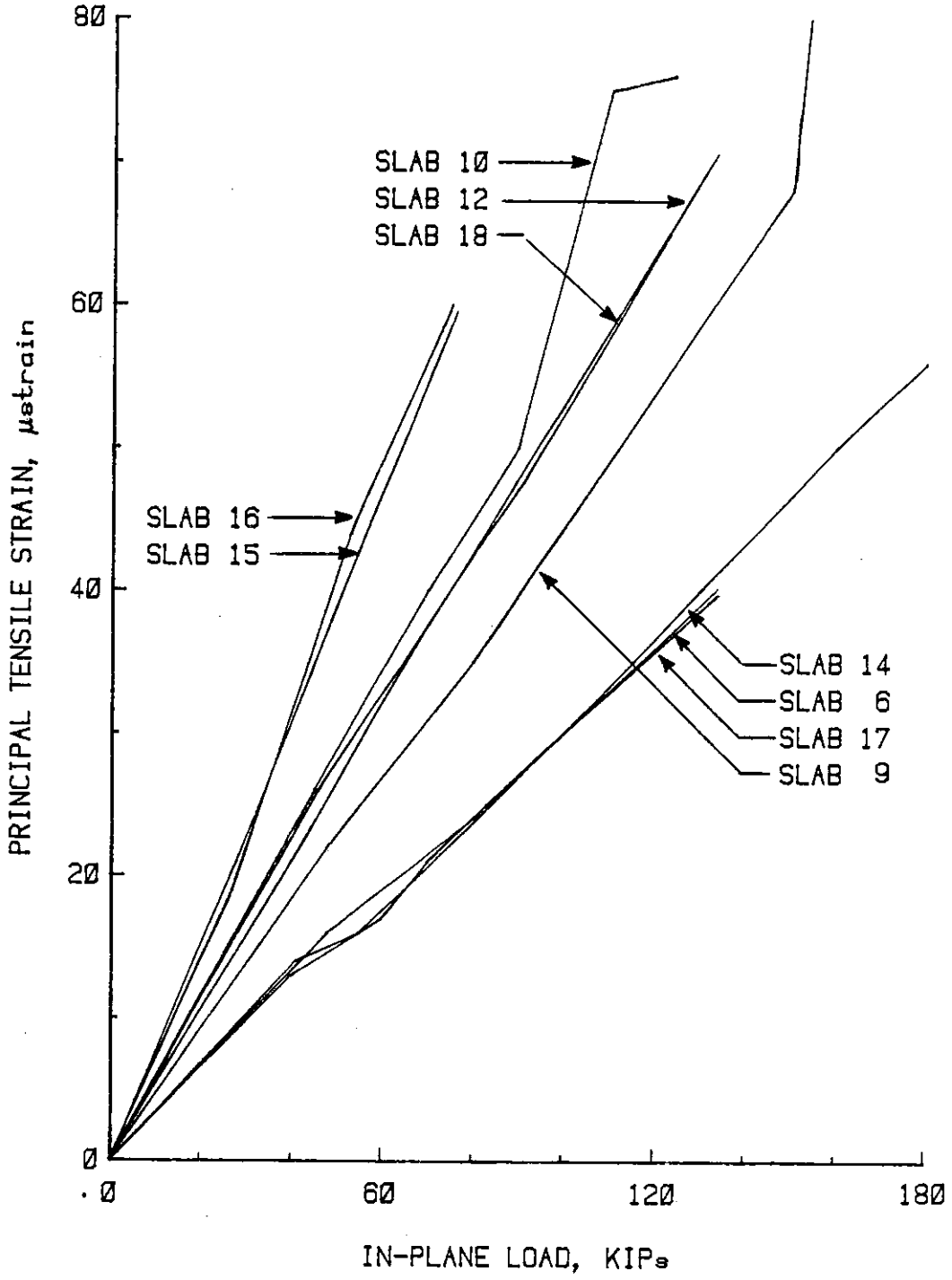

Figure 47. Principal strains caused by in-plane load

concrete and concrete compressive strength. The modulus of elasticity for concrete is related to its compressive strength according to ACI 318-83 (1).

Principal concrete surface strains near the edges were negligible when the vertical load was applied. When in-plane load was applied, these principal strains were equal to principal strains at the center of the diaphragm. The orientation of these principal strains became random and the magnitude of these strains was significantly reduced as soon as slip had occurred near the edges of the diaphragm. Embedment gages used on Slab 10 malfunctioned. Embedment gages used in the previous research effort (30) on Slabs 7 and 8 indicated that strains were constant throughout the thickness of the slab initially, but not near and not after ultimate load.

Deck strains on all diaphragms were small until slip between the deck and concrete occurred. Because of the geometry of the steel deck, strains perpendicular to the corrugations and away from the edges remained negligible throughout the entire test. Deck strains parallel to the corrugations and away from the edges remained small until ultimate load was reached and large vertical displacements occurred. After ultimate, the largest deck strains were oriented in a direction parallel to the deck corrugations. These deck strains became quite large on slabs that were subjected to vertical load. Some of these deck strains exceeded the yield strain when the frame was cycled at a displacement limit of 1.000 in.

Uniaxial strain gages mounted on the webs of the W24 X 76 edge beams were used to measure strains along the beams. These measurements were used to determine moments and axial forces along the edge beams. Axial strains measured along the edge beams while testing Slab 12 are shown in Figure 48. Results indicated that the axial load varied linearly before ultimate but became non-linear after ultimate. Based on these results, shear forces are assummed to be transferred uniformly from the beams to the diaphragm prior to ultimate load but non-uniformly after ultimate load. The proposed analysis in Section 5 does not require an understanding of this post-ultimate behavior.

4.3. Summary of Experimental Results

Ultimate loads, initial stiffnesses and failure modes are listed in Table 4. This list contains the results from all diaphragms tested to date. Ultimate loads were determined by the data acquisition system (DAS). The DAS continuously monitored the in-plane load cells and recorded the maximum load and the displacement of the load beam when maximum load was reached. Because the load program was based on displacement control, the experimental initial stiffness was defined as the slope of a line through the origin and the point on the load-displacement curve corresponding to the first nominal displacement of 0.025 in. The use of a common displacement provided for a consistent stiffness comparison for the same cycle of loading. The following

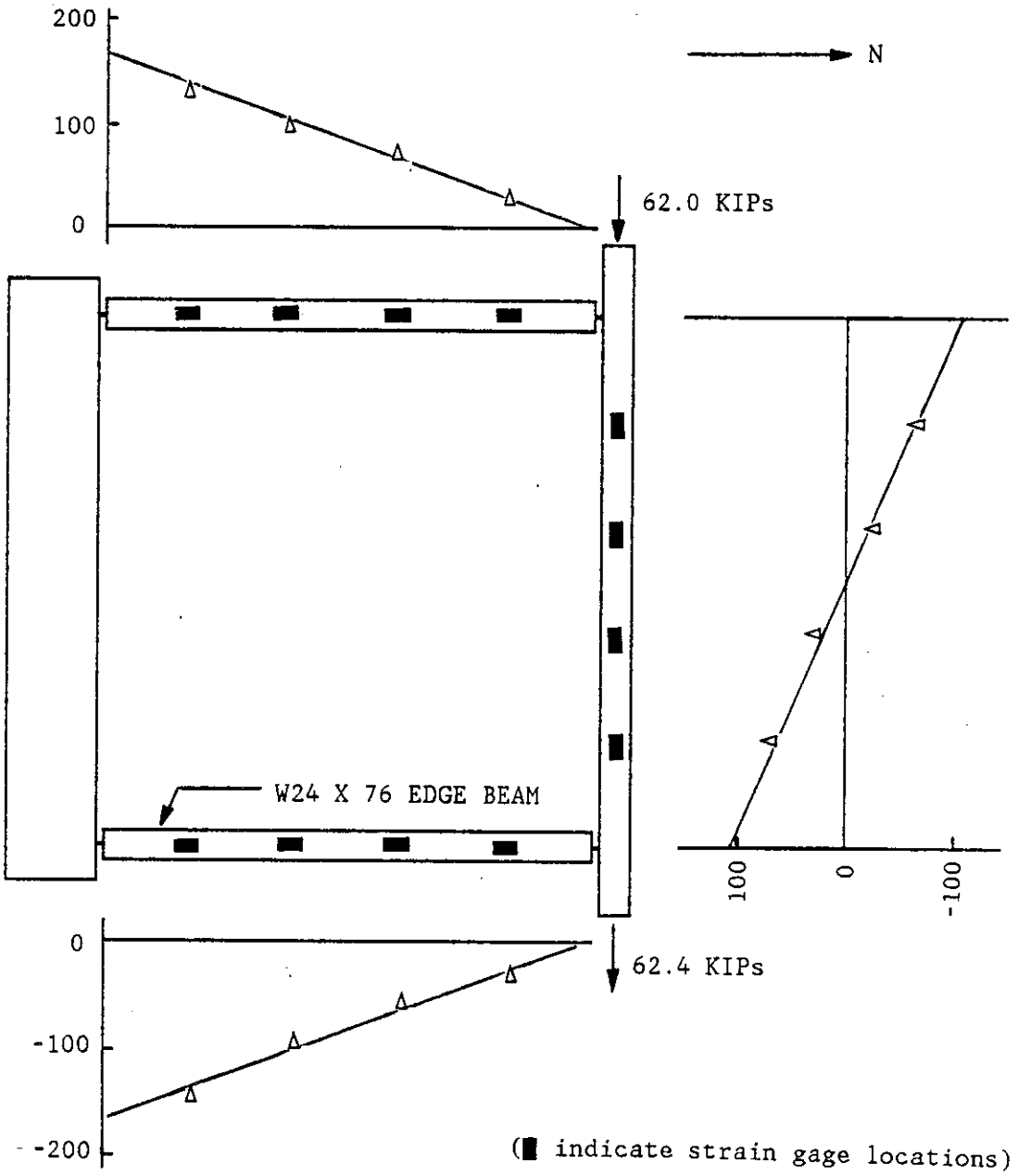

Figure 48. Axial strains along the edge beams (μstrains)

Table 4. Summary of experimental results

Slab Number	Initial Stiffness (kips/in.)	V_u (kips)	Failure Mode	Designation in Table 1
1	1800	168	Diagonal tension	1.a.1
2	2000	186	Diagonal tension	1.a.1
3	1600	97.8	Deck foldover	2.b.2
4	1300	87.7	Deck foldover	2.b.2
5	1700	116	Diagonal tension	1.a.1
6	2600	147	Interfacial shear parallel	2.a
7	1500	137	Deck foldover	2.b.2
8	1100	54.4	Edge fastener failure	3.b.2
9	1900	220	Diagonal tension	1.a.1
10	1700	161	Diagonal tension	1.a.1
11	1600	95	Interfacial shear parallel	2.a
12	1800	180	Diagonal tension	1.a.1
13	1900	250	Diagonal tension	1.a.1
14	1900	208	Interfacial shear	2.a, 2.b.1
15	1300	103	Concrete rib failure	2.b.3
16	1300	124	Diagonal tension	1.a.1
17	2200	146	Interfacial shear parallel	2.a
18	1700	161	Diagonal tension	1.a.1

section includes a summary of experimental results from slabs that are of interest to this research study.

Slabs 6 and 17 had the highest initial stiffness of all slabs tested. Both slabs failed in interfacial shear parallel to the corrugations and reached nearly the same ultimate load. The only differences between Slabs 6 and 17 was that Slab 17 was subjected to an applied vertical load of 100 psf and had a lower concrete strength than Slab 6.

Slabs 9 and 13 were the only slabs constructed using cellular deck. The primary difference between Slab 9 and Slab 13 was that Slab 13 was subjected to an applied vertical load of 200 psf prior to being loaded in-plane and Slab 9 was not. These slabs had the same initial stiffness and both failed in diagonal tension. Slab 13 had a higher concrete compressive strength and a higher ultimate capacity.

Slabs 10, 12 and 18 all failed in diagonal tension. Slabs 10 and 18 had the same initial stiffness and ultimate capacity. Slab 12 had a higher concrete strength, initial stiffness and ultimate capacity. The primary difference between Slabs 10, 12 and 18 was in the amount of applied vertical load. Slab 10 was subjected to no applied vertical load. Slabs 12 and 18 were subjected to applied vertical loads of 65 and 135 psf, respectively.

Slab 14 was constructed from the same deck type as Slabs 10, 12 and 18 but had a larger concrete thickness. Slab 14 was subjected to an applied vertical load of 135 psf prior to being loaded in-plane. Slab 14 had a higher initial stiffness than Slabs 10, 12 and 18. And

unlike the other Deck Type 5 slabs, Slab 14 failed by interfacial shear tranverse and parallel to the corrugations. Slab 14 had the highest ultimate capacity of any Deck Type 5 slab.

Slab 15 failed in interfacial shear perpendicular to the corrugations. Slab 16 was constructed exactly like Slab 15 but was subjected to an applied vertical load of 35 psf prior to being loaded in-plane. Slab 16 failed in diagonal tension. Slabs 15 and 16 had the same initial stiffness.

Vertical load had little effect on the initial stiffness of composite diaphragms. Vertical load had little effect on the ultimate capacity of diaphragms that experienced diagonal tension or interfacial shear parallel to the corrugations. Vertical load increased the capacity of composite diaphragms that experience interfacial shear transverse to the corrugations. All diaphragms experienced some parallel and transverse slip prior to ultimate. Similar diaphragms with applied vertical load experienced less transverse slip than diaphragms without applied vertical load.

To compare the degradation of stiffness, an average cyclic stiffness was defined as the slope of a line between the maximum positive and negative load values of the third cycle hysteresis loop at each displacement limit as shown in Figure 49. The stiffness degradation is illustrated in Figure 50 with a plot of cyclic stiffness versus nominal cyclic displacement. The stiffness of the slabs degraded quite rapidly. The cyclic stiffness of slabs without applied vertical load tended to degrade faster than the cyclic stiffness of similar

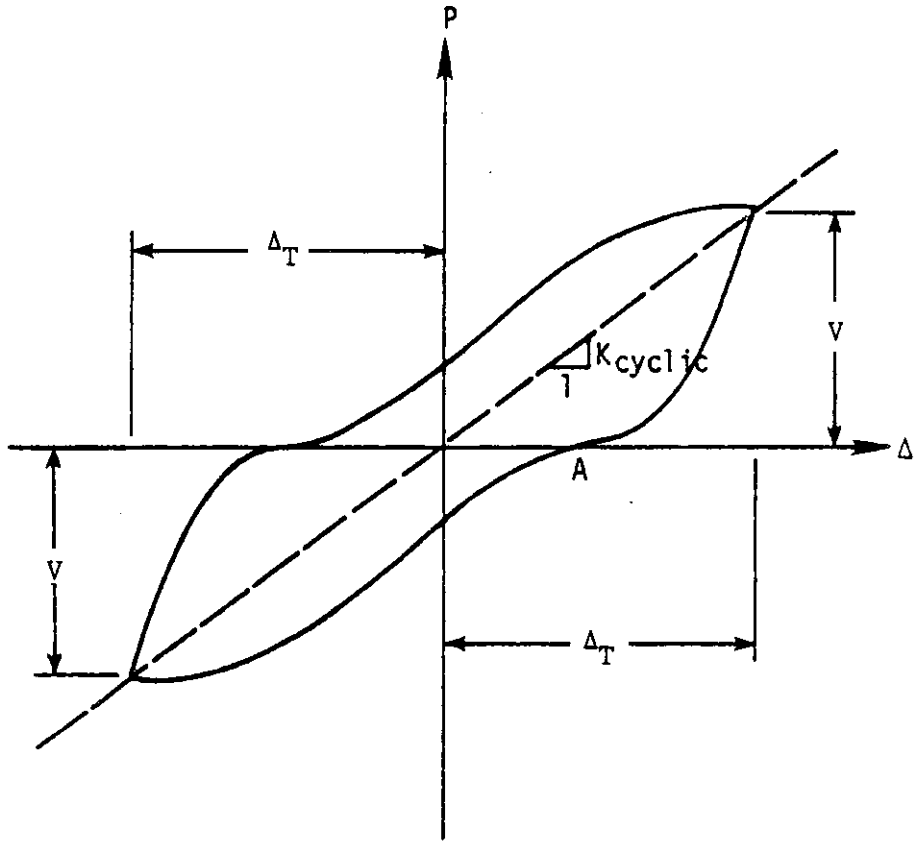

Figure 49. Calculation of average cyclic stiffness from load-displacement hysteresis loop (30)

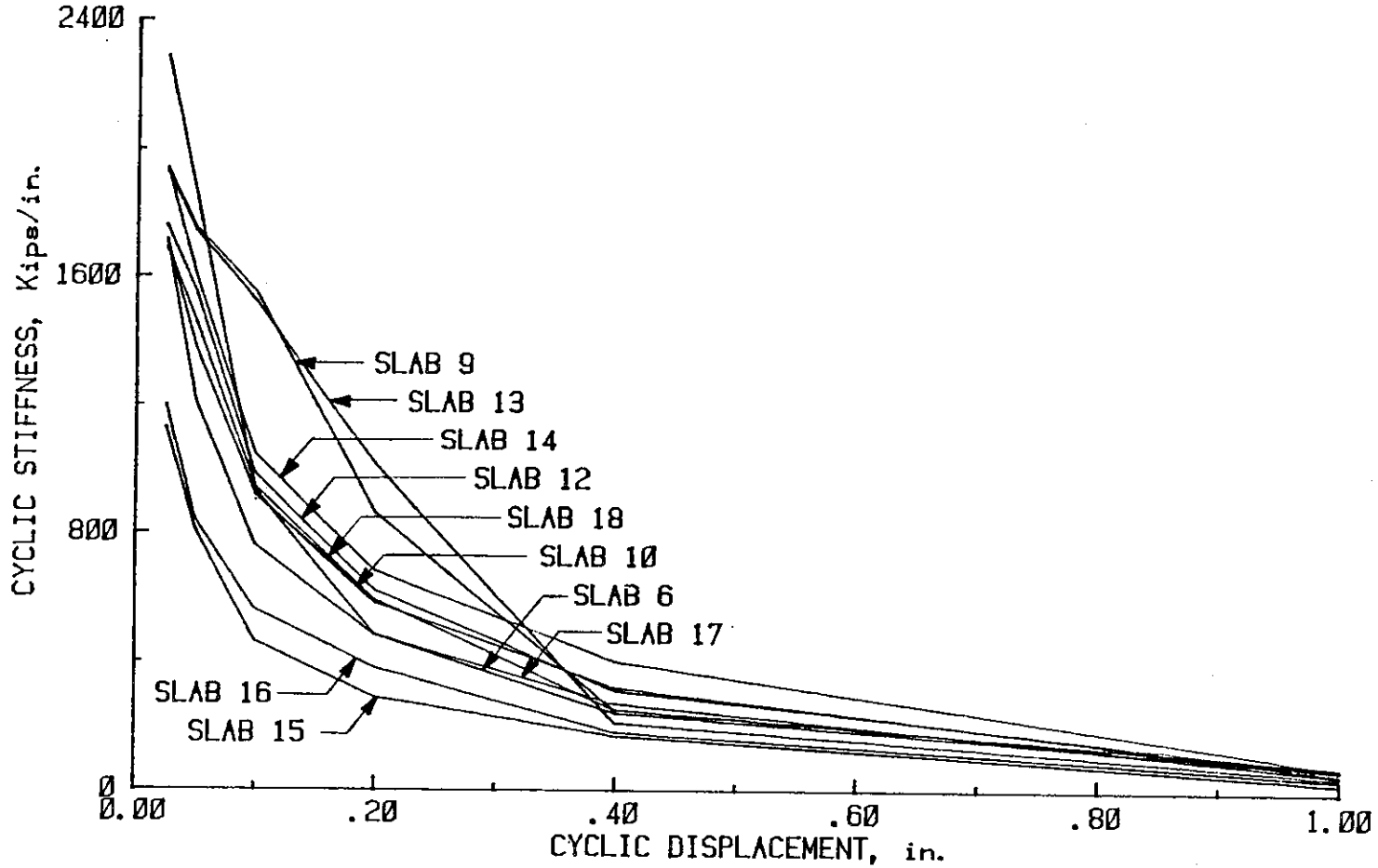

Figure 50. Stiffness degradation after three cycles of reversed loading at each displacement limit

slabs with applied vertical load. The stiffness of slabs that experienced concrete failure tended to degrade faster than the stiffness of slabs that experienced interfacial failure. Slabs that experienced interfacial failure tranverse to the corrugations had nearly the same rate of stiffness degradation as slabs that experienced interfacial failure parallel to the corrugations.

5. ANALYTICAL INQUIRY

5.1. Review of Previous Methods of Analysis

5.1.1. Methods developed for reinforced concrete diaphragms

Methods for designing reinforced concrete diaphragms were developed by the American Concrete Institute (1) and the Applied Technology Council (6). Both methods use a strength design design approach. The basic requirement for strength design is that the required strength of a structural element must be less than or equal to the design strength. Required strength is determined by multiplying expected loads by appropriate load factors. Design strength is determined by multiplying the nominal strength by an appropriate strength reduction factor.

In both methods, the nominal in-plane shear strength of a reinforced concrete diaphragm is given by

$$V = A_{cv} \left(\alpha \sqrt{f'_c}/1000 + \rho\, f_y\right) \qquad 5\text{-}1$$

where the coefficient α varies linearly from 3.0 for h/l equal to 1.5 to 2.0 for h/l equal to 2.0, f'_c is the concrete compressive strength, ρ is the shear reinforcement ratio, f_y is the specified yield strength of reinforcement and A_{cv} is the net area of concrete section bounded by web thickness and length of section in the direction of shear force considered. A strength reduction factor of 0.6 is recommended in Reference 6. Also, edges around and openings in diaphragms must be provided with boundary members unless it is shown that the unit compressive stresses are less than 0.2 f'_c at the edges, when calculated

on an elastic basis for any loading condition including earthquake effects (6). Boundary members can consist of reinforced concrete or structural steel members encased in, or continuously attached to, the diaphragm (6). Methods for determining required strength can be found in Reference 6.

5.1.2. Method developed by Pinkham

Empirical equations for predicting the stiffness and strength of steel-deck reinforced concrete diaphragms were developed by C.W. Pinkham of S.B. Barnes and associates of Los Angeles, California and were published by the Department of Defense in the Tri-Service design manual, "Seismic Design of Buildings" (12). A "guided cantilever" concept was used in the equation development. The equations, used to predict the diaphragm's strength, were based on the capacity of edge fasteners and the contribution made by the concrete across the seams.

Accurate ultimate load predictions were obtained from these equations for only a limited number of composite diaphragms (8). One possible reason for this limited accuracy is that several potential failure modes were not considered in the development of these equations. Therefore, an alternate method of analysis was proposed upon completion of the first three phases of this overall research project. A review of this alternate method is included next.

5.1.3. Method developed by ISU

An alternate method of analysis for predicting the stiffness and strength of steel-deck reinforced concrete diaphragms was included in a final report to the National Science Foundation by researchers

at Iowa State University's Engineering Research Institute (30). This method of analysis was, in part, based on the assumption that the transfer of forces from the frame to concrete slab through the interface effectively occurs within a relatively narrow band along the lengths of the edge beams. Throughout this section, interface will mean interface between the steel deck and concrete unless specified otherwise.

To calculate the initial in-plane deflections for a composite diaphragm, the diaphragm with edge beams was idealized as a plate girder. The total deflection was then given by

$$\Delta_T = \Delta_b + \Delta_s + \Delta_z \qquad 5\text{-}2$$

where Δ_b was the bending deflection of the composite diaphragm together with the edge beams acting as a plate girder, Δ_s was the shear deflection of the composite web and Δ_z was the deflection due to deformation in the "edge zone", which included the effects of fastener deformations. The bending deflection, Δ_b, at the free end of the cantilevered girder was given by

$$\Delta_b = \frac{Va^3}{3(E_c I_c + E_s I_s)} = \frac{V}{K_b} \qquad 5\text{-}3$$

where V was the applied shear force, a was the length of the cantilever, I_s was the moment of inertia of the edge beams, and I_c, the moment of of inertia of the composite web, was based on the average thickness of the concrete plus n times the thickness of the steel deck where

$n = E_s/E_c$. The shear deflection was given by

$$\Delta_s = \frac{Va}{G_c t_e b} = \frac{V}{K_s} \qquad 5\text{-}4$$

where t_e is the average thickness of the concrete plus n_s times the thickness of the deck where $n_s = G_s/G_c$ and b was the depth of the cantilevered girder. The "edge zone" deflection, Δ_z, was based on push-off test results.

Elemental push-off tests were conducted to determine the stiffness of the "edge zone" and the ultimate capacity of the interface between the steel deck and concrete. Push-off tests corresponding to both parallel and transverse sections of the composite diaphragm (Fig. 51) were conducted. The push-off model and the composite diaphragm's "edge zone" were shown to be subjected to similar interfacial stresses due to in-plane loading (30). Results from the push-off tests are given in Table 5. Table 5 includes parameters for both this ISU method and the proposed method in Section 5.3.

To develop an equation to predict the initial stiffness, the "edge zone" force distribution was assumed as shown in Figure 52. The corresponding forces on the edge members are shown in Figure 53. The "edge zone" in the linear range was idealized by a series of springs, K_t, K_t', K_p and K_p', as shown in Figure 54. The forces in Figure 53 were then written as

$$q_p = K_p\Delta_p,\ q_p' = K_p'\Delta_p,\ q_t = K_t\Delta_t,\ q_t' = K_t'\Delta_t \qquad 5\text{-}5$$

where Δ_t and Δ_p where the relative displacements between the framing

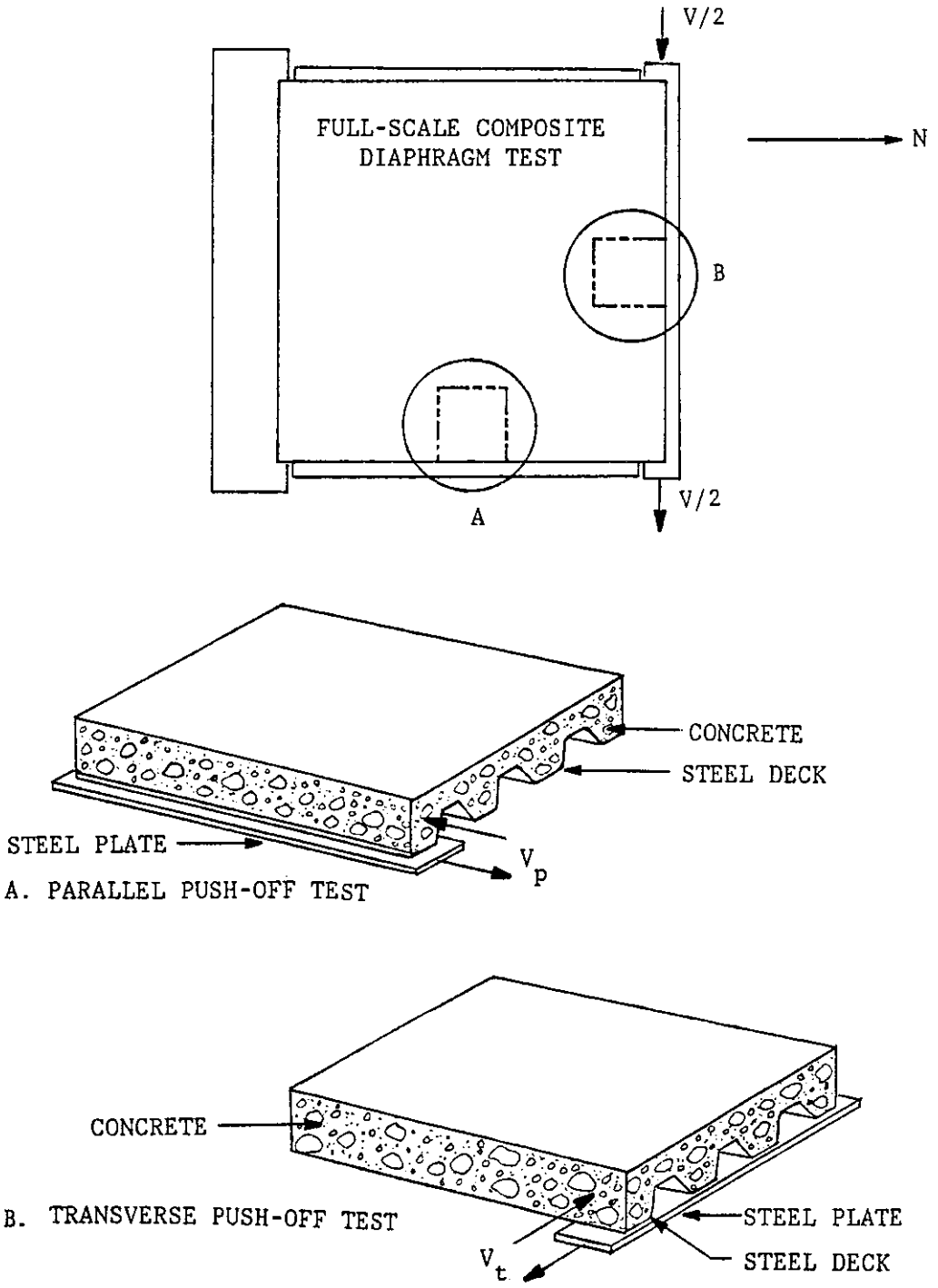

Figure 51. Composite diaphragm sections modeled with elemental push-off tests

Table 5. Results from push-off tests

Deck Type	Q_t (lb/in)	Q_p (lb/in)	σ_{ut} (psi)	σ_{up} (psi)	K_t (K/in/in)	K_p (K/in/in)	μ_t
1	454	468	25.2	26.0	47	55	0.70
2	933	493	51.8	27.4	65	42	3.53
3	-[a]	-[a]	-[a]	-[a]	-[a]	-[a]	-[a]
4	805	773	44.7	42.9	63	37	2.31
5	627	625	34.8	34.7	72	60	2.54
6	521	293	28.9	16.3	68	46	0.70
7	531	563	29.5	31.3	46	63	1.01

[a]Data not available due to a shortage of this deck type.

members and a rigid slab. From statics, the following equations were developed

$$V = (K_t b + K_t, l_t)\ \Delta_t \qquad 5\text{-}6$$

$$V = (K_p b + K_p, l_p)\ \Delta_p \qquad 5\text{-}7$$

where V is the applied shear force, $l_t = a' - 2a'^2/3a$ and $l_p = (b^2 + 3bb' - 2b'^2)/6a$. The values of a' and b' were taken as b/12 and a/12, respectively. Assuming small displacements, the relationships between Δ_t, Δ_p and Δ_z were given by

$$\Delta_t = \Delta_z/2 + \theta a/2 \qquad 5\text{-}8$$

$$\Delta_p = -\theta b/2 \qquad 5\text{-}9$$

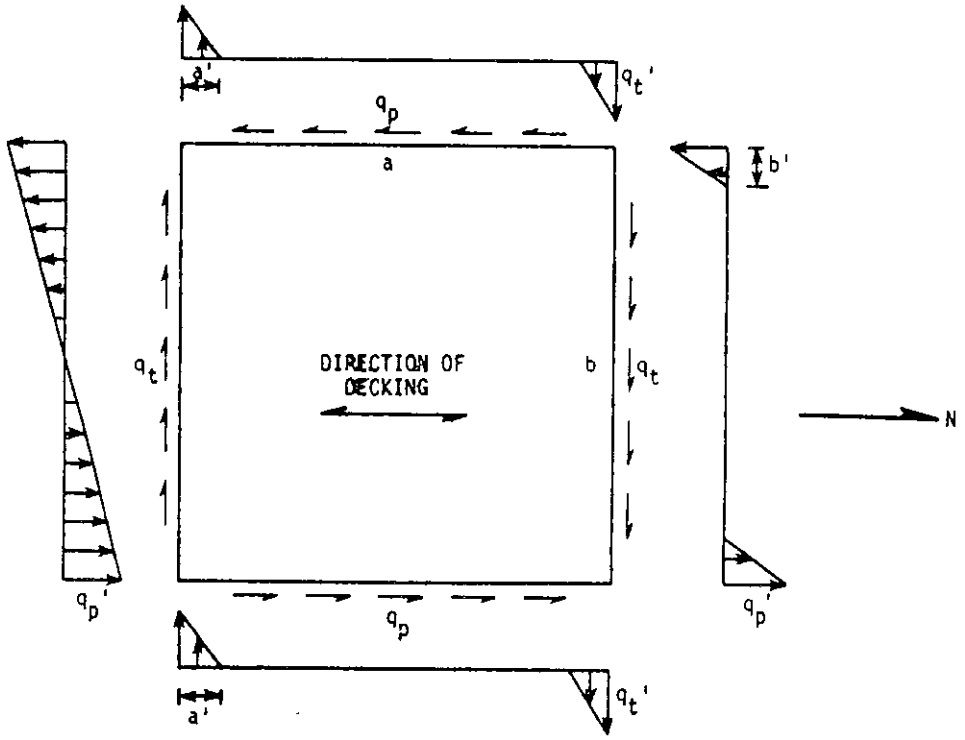

Figure 52. Interfacial edge forces (30)

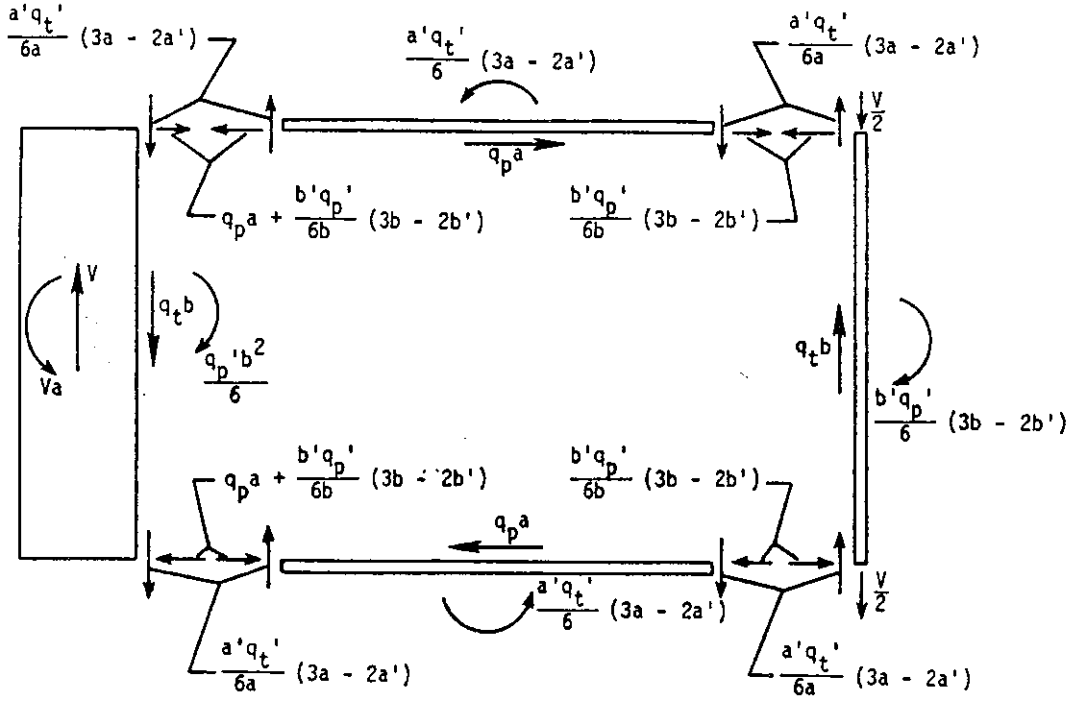

Figure 53. Edge member forces (30)

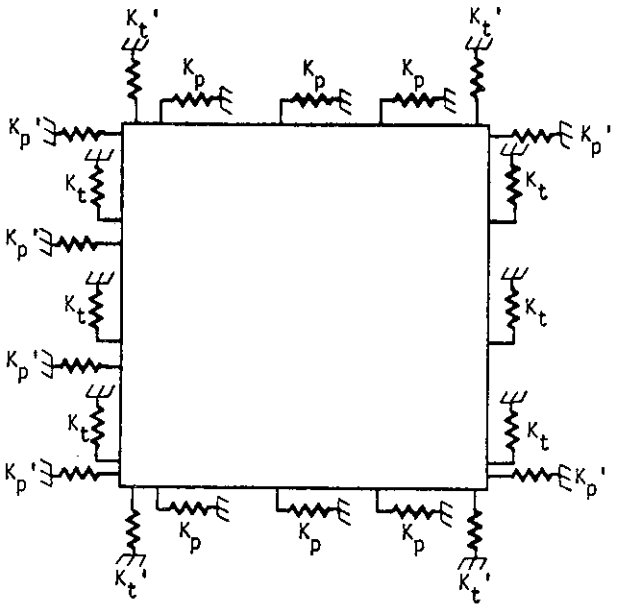

Figure 54. Idealized spring stiffness of edge zone (30)

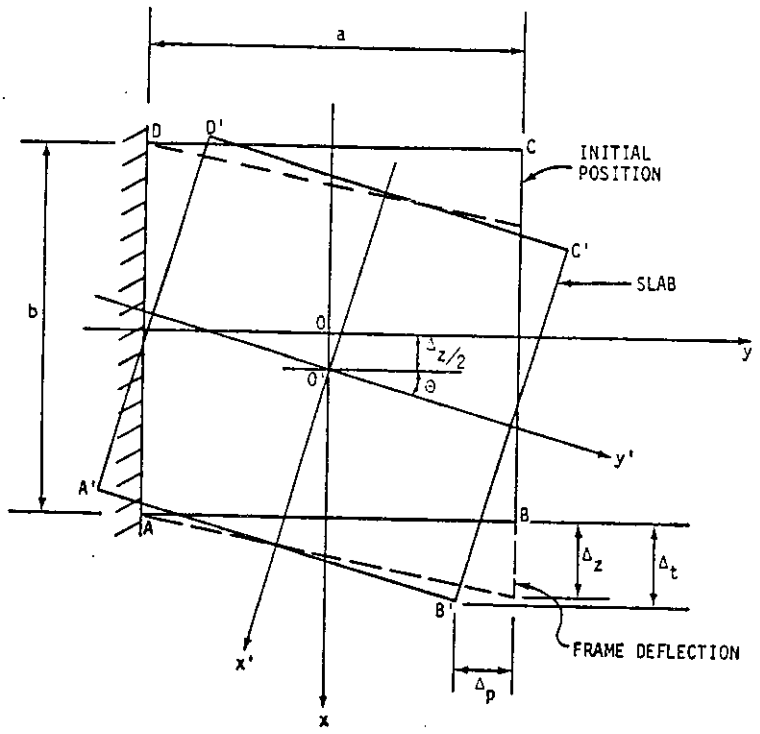

Figure 55. Displacement of slab with respect to frame (30)

where θ is the rotation of the concrete about its center as shown in Figure 55. This figure indicates that slip is measured relative to the frame in its original position. An accurate figure would indicate that slip is measured relative to the frame in its displaced position. Also, this figure indicates that the concrete slab rotates more than the frame. Experimental results indicate that the concrete slab moves relative to the frame and steel deck as shown in Figure 56. By using this figure, the relationships between Δ_t, Δ_p and Δ_z are given by the following equations.

$$\Delta_t = \Delta_z/2 - \theta a/2 \qquad 5\text{-}10$$

$$\Delta_p = \theta b/2 \qquad 5\text{-}11$$

By using either equations 5-8 and 5-9 or 5-10 and 5-11 and eliminating θ, the following equation for Δ_z in terms of Δ_p and Δ_t is developed

$$\Delta_z = 2(\Delta_t + a\Delta_p/b) \qquad 5\text{-}12$$

Finally, by substituting for Δ_p and Δ_t in Equation 5-12 and assuming that $K_t = K_t'$ and $K_p = K_p'$, the "edge zone" deflection was given by the following equation.

$$\Delta_z = \frac{2V}{K_t(b + l_t)} + \frac{2Va}{K_p(b^2 + b\, l_p)} = \frac{V}{K_z} \qquad 5\text{-}13$$

The stiffness factors K_p and K_t were obtained from push-off tests and are listed in Table 5. Since no push-off tests were performed on studded specimens, the values of K_p and K_t for studded slabs were

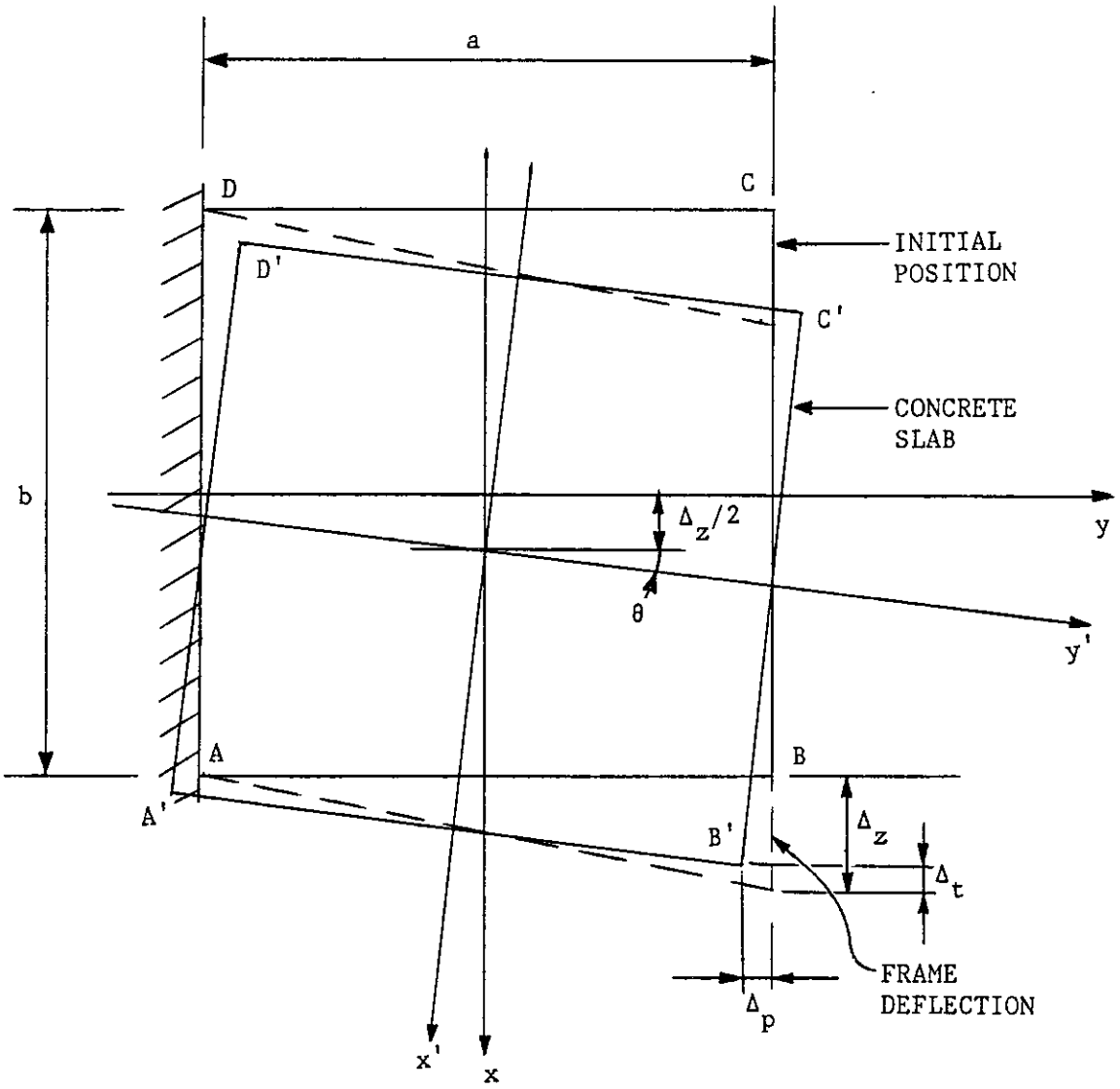

Figure 56. Displacement of slab with respect to frame

calculated using empirical load-slip equations for studs developed by Ollgaard, Slutter and Fisher (22). The total initial stiffness of the composite diaphragm was given by

$$K_T = \frac{1}{\frac{1}{K_b} + \frac{1}{K_s} + \frac{1}{K_z}} \qquad 5\text{-}14$$

where K_b is the bending stiffness of the composite diaphragm together with edge beams acting as a plate girder, K_s is equal to the shear stiffness of the composite web and K_z is equal to the "edge zone" stiffness.

The ultimate capacity of composite diaphragms was expected to be limited by one of three things: the shear capacity of the concrete web, the capacity of the interface between the concrete and the steel deck or the strength of the edge fasteners. Ultimate capacity based on diagonal tension failure of the concrete web was calculated using the shear wall equation from the American Concrete Institute (ACI) Code 318-83 (1). Assuming no axial loads, this equation was written as

$$V = 3.3 \sqrt{f'_c}\ h\ d\ /\ 1000 \qquad 5\text{-}15$$

In applying this equation, h was taken as the effective concrete thickness, t_e, where $t_e = t_a + n_s t_s$ and the value of d was taken as the width of the diaphragm. Equation 5-15 was then written as follows.

$$V = 3.3 \sqrt{f'_c}\ t_e\ b\ /\ 1000 \qquad 5\text{-}16$$

To predict the capacity of diaphragms that experience interfacial failure at ultimate, the "edge zone" force distribution was assumed to approach that shown in Figure 57 at ultimate load. The related forces on the framing members are shown in Figure 58. From statics, the following equations were developed

$$V = q_t\ b + q_{t'}\ l_{t'} \qquad 5\text{-}17$$

$$V = q_p\ b + q_{p'}\ l_{p'} \qquad 5\text{-}18$$

where $l_{t'} = 2a' - 2a'^2/a$ and $l_{p'} = (b^2 + 4bb' - 4b'^2)/4a$. The limiting values of q_t and $q_{t'}$ were assumed to be equal to Q_t, the maximum load from the transverse push-off tests. The limiting value of q_p was assumed to be Q_p, the maximum load from the parallel push-off tests. The limiting value of $q_{p'}$ was assumed to be the sum of two forces. The first of these two forces was the cohesion between the concrete and steel deck. The second of these forces was a frictional force, equal in magnitude to the normal force against the up corrugations, q_t, times the coefficient of friction between the steel deck and concrete. In equation form.

$$Q_{p'} = Q_p + \mu\ q_t \qquad 5\text{-}19$$

By substitution of Equation 5-17 into Equation 5-19 and assuming that $q_t = q_{t'}$, the following equation was obtained

$$Q_{p'} = Q_p + \frac{\mu V}{(b + l_{t'})} \qquad 5\text{-}20$$

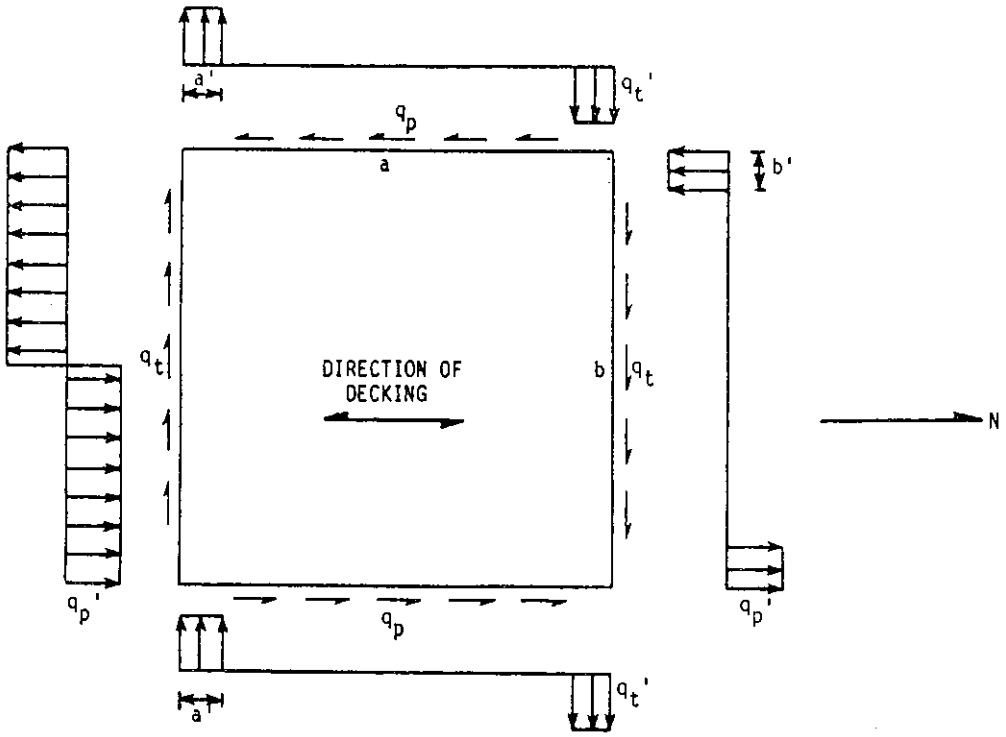

Figure 57. Assumed edge force distribution at ultimate (30)

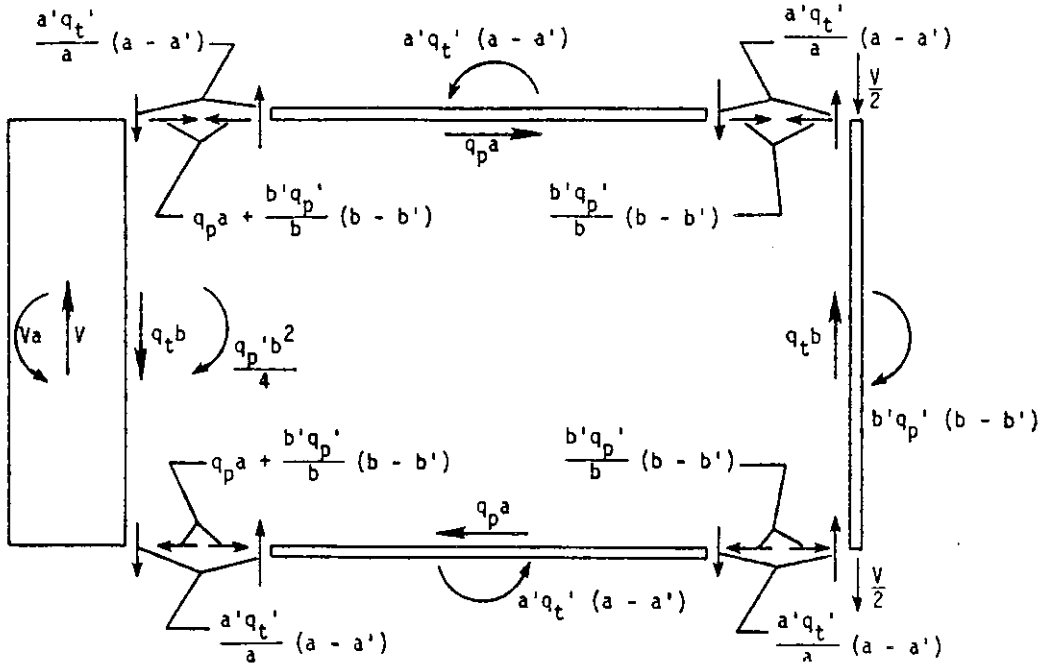

Figure 58. Edge member forces at ultimate (30)

where V is the applied shear force on the diaphragm and Q_p is the maximum load per unit length from the parallel push-off tests. Finally, the ultimate capacity of diaphragms that experience interfacial shear failure at ultimate was given by the following equation.

$$V = \text{minimum} \begin{cases} Q_t (b + l_{t'}) \\ Q_p \left[\dfrac{(b + l_{p'})\ (b + l_{t'})}{(b + l_{t'} - \mu l_{p'})} \right] \end{cases} \qquad 5\text{-}21$$

A value of 0.7 was used for μ based on ACI 318-83, 11.7.5 (1).

The ultimate capacity based on edge fastener capacity was determined by assuming that the force distribution shown in Figure 57 existed at ultimate. Ultimate capacity was assumed to be controlled by either edge fastener capacity in the corners or along the edge beams depending on the edge fastener spacing. The edge fasteners near the corners were expected to fail if the vector sum of perpendicular forces acting on them exceeded their capacity. The capacity of edge fasteners near the corners in the perpendicular "edge zone" was given by

$$V = \frac{Q_{ut}}{\left[\left(\dfrac{b}{(b + l_{t'})\ n_b} \right)^2 + \left(\dfrac{l_c}{(b + l_{p'})\ n_c} \right)^2 \right]^{1/2}} \qquad 5\text{-}22$$

where Q_{ut} is the ultimate strength of a fastener with the deck perpendicular to the edge, n_b and $n_{b'}$ are the numbers of fasteners in lengths b and l_c, respectively, and l_c was taken as b' or the distance from the

edge of the slab to a point halfway between the connectors at the corner and the middle connectors, whichever is less. The ultimate capacity of fasteners, near the corners, in the parallel "edge zone" was given by

$$V = \frac{Q_{up}}{\left[\left(\frac{a}{(b + l_{p'})\ n_a}\right)^2 + \left(\frac{a'}{(b + l_{t'})\ n_{a'}}\right)^2\right]^{1/2}} \qquad 5\text{-}23$$

where n_a and $n_{a'}$ are the numbers of connectors in lengths a and a', respectively, and Q_{up} is the ultimate strength of a fastener with the deck parallel to the edge. Also, if there were enough middle fasteners to carry additional load after the corner fasteners had failed, the ultimate capacity was given by

$$V = Q_{up}\ (n_a - 2n_{a'}) \qquad 5\text{-}24$$

When studs were used, Q_{up} and Q_{ut} were determined using empirical equations for studs developed by Ollgaard, Slutter and Fisher (22). When arc spot welds were used, Q_{ut} and Q_{up} were assumed to be equal to Q_u, the ultimate strength of one weld. The ultimate strength of one weld was determined using AISI and AWS specifications (3, 9) and was given by

$$Q_u = \text{minimum} \begin{cases} 2.2\ t_s\ d_a\ \sigma_{ult} & \text{tearing of the deck} \\ \\ \pi\ d_e^{\,2}\ F_{xx}/4 & \text{shearing of the weld} \end{cases} \qquad 5\text{-}25$$

where t_s is equal to the net thickness of the deck (single or double

sheet minus any coatings), d_a is equal to the average diameter of the weld (surface diameter minus the thickness of the deck), σ_{ult} is the ultimate tensile strength of the steel, d_e is the effective diameter of fused weld area (0.7 x surface diameter minus 1.5 x deck thickness), and F_{xx} is the arc spot weld strength level designation in AWS electrode classification. Finally, the ultimate strength based on edge fastener failure was given by the following equation.

$$V = \text{minimum} \begin{cases} \text{Equation 5-22} \\ \text{maximum} \begin{cases} \text{Equation 5-23} \\ \text{Equation 5-24} \end{cases} \end{cases} \qquad 5\text{-}26$$

This ISU method of analysis considers several potential failure modes. The equations usually produced reasonable predictions of the diaphragm's initial stiffness and ultimate capacity. A critical review of this method of analysis is included next.

The equation used to predict the ultimate capacity based on diagonal tension failure of the concrete web is a modified version of the shear wall equation from the ACI Code 318-83 (1). This shear wall equation was based on the assumption that failure occurs when a maximum principal tensile stress of $4\sqrt{f'_c}$ is reached (11). In a shear wall, the shear stress distribution was assumed parabolic with the maximum shear stress as a function of load given by the following equation

$$v_{max} = 3\ V\ (1000)\ /\ 2\ 1\ h \qquad 5\text{-}27$$

where l is the width of the shear wall and h is the depth. By substituting d/0.8 for l and $4\sqrt{f'_c}$ for v_{max}, the shear wall equation was developed.

$$V = \frac{2}{3}\frac{4}{0.8}\frac{\sqrt{f'_c}}{1000} h\,d \cong 3.3\,\frac{\sqrt{f'_c}}{1000} h\,d \qquad 5\text{-}28$$

This empirical equation would only apply to composite diaphragms if all the assumptions made in its development were still valid. Because of the relatively large edge beams on the test frame, the actual shear distribution, in the concrete slab, is nearly uniform and not parabolic. Therefore, this shear wall equation does not apply to composite diaphragms with large edge beams. Also, in applying the shear wall equation, h was taken as the effective concrete thickness, t_e, where t_e was equal to $t_a + n_s t_s$ where t_a is the average thickness of the concrete, n_s is the ratio of shear moduli for the steel deck and concrete, and t_s is the thickness of the steel. By including the term, $n_s t_s$, an assumption that the steel is straining as much as the concrete in shear at ultimate has been made. A new, alternate assumption would be that when diagonal tension failure of the concrete web occurs, localized interfacial failure (in a narrow band on either side of the diagonal tension crack) occurs simultaneously. The interfacial capacity of this narrow band is assumed as small when compared with the capacity of the concrete.

Interfacial shear capacity equations used results from elemental push-off tests to predict the interfacial capacity of the composite

diaphragms. To be valid, these equations must consider any differences that exist between the push-off model and the composite diaphragm. The "edge zone" in the composite diaphragm and the push-off model were shown to be subjected to similar in-plane loads (30). However, no consideration of vertical loads was included. The transverse push-off model is not subjected to nearly the same amount of vertical load as the transverse "edge zone" of the composite diaphragm. The effect of vertical load needs to be included in the predictive equations.

The edge fastener capacity equations seem to produce reasonable predictions. However, since failure of the edge fasteners has controlled the ultimate capacity only once, no evaluation of the validity of these equations was made. These proposed equations were tentative.

Results from the composite diaphragm tests, reported in Chapter 4, indicated that vertical load had no significant effect on the initial stiffness of composite diaphragms. The ISU method of analysis produced reasonable predictions of the diaphragm's initial stiffness. Therefore, no alternate methods for predicting the initial stiffness of composite diaphragms were developed as part of this study. These experimental results also indicated that gravity load had a significant effect on the ultimate capacity of some composite diaphragms, depending on the mode of failure. This gravity load effect was not considered in the ISU method of analysis. Therefore, an alternate method of analysis for predicting the ultimate capacity of composite diaphragms was developed and is included next.

5.2. Proposed Method of Analysis

This proposed method of analysis is based on the following assumptions. The ultimate capacity of composite diaphragms can be limited by the capacity of the concrete slab, steel deck, support beams or the interfaces between these elements. The interfaces are idealized as sets of translational springs oriented normal to the plane of the interface and parallel and perpendicular to the corrugations in the plane of the interface. In-plane loads are transferred from the support beams through the interface between the support beams and the steel deck, through the steel deck, through the interface between the steel deck and concrete, and into the concrete slab as in-plane shear.

Diagonal tension failure of the concrete slab occurs when the tensile strength of the concrete is exceeded. Several empirical equations that relate the tensile strength of concrete to its compressive strength have been developed (23). An empirical equation developed by Cardenas, Hanson, Corley and Hognestad (11) for shear walls, states that web-shear failure occurs when a principal tensile stress of $4\sqrt{f'_c}$ causing web-shear cracking is reached. This empirical equation was based on the results from several different research projects on shear walls and is used as the basis for the shear wall equation currently used in the ACI Code 318-83 (1).

To develop an equation to predict the capacity of diaphragms that experience diagonal tension failure of the concrete web, the

stress distribution, in the concrete slab, was assumed to be uniform (Fig. 59) at ultimate. With this stress distribution, the concrete is subjected to a uniform shearing stress distribution on any plane oriented parallel to the edges of the concrete slab. Principal tensile and compressive stresses, equal in magnitude to the shearing stresses, are assumed to occur on planes oriented 45° from the edges of the concrete slab (Fig. 59). Failure of the concrete web is assumed to occur when the maximum shearing stress and principal stresses reach a magnitude greater than or equal to $4\sqrt{f'_c}$. With these assumptions, the ultimate capacity of diaphragms that fail in diagonal tension is given by

$$V = 4\sqrt{f'_c}\ t_a\ b\ /\ 1000 \qquad 5\text{-}29$$

where V is the predicted capacity, f'_c is the concrete compressive strength, t_a is the average thickness of the concrete, b is the width of the diaphragm, and 1000 is a conversion factor from pounds to kips. Experimental results, reported in Section 4, indicated that vertical load had no significant effect on the ultimate capacity of diaphragms that experience diagonal tension failure. Therefore, no consideration of flexural stresses caused by vertical load were included in the development of Equation 5-29.

When interfacial shear failure transverse to the corrugations occurs, the frame moves relative to the concrete as shown in Figure 60. When non-cellular deck types are used, movement between the steel

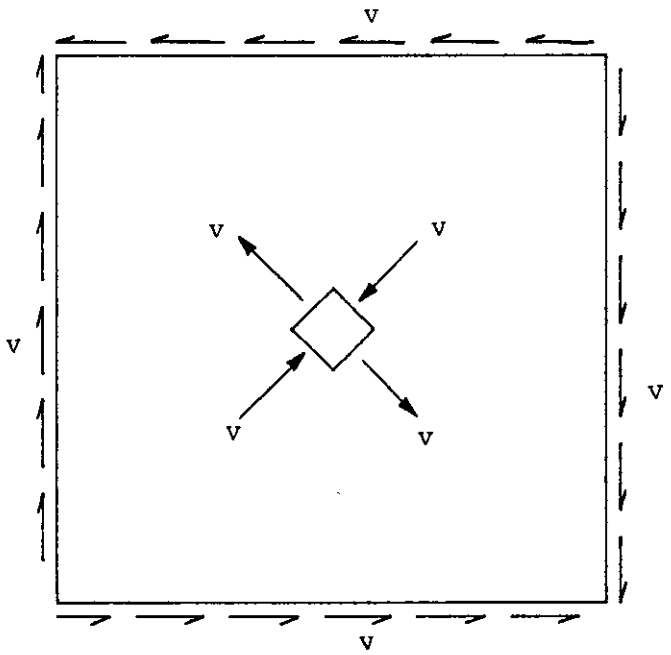

Figure 59. Stresses on the concrete slab

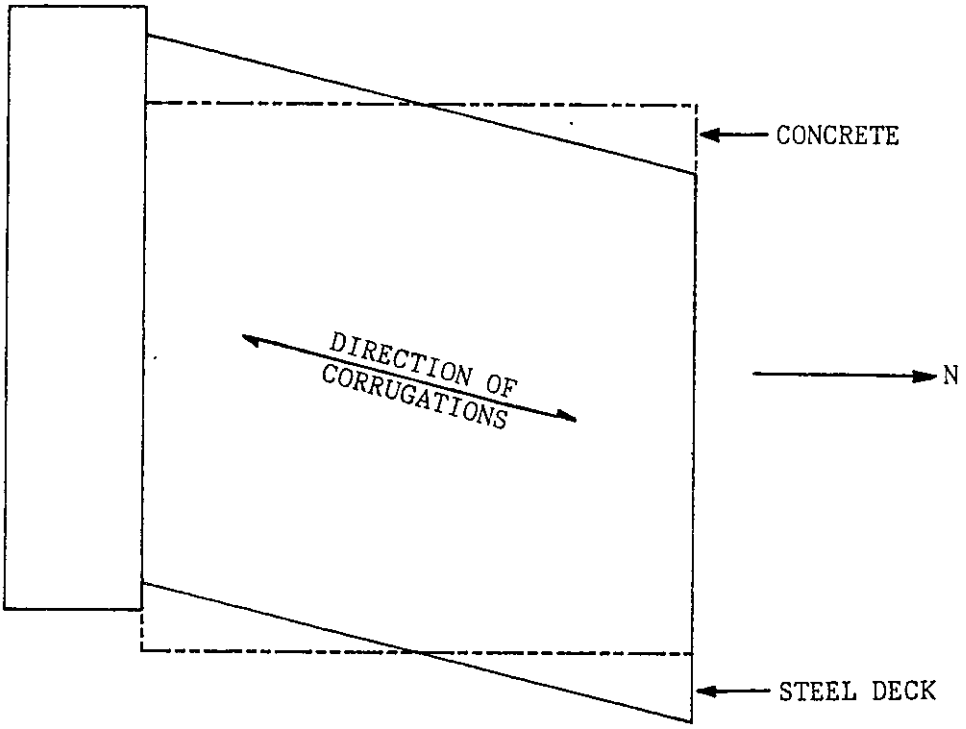

Figure 60. Interfacial failure perpendicular to the corrugations

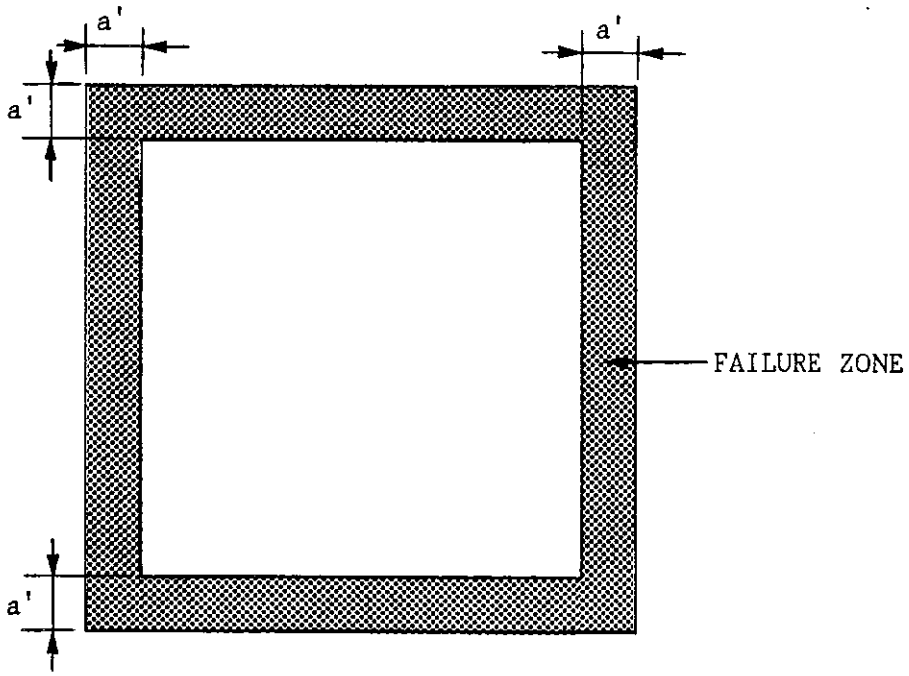

Figure 61. Interfacial failure zone

deck and concrete is assumed to occur only in the "edge zone" (Fig. 61). This behavior occurs because the steel deck is not as strong as the interface perpendicular to the corrugations.

Elemental tests were conducted to determine the stiffness and strength of the interface between the steel deck and concrete. The transverse elemental tests are assumed to model a section along the north or south edges of the composite diaphragm (Fig. 51). On the elemental specimens, the deck moves relative to the concrete as shown in Figure 62. The "edge zone" width, a', varied with deck type but was approximately equal to 18 in. for all non-cellular deck types. A typical load-displacement curve from a transverse push-off test is shown in Figure 63. Transverse interfacial stresses and edge forces on the steel deck are assumed to be as shown in Figure 64 when Point A on the load-displacement curve (Fig. 63) is reached. While moving to Point B on the load-displacement curve, additional interfacial area reaches ultimate. At ultimate (Point B) on the load-displacement curve, the transverse interfacial stress distribution is assumed to approach that shown in Figure 65. Interfacial stresses parallel to the corrugations existed but are not shown on this figure. Based on this stress distribution, the ultimate interfacial capacity transverse to the deck corrugations per unit of projected area is given by

$$\sigma_{ut} = Q_t / a' \qquad 5\text{-}30$$

where Q_t is the force per unit length required to cause failure of the elemental push-off tests. This force per unit length, Q_t,

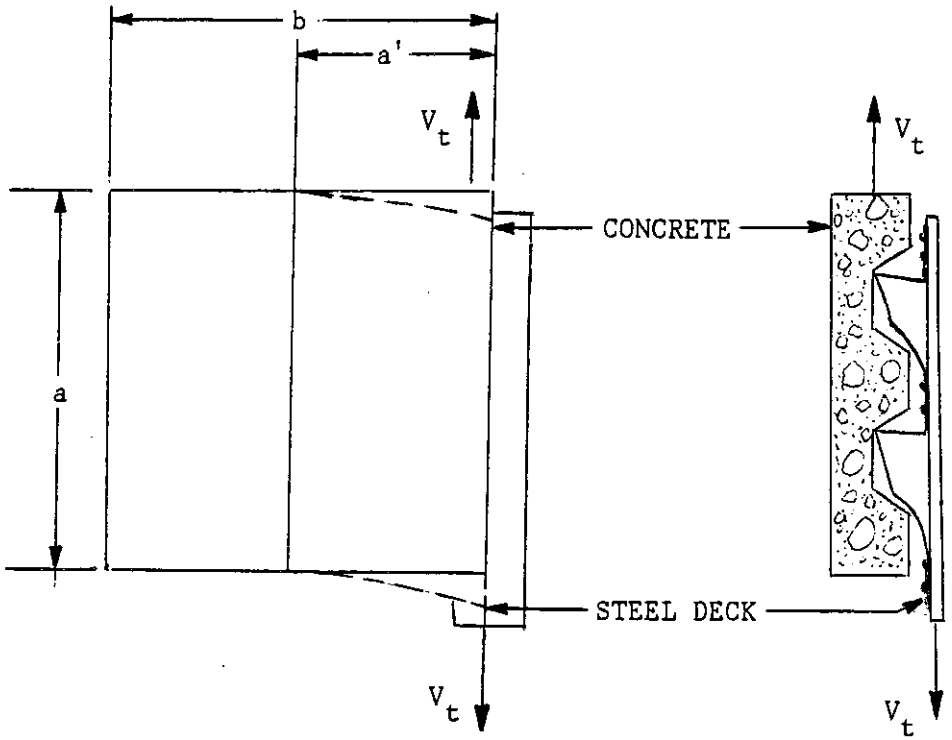

Figure 62. Elemental transverse push-off test

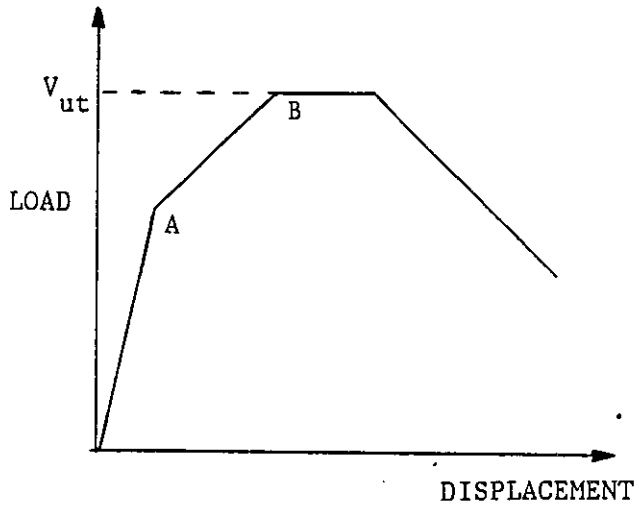

Figure 63. Load-displacement diagram from transverse push-off test

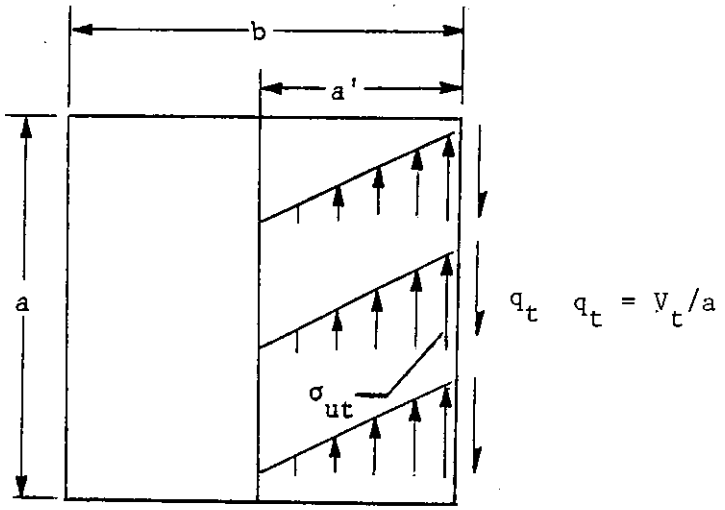

Figure 64. Transverse interfacial stresses and edge forces on the steel deck corresponding to Point A on the load-displacement diagram from push-off test

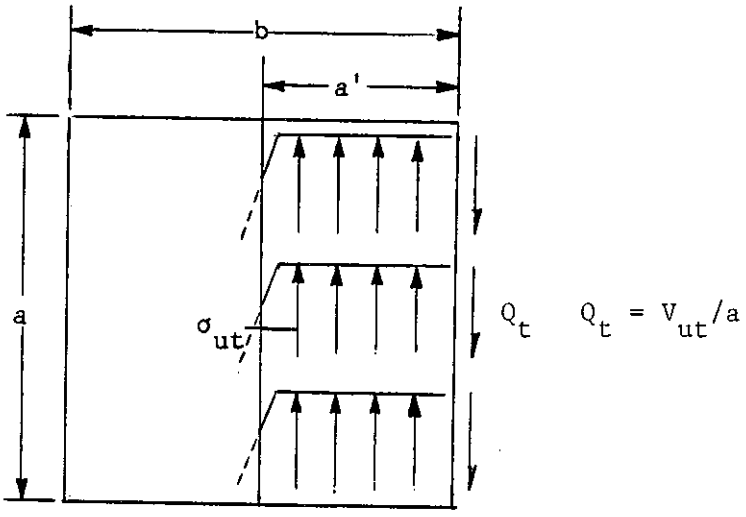

Figure 65. Transverse interfacial stresses and edge forces on the steel deck corresponding to Point B (ultimate) on the load-displacement diagram from push-off test

actually represents the force required to cause interfacial failure and to deform the steel deck. By using the above equation, the force required to deform the steel deck is included as part of the expected interfacial capacity.

On composite diaphragms, the interface between the steel deck and concrete is idealized as a series of translational springs. With this idealization, interfacial stresses only exist in areas where interfacial movement occurs and the amount of interfacial stress is directly related to the amount of interfacial movement. When interfacial failure transverse to the corrugations occurs, the transverse interfacial stresses on the steel deck only exist in the "edge zone" (Fig. 66). Parallel interfacial stresses exist but are not shown on this figure. The corresponding forces on the edge beams are shown in Figure 67. By summing forces on the north edge beam in the transverse direction, an equation for the ultimate capacity of composite diaphragms that experience interfacial failure, transverse to the corrugations, is developed

$$V = \sigma_{ut} a'(b + 4(a/2-a')^2/3a) \qquad 5\text{-}31$$

where σ_{ut} is the ultimate capacity of the interface per unit of projected area and a' is the transverse "edge zone" width.

This prediction for diaphragms that experience interfacial shear failure transverse to the corrugations must be corrected for a difference in out-of-plane stress that exists between the push-off

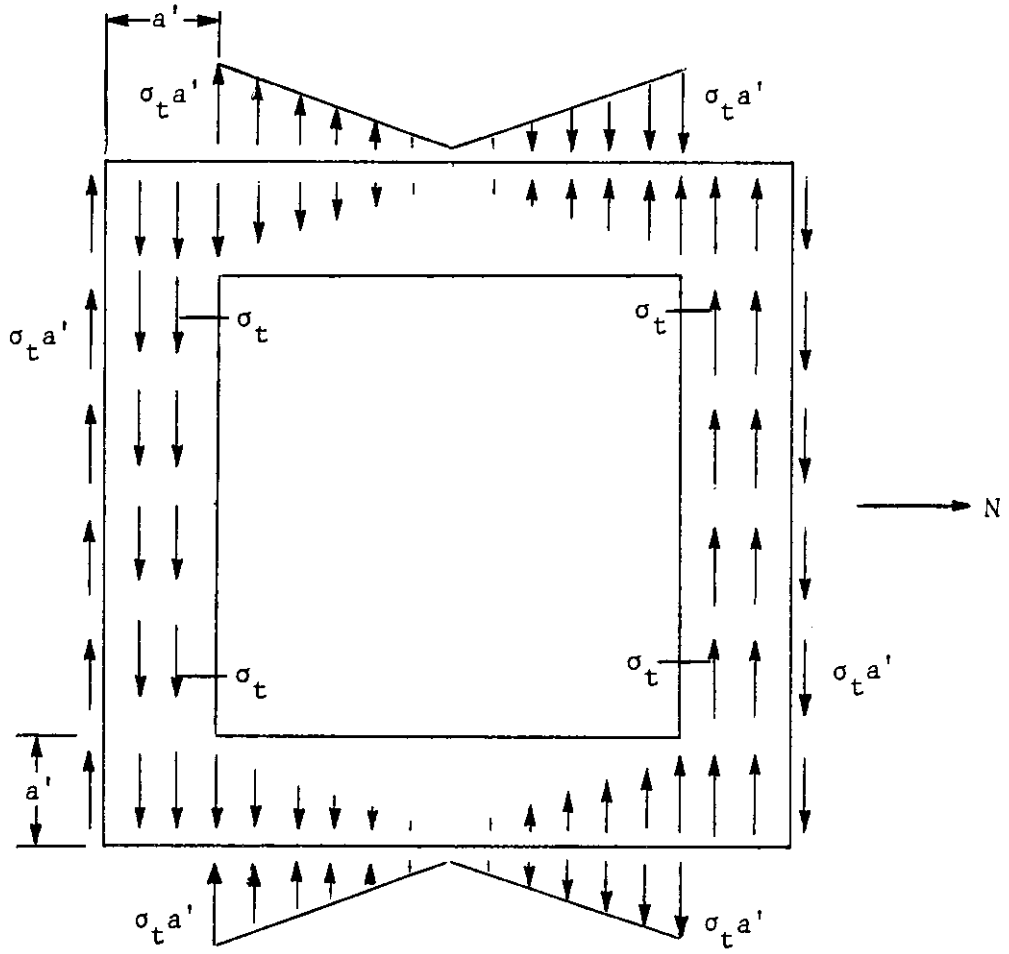

Figure 66. Transverse interfacial stresses and edge forces on the steel deck

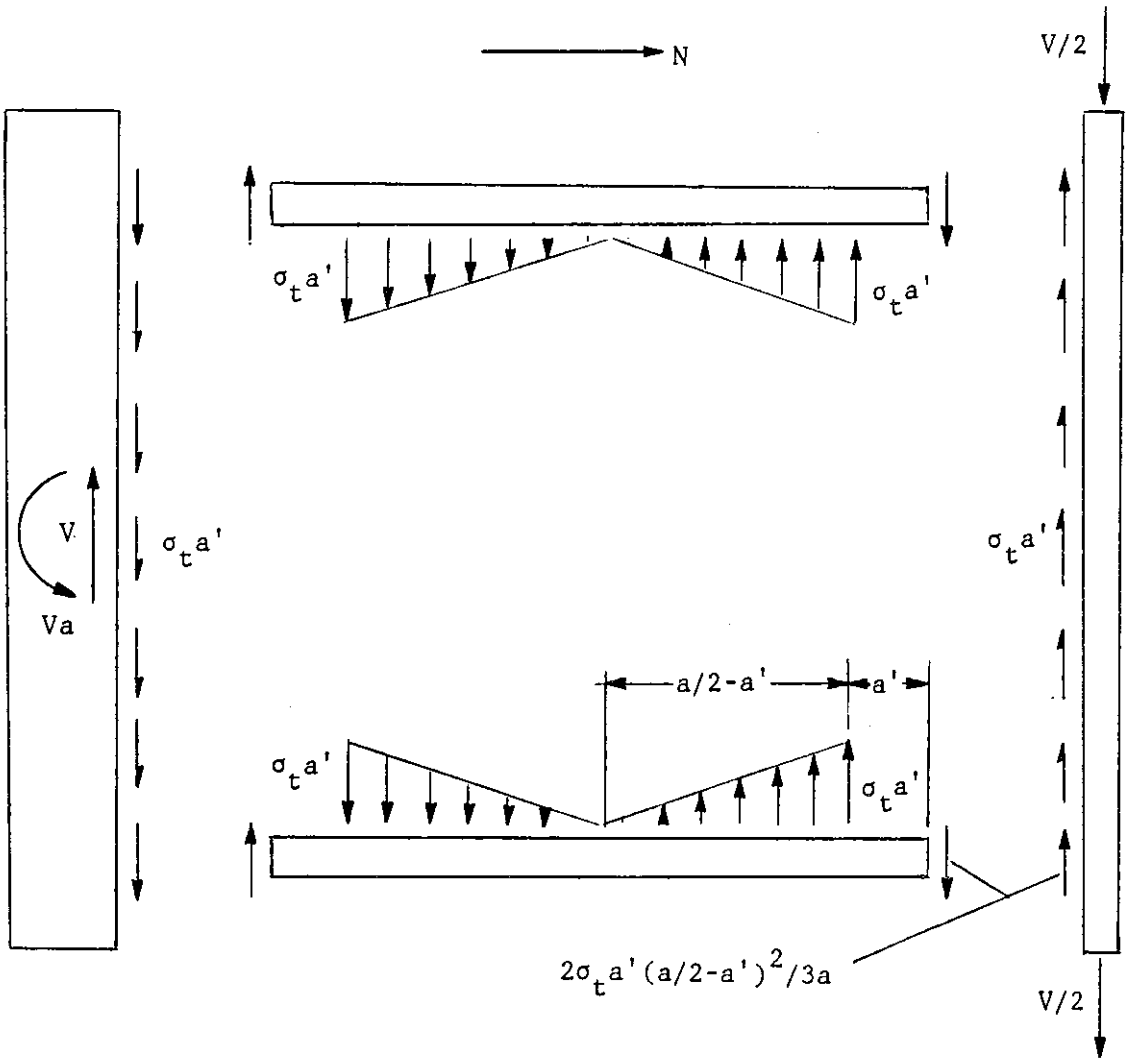

Figure 67. Transverse forces on the edge beams

model and the composite diaphragm. Previous research has shown that steel-deck reinforced concrete slabs, simply supported on all four sides, behave as one-way slabs (29). By assuming that vertical load is transferred in one direction through the interface in the transverse "edge zone", the normal load transferred through the interface at each end is given by

$$(w_c + w_l)\ b\ a\ /\ 2 \qquad 5\text{-}32$$

where w_c is the weight of the concrete in ksi and w_l is any applied vertical load in ksi. Then, the shear required to cause interfacial shear failure, transverse to the corrugations, is given by the following equation

$$V = \sigma_{ut} a'(b + 4(a/2 - a')^2/3a) + \mu_t(w_c + w_l)ba/2 \qquad 5\text{-}33$$

where μ_t is the cell force coefficient. This cell force coefficient relates the amount of vertical load to its contribution to the in-plane capacity of the diaphragm. The value of μ_t is a function of the failure mode that occurs at ultimate. When Failure Mode 2.b.1 (pop-up) occurs, a conservative value for μ_t was taken as the slope of the inclined web as shown in Figure 68. This value was based on the horizontal force required to push the concrete up the inclined web against the action of gravity. Any contribution made by the frictional force between the steel deck and concrete has been assumed as included in the σ_{ut} term. When Failure Mode 2.b.2 (deck foldover) occurs, μ_t

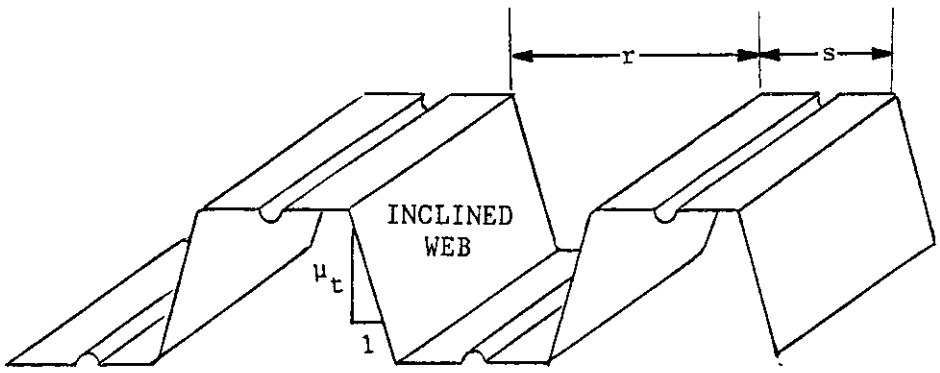

Figure 68. Determination of μ_t

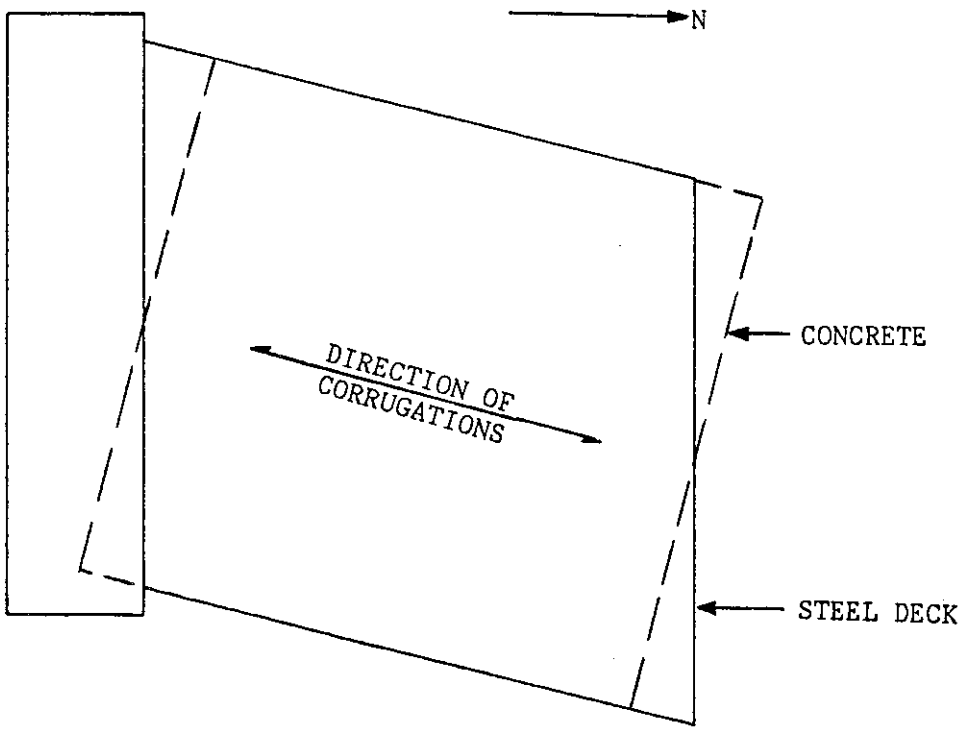

Figure 69. Interfacial failure parallel to the corrugations

was assumed to be equal to 0.7 based on ACI Code 318-83, 11.7.4.3. By using this value for μ_t, the capacity was increased only because of the frictional force between the steel deck and concrete. When Failure Mode 2.b.3 (concrete rib failure) occurs, μ_t was given by

$$\mu_t = (1.4\ r + 0.7\ s) / (r + s) \qquad 5\text{-}34$$

where r is the width of one concrete rib and s is the width of one top section of steel (Fig. 68), 1.4 is based on ACI Code 318-83 for concrete placed monolithically, and 0.7 is based on the same code for concrete placed against steel. When a combination of the above failure modes occurs at ultimate, various values for μ_t could be used. A conservative estimate of ultimate capacity would be obtained by using the smallest possible value for μ_t.

When interfacial shear failure parallel to the corrugations occurs, the frame moves relative to the concrete as shown in Figure 69. Movement between the steel deck and concrete occurs across the entire interface. This behavior occurs because the strength of the steel deck in the direction parallel to the corrugations is greater than the strength of the interface in this direction.

Elemental tests were conducted to determine the stiffness and capacity of the interface between the steel deck and concrete. Parallel elemental tests are assumed to represent a section along the east or west edges of the diaphragm (Fig. 51). On the parallel elemental specimens, the steel deck moves relative to the concrete as shown in

Figure 70. A typical load-displacement curve from a parallel push-off test is shown in Figure 71. The load carrying capacity increased linearly with respect to displacement prior to ultimate. When ultimate was reached the load carrying capacity immediately decreased. Interfacial stresses parallel to the corrugations on the steel deck are assumed to be as shown in Figure 72 at ultimate. Interfacial stresses transverse to the corrugations also exist but are not included on this figure. Based on this stress distribution, the ultimate interfacial capacity per unit of projected area is given by

$$\sigma_{up} = 2\ Q_p\ /\ b \qquad 5\text{-}35$$

where b is the width of the push-off specimen and Q_p is the force per unit length required to cause failure of the elemental push-off test. This force, Q_p, actually represents the force required to cause interfacial failure and to deform the steel deck. By using the above equation, the force required to deform the steel deck is included as part of the expected interfacial capacity.

When a composite diaphragm experiences interfacial failure parallel to the deck corrugations, the parallel interfacial stresses and edge forces are assumed to be as shown in Figure 73. Transverse interfacial stresses also exist but are not shown on this figure. The corresponding forces of the support beams are as shown in Figure 74. By summing moments on the south reaction block, an equation for the ultimate capacity of composite diaphragms that experience interfacial

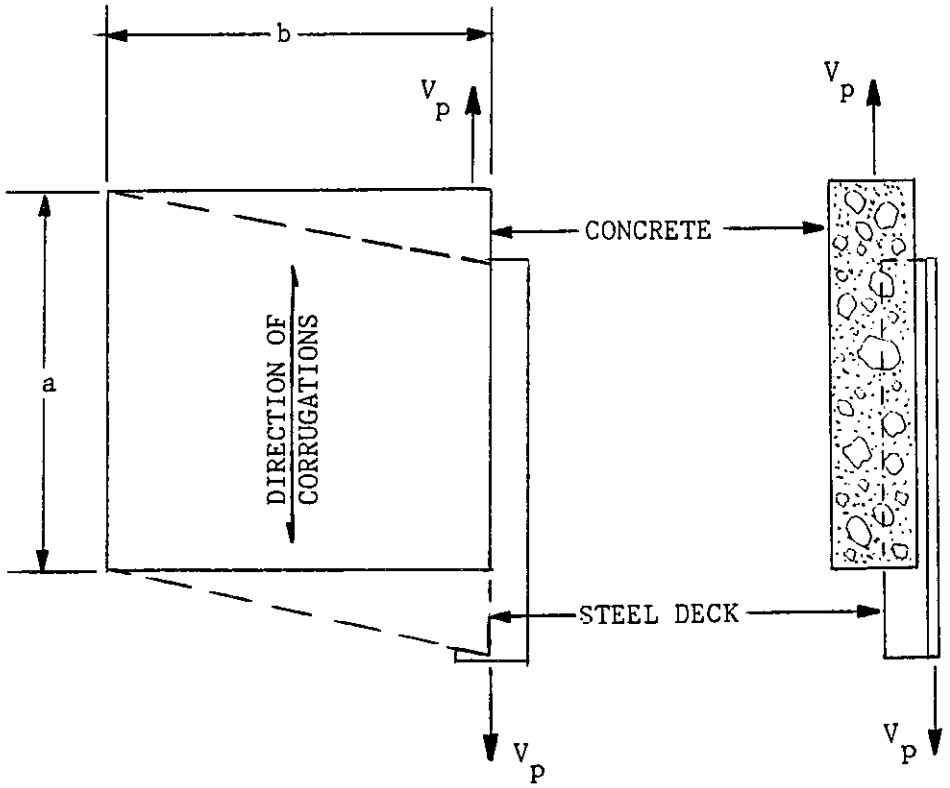

Figure 70. Elemental parallel push-off test

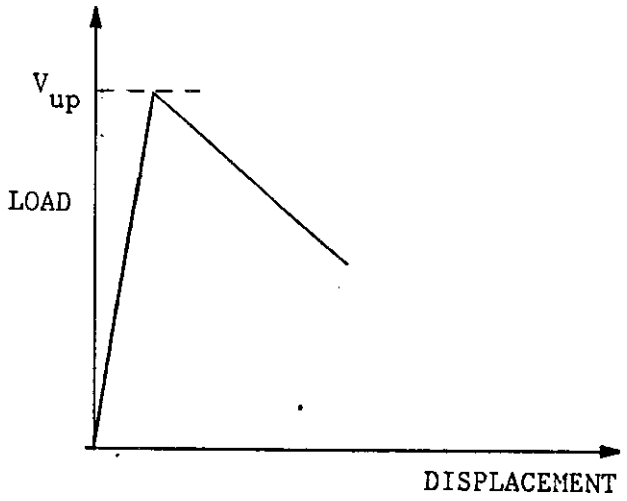

Figure 71. Load-displacement diagram from parallel push-off test

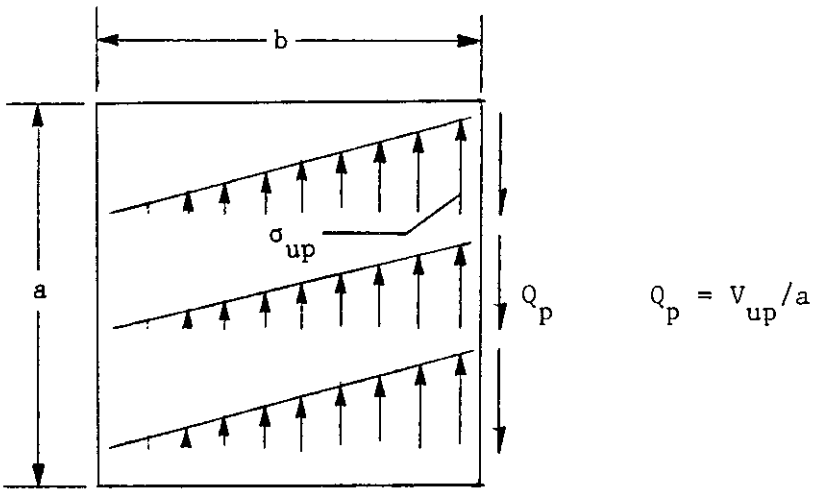

Figure 72. Parallel interfacial stresses and edge forces on the steel deck corresponding to ultimate on the load-displacement diagram from push-off test

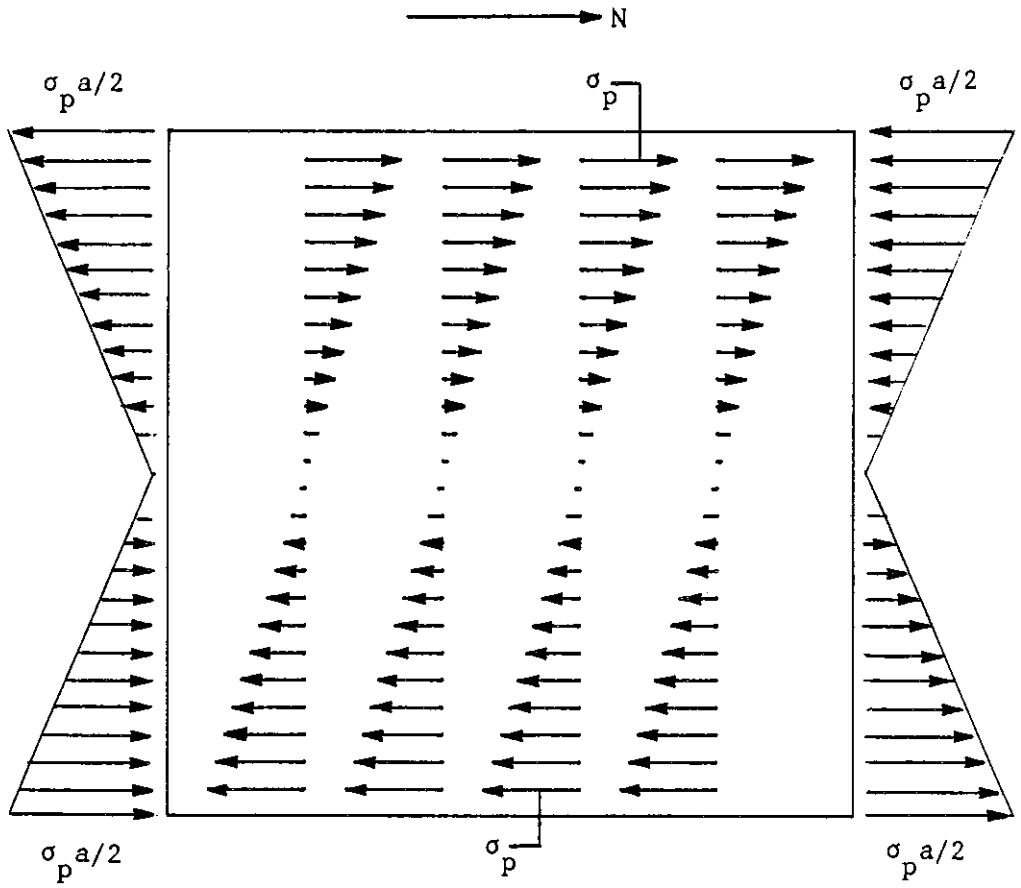

Figure 73. Parallel interfacial and edge forces on the steel deck

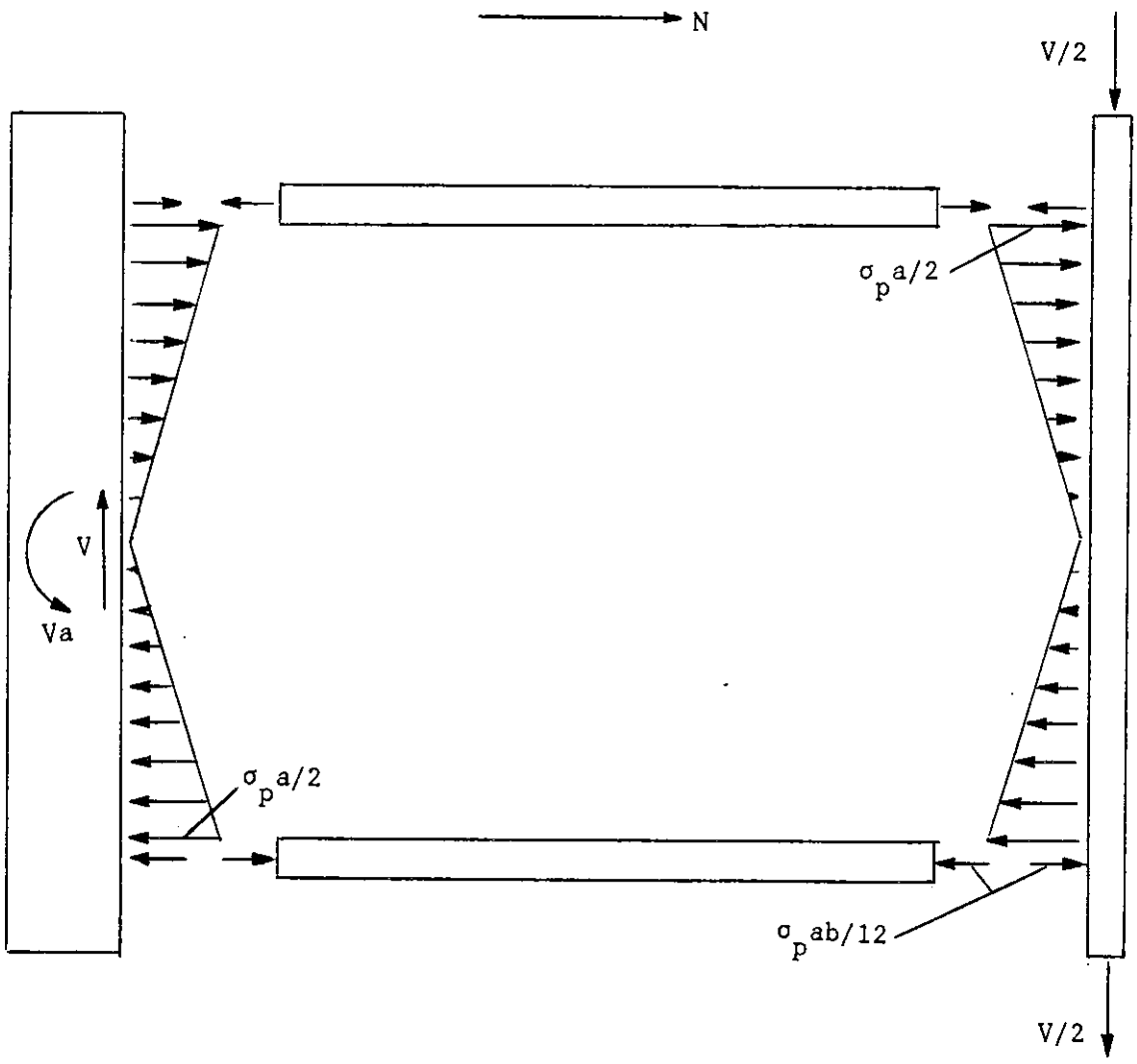

Figure 74. Forces on the edge beams

failure parallel to the corrugations is developed

$$\sigma_{up} b^2 / 6 \qquad 5\text{-}36$$

where σ_{up} is the ultimate interfacial capacity parallel to the corrugations.

This equation does not include the effects of gravity load on the ultimate capacity and must be modified. Gravity load is expected to be transferred one-way to the transverse edges of the diaphragm. The normal interfacial forces generated by the gravity load are assumed to be uniformly distributed along the transverse edge. The total distributed load along both transverse edges is given by

$$(w_c + w_l)\ a \qquad 5\text{-}37$$

where w_c is the weight of the concrete in ksi and w_l is any applied vertical load in ksi. Frictional forces generated when the concrete moves relative to the steel deck are also assumed to be uniformly distributed. By summing moments on the south reaction block, an equation to predict the ultimate capacity of composite diaphragms that experience interfacial failure parallel to the corrugations is given by

$$V = \sigma_{up} b^2/6 + \mu(w_c + w_l)b^2/4 \qquad 5\text{-}38$$

where V is the predicted ultimate capacity in kips and μ is the

coefficient of friction between the steel deck and concrete. This coefficient of friction, μ, is assumed to be equal to 0.7 based on ACI Code 318-83 (1), 11.7.4.3.

Cellular deck is relatively rigid in both the parallel and transverse directions. When this deck type is used and either type of interfacial failure occurs, movement between the steel deck and concrete occurs across the entire interface. The ultimate capacity of composite diaphragms constructed from cellular deck, that experience interfacial failure transverse to the corrugations, can be predicted by using an equation similar to the one developed for interfacial failure parallel to the corrugations. The ultimate capacity of diaphragms, constructed from cellular deck, that experience interfacial failure transverse to the corrugations is given by

$$V = \sigma_{ut} ba/6 + \mu_t (w_c + w_1) ba/2 \qquad 5\text{-}39$$

where μ_t is the cell force coefficient as previously defined. The effect of gravity load on interfacial capacity is the same for both cellular and non-cellular deck types. The ultimate interfacial capacity of diaphragms, constructed from non-cellular deck types, is given by the following equation.

$$V = \text{minimum} \begin{cases} \text{Equation 5-38} \\ \\ \text{Equation 5-33} \end{cases} \qquad 5\text{-}40$$

The ultimate interfacial capacity of diaphragms, constructed from cellular deck types, is given by the following equation.

$$V = \text{minimum} \begin{cases} \text{Equation 5-38} \\ \\ \text{Equation 5-39} \end{cases} \qquad 5\text{-}41$$

The ultimate capacity of diaphragms that experience edge fastener failure can be calculated using the ISU method of analysis. The effects of vertical load on edge fastener capacity were not investigated as part of this study.

These proposed equations were designed to be used in a strength design method. Nominal in-plane shear strength of a diaphragm could be determined using these proposed equations. A conservative estimate of nominal in-plane shear strength would be obtained by assuming the applied gravity load, w_1, is equal to zero. Design in-plane shear strength would be determined by multiplying the nominal in-plane shear strength by an appropriate strength reduction factor. Additional testing and a reliability study must be completed before an appropriate strength reduction factor can be proposed.

5.3. Comparison of Experimental and Analytical Results

The experimental initial stiffnesses and the stiffnesses predicted by ISU equations and Tri-Service equations are listed in Table 6. The ISU equations are based on the assumption that the diaphragm together with edge beams can be idealized as a plate girder. The total stiff-

Table 6. Experimental versus predicted initial stiffness

Slab Number	Experimental (k/in)	Stiffness predicted by: ISU Equations (k/in)	Tri-Service Equations (k/in)
1	1800	3000	4500
2	2000	2900	4300
3	1600	1600	2900
4	1300	1500	2600
5	1700	1400	1600
6	2600	1900	3900
7	1500	1600[a]	4600
8	1100	1100	3400
9	1900	1600	7000
10	1700	1800	3100
11	1600	1600	1100
12	1800	1800	3200
13	1900	1600	7100
14	1900	2100	5200
15	1300	1400	1700
16	1300	1400	1700
17	2200	1800	3800
18	1700	1700	3000

[a]Calculated using push-off test results for Deck Type 1.

ness is then a function of the bending stiffness of the equivalent plate girder, the shear stiffness of the composite web, and the stiffness of the "edge zone". The "edge zone" stiffness was based on results from elemental push-off tests. Since no push-off tests were completed on studded specimens, the "edge zone" stiffness of studded diaphragms was calculated using empirical load slip equations for studs given by Ollgaard, Slutter and Fisher (22). Studs were used on Slabs 1, 2 and 8. Stiffness predictions for Slabs 1 and 2 were not very good. Stiffness predictions for the rest of the slabs were good. Stiffness predictions using the Tri-Service equations were not very good.

Experimental and predicted ultimate loads based on the ISU equations and the Tri-Service equations are given in Table 7. The ISU equations include the consideration of four possible failure modes. Only two possible failure modes are considered on studded specimens because interfacial failure does not occur when studs are used. The lowest prediction calculated corresponds to the failure mode that will occur first and is used as the predicted ultimate strength of the diaphragm. The Tri-Service equations produced good predicted ultimate strengths for only a few of the diaphragms. One possible reason for this limited accuracy is that several potential failure modes were not considered in the equation development. The ISU equations produced good predicted strengths for most of the diaphragms but tended to predict too low a value for the transverse interfacial slip mode of failure. This probably occurred because the

Table 7. Experimental versus predicted ultimate loads

Slab Number	Experimental (kips)	ISU Equations				Tri-Service Equations (kips)
		Mode 1 (kips)	Mode 2a (kips)	Mode 2b (kips)	Mode 3 (kips)	
1	168	182	-[a]	-[a]	448	-[a]
2	186	181	-[a]	-[a]	490	-[a]
3	98	166	139	94	145	104
4	88	148	139	94	145	93
5	116	115	147	194	182	82
6	147	295	147	194	290	196
7	137	186	139[b]	94[b]	275	123
8	54	146	-[a]	-[a]	80	-[a]
9	220	201	230	167	261	146
10	161	150	186	130	255	99
11	95	163	87	108	345	96
12	180	154	186	130	255	101
13	250	221	230	167	261	150
14	208	255	186	130	255	166
15	103	116	168	110	346	85
16	124	117	168	110	346	85
17	146	288	147	194	290	191
18	161	145	186	130	255	97

[a]Does not apply.

[b]Calculated using push-off test results for Deck Type 1.

ISU equations did not consider the effects of gravity load on composite diaphragm behavior.

The experimental and predicted strengths based on the proposed equations and the ISU equations are given in Table 8. The proposed equations are similar to the ISU equations but include a consideration of gravity load effects. These proposed equations produced good predicted strengths and failure modes for most of the diaphragms. The difference between the predicted ultimate capacity and experimental ultimate capacity was less than 17 percent for all slabs except Slabs 1, 7 and 8. The predicted ultimate capacity for Slab 1 was 25 percent greater than the measured experimental capacity. The predicted ultimate capacity for Slab 7 was 25 percent less than the measured experimental capacity. The predicted ultimate capacity for Slab 8 was 48 percent greater than the measured experimental capacity. Predictions for Slab 8 were calculated using the ISU equations for edge fastener failure.

Slabs 1 and 2 failed in diagonal tension prior to reaching the load predicted by the proposed equations. One possible reason for this behavior would be that the studs generated discrete regions of high stress that cause these diaphragms to fail prematurely. Slabs 3 and 4 failed in transverse interfacial shear. This failure mode was predicted by the proposed equations. Transverse elemental tests for Deck Types 2, 4, and 5 indicated that pop-up failure would occur if failure transverse to the corrugations occurred. Thus, a conservative value for μ_t was taken as the slope of the inclined web for slabs constructed from these deck types. Slabs 6, 11, and 17 failed

Table 8. Experimental versus predicted ultimate loads

Slab Number	Experimental (kips)	Proposed Equations Mode 1 (kips)	Proposed Equations Mode 2a (kips)	Proposed Equations Mode 2b (kips)	ISU Equations (kips)
1	168	210	-[a]	-[a]	182
2	186	209	-[a]	-[a]	181
3	98	191	142	103	94
4	88	169	142	103	94
5	116	119	149	219	115
6	147	337	151	237	147
7	137	207	142[b]	103[b]	94
8	54	165	-[a]	-[a]	80
9	220	205	234	253	167
10	161	161	189	150	130
11	95	181	90	118	87
12	180	166	192	169	130
13	250	228	241	306	167
14	208	287	196	198	130
15	103	123	171	120	110
16	124	124	172	124	110
17	146	329	155	277	147
18	161	155	196	189	130

[a]Does not apply.

[b]Calculated using push-off test results for Deck Type 1.

in interfacial shear parallel to the corrugations and this behavior was predicted. Slabs 5, 9, 12, 13, 16, and 18 failed in diagonal tension and this behavior was predicted. No elemental push-off tests were completed using Deck Type 3 due to a shortage of this deck type. Ultimate capacity predictions for Slab 7 were calculated by using results from elemental push-off tests for Deck Type 1. The embossment pattern on Deck Type 1 was similar to the embossment pattern on Deck Type 3. Deck Type 1 was made from 20-gauge steel and Deck Type 3 was made from 16-gauge steel. The predicted ultimate capacity for Slab 7 was conservative. Slab 10 failed in diagonal tension but transverse interfacial shear was predicted. This was probably caused by using a conservative value for μ_t. Slab 14 failed in interfacial shear both parallel and perpendicular to the corrugations and the predicted values for these two failure modes were very close. Slab 15 experienced transverse interfacial shear and this behavior was predicted.

6. SUMMARY, CONCLUSIONS AND RECOMMENDATIONS

6.1. Summary

A mechanism was designed and constructed to apply vertical load to diaphragms. Ten full-scale diaphragms were tested using a cantilever type test frame. Four diaphragms were subjected to in-plane loading only and were used as a control series. Six diaphragms were subjected to distributed vertical load and in-plane load. These tests were conducted to study the effects of distributed vertical load on composite diaphragm behavior.

Slabs 6 and 17 were constructed from the same deck type and had nearly the same concrete thickness. Slab 6 was subjected to no applied vertical load and Slab 17 was subjected to an applied vertical load of 100 psf. The initial stiffness and concrete strength for Slab 17 was less than it was for Slab 6. Both slabs failed by interfacial shear parallel to the corrugations and reached nearly the same ultimate load.

Slabs 10, 12, and 18 were constructed from Deck Type 5 and had nearly the same concrete strength and concrete thickness. Slabs 10, 12, and 18 were subjected to applied loads of 0, 65, and 135 psf, respectively. All of these slabs had nearly the same initial stiffness and ultimate capacity. Slab 12 had a slightly higher concrete strength, initial stiffness, and ultimate capacity. All of these slabs experienced diagonal tension failure of the concrete web at ultimate. The rate of stiffness degradation was less for Slabs 12 and 18 than for Slab 10.

Slab 14 was constructed from Deck Type 5 but had a larger concrete thickness than Slab 18. Slab 14 was subjected to an applied vertical load of 135 psf just like Slab 18. The initial stiffness of Slab 14 was greater than the initial stiffness of Slab 18. Slab 14 failed by interfacial shear at ultimate and reached a maximum load significantly higher than the maximum load for Slab 18.

Slabs 9 and 13 were both constructed from cellular Deck Type 4 and had nearly the same concrete thickness. Slab 13 was subjected to an applied vertical load of 200 psf in addition and prior to being loaded in-plane like Slab 9. These slabs had the same initial stiffness and failed by diagonal tension of the concrete web. Slab 13 had a higher concrete compressive strength and reached a higher ultimate load. The rate of stiffness degradation was less for Slab 13.

Slabs 15 and 16 were constructed from Deck Type 7 and had nearly the same concrete thickness and concrete strength. Slab 16 was subjected to an applied vertical load of 35 psf in addition and prior to being loaded in-plane like Slab 15. These slabs had the same initial stiffness. Slab 15 experienced concrete rib faliure. Slab 16 failed by diagonal tension of the concrete web. Prior to ultimate, the rate of stiffness degradation was nearly the same for these slabs.

A method of analysis was developed to estimate the ultimate capacity of steel-deck reinforced concrete diaphragms. This method included a consideration of vertical load effects on diaphragm capacity. Ultimate strengths were calculated using this proposed method of analysis. Initial stiffnesses and strengths were calculated using

the ISU method of analysis (30) and the Tri-Service method of analysis (12). Results from all three methods were compared with the experimental results.

6.2. Conclusions

Distributed vertical load has no significant effect on the initial stiffness of composite diaphragms. The initial stiffness of similar diaphragms with and without vertical load was nearly the same. Distributed vertical load tends to reduce the rate of stiffness degradation.

Distributed vertical load has very little effect on the ultimate capacity of composite diaphragms that fail in diagonal tension. The capacity of these slabs is primarily a function of the concrete thickness and strength. Distributed vertical load also has little effect of the capacity of composite diaphragms that fail in interfacial shear parallel to the corrugations.

Distributed vertical load has a significant effect on the ultimate capacity of composite diaphragms that fail in interfacial shear transverse to the corrugations. The vertical load tends to create a large force normal to the interfacial plane in the transverse "edge zone". This normal force helps to prevent interfacial shear failure.

The Tri-Service equations produced good ultimate load predictions for only a few of the diaphragms. These equations do not produce satisfactory predictions for certain failure modes. The previously proposed ISU equations produced good initial stiffness predictions

for most of the diaphragms. The ISU equations also produced good ultimate load predictions for some of the diaphragms. These equations tend to underestimate the capacity of diaphragms that fail by interfacial shear transverse to the corrugations. The proposed equations produced good ultimate load predictions for most diaphragms that have been tested to date. However, the effects of changes in slab dimensions and edge fastener failures need to be studied further before a final design method can be proposed.

6.3. Recommendations for Continued Study

Additional experimental research should be completed to determine the strength and behavior of composite diaphragms that experience edge fastener failure. Composite diaphragms with various fastener spacings and types should be tested. This research should also include an investigation of the effects of gravity load on edge fastener failure.

Composite diaphragms with different length to width ratios should be tested to determine the effects of this variable on strength and behavior. Elemental push-off tests for Deck Type 3 should be completed to determine values for interfacial strength and stiffness. Effects of adjoining panels on diaphragm behavior should be investigated by conducting tests with continuous slab elements. Composite diaphragms with concentrated gravity loads and pattern gravity loads should be tested to determine the effects of these types of loads on diaphragm behavior.

Additional analytical and experimental research should be completed to determine the damping and energy dissipation characteristics of steel-deck reinforced concrete diaphragms. Damping is a very important variable in the design of structures subjected to seismic forces. Further analysis is required to better understand the behavior of composite diaphragms as part of an entire structure.

7. REFERENCES

1. American Concrete Institute. Building Code Requirements for Reinforced Concrete. ACI Standard 318-83. Detroit, Michigan: American Concrete Institute, 1983.

2. American Institute of Steel Construction, Inc. "Specification for the Design, Fabrication and Erection of Structural Steel for Building." New York: AISC, 1978.

3. American Iron and Steel Institute. Cold-Formed Steel Design Manual. Washington, D.C.: AISI, 1983.

4. Ammar, A. A. and Nilson, A. H. "Analysis of Light Gage Steel Shear Diaphragms, Part I." Research Report 350. Department of Structural Engineering, Cornell University, August 1972.

5. Ammar, A. A. and Nilson, A. H. "Analysis of Light Gage Steel Shear Diaphragms, Part II." Research Report 351. Department of Structural Engineering, Cornell University, August 1973.

6. Applied Technology Council. "Tentative Provisions for the Development of Seismic Regulations for Buildings." ATC 3-06. Washington D.C.: U.S. Government Printing Office, June 1978.

7. Apparao, T. V. "Tests on Light Gage Steel Diaphragms." Research Report 328. Department of Structural Engineering, Cornell University, December 1966.

8. Arnold, V. E., Greimann, L. F. and Porter, M. L. "Pilot Tests of Composite Floor Diaphragms." Progress Report, ERI-79011. Engineering Research Institute, Iowa State University, Ames, Iowa, September 1978.

9. Blodgett, O. W. "Report on Proposed Standards for Sheet Steel Structural Welding." Welding Journal, 57, No. 4 (April 1978), 15-24.

10. Brangwin, D.J. "Interfacial Shear of Composite Floor Diaphragms." Unpublished Master's thesis. Iowa State University, Ames, Iowa, 1979.

11. Cardenas, A. E., Hanson, J. M., Corley, W. G. and Hognestad, E. "Design Provisions for Shear Walls." Journal of the American Concrete Institute, Proceedings 70, No. 3 (March 1973), 221-230.

12. Department of the Army, Navy and the Air Force. Seismic Design of Buildings. Army TM5-809-10. Washington, D.C.: U.S. Government Printing Office, April 1973.

13. Ellifritt, D. S. and Luttrell, L. D. "Strength and Stiffness of Steel Deck Shear Diaphragms." Proceedings of First Specialty Conference on Cold-Formed Steel Structures. Department of Civil Engineering, University of Missouri-Rolla, August 1971.

14. Grant, J. A., Fisher, J. W. and Slutter, R. G. "Composite Beams with Formed Steel Deck." AISC Engineering Journal, American Institute of Steel Construction, 14, No. 1, First Quarter (1977), 24-43.

15. Klaiber, F. W. and Porter M. L. "Uniform Loading for Steel-Deck Reinforced Slabs." Journal of the Structural Division, ASCE 107, No. ST11, Proc. Paper 16642 (November 1981), 2097-2110.

16. Krupicka, Gary L. "The Behavior and Analysis of Steel-Deck Reinforced Concrete Slabs with End-Span Studs." Unpublished Master's Thesis, Iowa State University, Ames, Iowa, 1979.

17. Luttrell, L. D. "Strength and Behavior of Light Gage Steel Shear Diaphragms." Cornell Engineering Research Bulletin No. 67-1. Department of Structural Engineering, Cornell University, July 1976.

18. Luttrell, L. D. "Structural Performance of Light Gage Steel Diaphragms." Research Report 319. Department of Structural Engineering, Cornell University, August 1965.

19. Nilson, A. H. "Shear Diaphragms of Light Gage Steel." Journal of the Structural Division, ASCE 86, No. ST11 (November 1960), 111-140.

20. Nilson, A. H. "Diaphragm Action of Light Gage Steel Construction." AISI Regional Technical Paper, 1960.

21. Nilson, A. H. and Ammar, A. R. "Finite Analysis of Metal Deck Shear Diaphragms." Journal of the Structural Division, ASCE 100, No. ST4 (April 1974), 711-726.

22. Ollgaard, J. G., Slutter, R. G. and Fisher, J. W. "Shear Strength of Stud Connectors in Lightweight and Normal-Weight Concrete." AISC Engineering Journal, American Institute of Steel Construction, 8, No. 2 (April 1971), 55-64.

23. Park, R. and Paulay T. Reinforced Concrete Structures. New York: John Wiley and Sons, Inc., 1975.

24. Porter, M. L. Commentary on the Tentative Recommendations for the Design of Composite Steel Deck Slabs. Manual. Washington, D.C.: American Iron and Steel Institute, December 1974.

25. Porter, M. L. and Ekberg, C. E., Jr. "Investigation of Cold-Formed Steel-Deck Reinforced Concrete Floor Slabs." Proceedings of First Specialty Conference on Cold-Formed Steel Structures. Department of Civil Engineering, University of Missouri-Rolla, August 1971.

26. Porter, M. L. and Ekberg, C. E., Jr. "Summary of Full-Scale Laboratory Tests of Concrete Slabs Reinforced with Cold-Formed Steel Decking." Preliminary Report. International Association for Bridge and Structural Engineering, Ninth Congress, Zurich, Switzerland, May 1972.

27. Porter, M. L. and Ekberg, C. E., Jr. "Design vs Test Results for Steel Deck Floor Slabs." Proceedings of Third International Speciality Conference on Cold-Formed Steel Structures, University of Missouri-Rolla, November 1975.

28. Porter, M. L. and Ekberg, C. E., Jr. "Design Recommendations for Steel Deck Floor Slabs." Journal of the Structural Division, ASCE 102, No. ST11, Proc. Paper 12528 (November 1976), 2121-2136.

29. Porter, M. L. and Ekberg, C. E., Jr. "Behavior of Steel-Deck Reinforced Slabs." Journal of the Structural Division, ASCE 103, No. ST3, Proc. Paper 12826 (March 1977), 663-677.

30. Porter, M. L. and Greimann, L. F. "Seismic Resistance of Composite Floor Diaphragms." Final Report, ERI-80133. Engineering Research Institute, Iowa State University, Ames, Iowa, May 1980.

31. Porter, M. L., Ekberg, C. E., Jr., Greimann, L. F. and Elleby, H. A. "Shear-Bond Analysis of Steel-Deck-Reinforced Slabs." Journal of the Structural Division, ASCE 102, No. ST12, Proc. Paper 12611 (December 1976), 2255-2268.

8. ACKNOWLEDGEMENTS

This investigation into the behavior of composite diaphragms was conducted by the Engineering Research Institute of Iowa State University with funds provided by the National Science Foundation. Steel deck was provided by the following manufacturers: Mac-Fab Products, Inc., H.H. Robertson Company, Wheeling Corrugating Company and Vulcraft, a division of Nucor Corporation.

The author wishes to express his appreciation to his major professor, Dr. M.L. Porter, for his support and guidance throughout this investigation. In addition, the author wishes to express his appreciation to Dr. F.W. Klaiber and Prof. W.F. Riley for serving on the author's graduate committee. A special thanks to graduate student, Mike Prins, for conducting elemental push-off tests and providing results from those tests. The author is also grateful for the assistance provided by Sam Easterling and Doug Wood, and the many undergraduate students during the experimental phases of this investigation.

Special thanks are given to my fiancee, Susanne, for her continued understanding and encouragement throughout my work.